ISSN 0371-9538
Vol. 115, April 2018 – March 2019

TRANSACTIONS

A Technical Publication of
The Mining, Geological and Metallurgical Institute of India

The Mining, Geological and Metallurgical Institute of India

MGMI COUNCIL FOR 2018-19

THE MINING GEOLOGICAL & METALLURGICAL INSTITUTE OF INDIA
1906
Established 1906

President

Anil Kumar Jha, Chairman, Coal India Limited

Vice - Presidents

Prabhat Kr Sinha, CMD, NCL

PR Mandal, Former Advisor, MoC

Avijit Ghosh, Former CMD, HEC

JP Goenka, Mng Partner, NMC

Immediate Past President

Dr NK Nanda, Director (Technical), NMDC

Honorary Secretary

Rajiw Lochan, General Manager (CBM), CMPDI

Honorary Jt Secretary

Ranajit Talapatra, Sr Manager (CP), CIL

Honorary Treasurer

Samir Kumar Ghosh, Former Mgr (Met), HCL

Immediate Past Honorary Secretary

Prasanta Roy, Sr Manager (Geol/CV), CIL

Honorary Editor

Prof (Dr) Khanindra Pathak, IIT Kharagpur

Members

LK Bose, Former Executive Director, CIL

BC Bhattacharya, Former Chief General Manager (WBPD), CIL

Prof (Dr) SK Mukhopadhyay, Former Professor IIT, Kharagpur

Bhaskar Chakraborti, Former Director (SG), GSI

Dr Amalendu Sinha, Former Director, CSIR-CIMFR

Amrita Acharya, Former Coal Controller

Prof (Dr) Ashis Bhattacharjee, IIT, Kharagpur

Prof (Dr) GP Karmakar, IIT, Kharagpur

Anil Kumar Singh, TS/GM to Director (Technical), MCL

Dr Kalyan Sen, Former Director, CIMFR

Prof (Dr) Sajal Dasgupta, VC, University of Engg & Mgmt

VK Arora, Chief Mentor (Coal), KCT & Bros

Anup Biswas, Former Deputy Director General, Mines Safety

Anil K Karmakar, Former General Manager (Admin), CIL

Akhilesh Choudhury, Former Deputy Director General, GSI

Prof Bhabesh Chandra Sarkar, Professor, IIT-ISM, Dhanbad

Dr Netai Chandra Dey, Professor, IIEST, Shibpur

Editorial Committee

Binay Dayal, Director (Technical), CIL
BC Bhattacharya, Former Editor, MGMI
Dr Anupendu Gupta, Former DDG, GSI

Prof (Dr) SK Mukhopadhyay, Former Professor, IIT Kharagpur
Dr Biswajit Samanta, Professor, IIT Kharagpur and Asso Edt, MGMI
Prof Atul Verma, Former HOD, Applied Geology, IIT-ISM

Chief Advisor to the Editorial Committee

Prof SP Banerjee, Former President, MGMI & Director ISM, Dhanbad

ISSN 0371-9538 Volume 115 : April 2018 – March 2019

TRANSACTIONS

A Technical Publication of
The Mining, Geological and Metallurgical Institute of India

MGMI
Established 1906

TRANSACTIONS of
THE MINING, GEOLOGICAL AND METALLURGICAL INSTITUTE OF INDIA
Inaugurated 1906 – incorporated 1909 – as the Mining and Geological Institute of India, the word Metallurgical was included in the title in 1937.

Price

- Free to Members
  (Rs. 100/- for each additional copy)
- Non – Members
  Rs. 200/- per copy
- Foreign US$ 25.00 per copy

Published by
Rajiw Lochan, Honorary Secretary
The Mining, Geological and Metallurgical Institute of India
GN – 38/4, Sector – V, Salt Lake City, Kolkata – 700 091

Printed at :
Graphique International
Kolkata

Contents

From Editor's Desk..... i
Prof (Dr) Khanindra Pathak

Presidential Address.....iv
Dr NK Nanda

60th Holland Memorial Lecture.....vi
Dr Kirit Shantilal Parikh

TECHNICAL PAPERS

Reliability and Availability Analysis of a Continuous..... 1
Miner Machine in an Indian Underground Coal Mine
Sumit Banerjee, Prof NC Dey

Geomorphic Indicator Model for Identifyig..... 8
Manganese Mineralization
Shaurav Kumar, Asim Chatterjee, Rajesh Mukherjee
Rajib Deb, Subhashbabu Ainampudi

Laboratory Measurement of Permeability..... 17
of Argon and Carbon-di-oxide in Coal
T Bakshi, Dr K Pathak, BK Prusty, SK Pal, AK Patra

Assessment of Occupational Stress Variability (OSV)..... 27
of Deep Underground Miners Including Estimation
of Skeletal Muscle Force, Fatigue, and its Recovery
Testing by Hand-Grip Dynamometry (HGD)
Shibaji Ch. Dey, Prof NC Dey

Development of a GUI Based Software - Tool for Surface..... 37
Deformation Mapping through DInSAR Processing :
A Case Study Over Jharia Coal Field
Tapas Kumar Dey, Biswajit Manna, Debashish Chakravarty
Biswajit Samanta, and Arundhati Misra

Comparison of Efficiency of use of Polyurethane..... 52
Coating of Hydro Transport Pipelines
and Steel Pipelines on the Basis
of Parameters of Abrasive Wear
Victor Alexandrov, Maria Vasilyeva and Prof Olga Kochergina

WATER RESOURCE DEVELOPMENT AND WATER MINING

Prof (Dr) Khanindra Pathak

Humanity is well aware of the fact that water is the most important natural resource. It has the sheer ability to define and maintain the existence of human beings on this planet. Inevitably, there has been a surge in the conflicts between the mining community and the general society regarding the interference of mining on potable waters. In this regard, there have been many instances which have proved that mining induced water resource interference is of great concern. To name a few, the rural community of Enyigba in South-Eastern Nigeria is currently facing acute problems of water resource contamination due to lead Zinc mining, villagers near Sukinda are exposed to Hexavalent chromium dispersed by tailing wash-off while the people of Kaudikasa village in the Ambagad Chowki block of Rajnandgaon district in Chhattisgarh facing Arsenic contaminated ground water after a venture of uranium mining. These examples clearly show that this problem is not local to any particular mine site, but is rather far reaching. As a result, there has been increasing pressure on the government to strengthen the rules regarding mining and water source management and make the law more stringent.

On a national scale, the hilltop surface mining of iron ores can be considered to be a potential threat to many perennial streams in Karo and Koina river basins in Saranda forest. It has also been observed that the large opencast mines in the Chattisgarh or West Bengal can disrupt the ground water flow patterns, giving rise to acute water shortage issues in the many generations to come. Thus, there is an urgent need for appropriate measures that would be required for ground water management in all the mining regions.

To address these issues, mining-industry pioneer, Tatasteel has successfully initiated rainwater harvesting in the mining areas of Barbill, while many other mining companies in India are yet to take some steps for ground water restoration. However, despite the numerous initiatives undertaken, the public remains largely unaware and unconvinced of the efforts taken for the same.

Water resource crisis is increasing at an alarming rate due to anthropogenic interferences. USA reveals that the extraction, transport, store, process and disposing of 1 ton of coal uses 800-3000 gallons of water. Areputed journal has been quoted to say that "Mining and burning coal accounts for half of all water withdrawals in the United States, which is the same amount of water that pours over Niagara Falls in five months". As a testimony to this, Mpumalanga coal mining belt in South Africa has caused a lot of damage to the water resources ultimately resulting in barren lands incapable of bearing crops for livelihood of common people. Consequently, the mine had to close, which left the miners in a pitiable, poverty-ridden state. Unless adequate steps are taken, similar situations are highly probable in the villages near any mine site of India as there have already been reports of the ground water level lowering, leading to water crisis.

Damages by Acid mine drainage could be threat to food security

During the large scale surface mining, many water holding sandy strata may get excavated. Backfilling if not properly planned may not restore the water regime of the premining conditions.

Stakeholder engagement in planning and apprising cumulative impacts, mitigating regional risks and creating opportunities for mine water management are now attempted through innovative programs and investments. Lare volumes of documents and guidelines are now available for the mining industry worldwide. Many research activities are still going on, however, visible mega projects to engineer the water resource restoration are rare.

However, it is doubtful if the ground water, aquifers and potable water reservoir issues have been properly addressed at a local level. Unfortunately, our laws and regulations are not implemented to achieve zero pollutant contamination of ground water. No policy has been introduced in any field to arrest migrating pollutants in the soil. Al the towns and villages in India now charging pollutants to grownwater through free discharge of contaminated water on earth surface without any protection measures. Every household and organizations in India are contributing to ground water contamination. Central Ground Water Board (CGWB), GSE and relevant mining companies must take joint initiatives for ensuring ground water security and to take necessary steps to eliminate water poverty in near future.

Such ongoing debates and disputes regarding the water reservoirs show how important water is for the sustainability of mankind. It had been realized in the late 20th century that this depleting resource requires collaborative global initiatives to handle it. To facilitate this, an international network called Global Water Partnership (GWP) was created in 1996 with the support of the World Bank, the United Nations Development Programme (UNDP) and the Swedish International Development Cooperation Agency (Sida). It was founded to foster an integrated approach to water resources management (IWRM) and provide practical advice for sustainably managing water resources. In 2002, the GWP became an intergovernmental organisation under international law and became known as the Global Water Partnership Organisation (GWPO). The Secretariat is based in Stockholm, Sweden.

India, also recognizing the need to monitor and develop on water allocation and management, housed a non-profit organization called India Water Partnership (IWP). IWP was primarily concerned with the promotion of Integrated Water Resources Management (IWRM) in India and possessed 12AA & 80G from Income Tax Department, Government of India. It was also accredited by the GWP as a Country Water Partnership of GWP and hence also known as GWP-India. This organization is working with a mission of building a water secure India, by integrating the actions of Sustainable and Integrated Development and Management of Water Resources initiatives taken at a national, regional, riverbasin/Sub-basin and local levels [along with the participation of all stakeholders]. However, while such organizations can sensation alise the issue to bring about reformative national discussions and policies, realistic action plans and demonstration projects are the real need.

To achieve this, six Zonal Water Partnerships have been established in India with the following composition of States and Union Territories :

1. **North Zone Water Partnership :** The North Water Partnership comprises of the States of Jammu & Kashmir, Himachal Pradesh, Uttarakhand, Uttar Pradesh, Punjab, Haryana, Rajasthan, Chandigarh & Delhi;
2. **South Zone Water Partnership :** The South Zone Water Partnership consists of the States like; Andhra Pradesh, Kerala, Karnataka, Tamil Nadu & Pondicherry;
3. **East Zone Water Partnership :** Bihar, Jharkhand, West Bengal & Orissa States form part of East Zone Water Partnership
4. **West Zone Water Partnership :** The West Zone Water Partnership comprises of States of Gujarat, Maharashtra & Goa;
5. **Central Zone Water Partnership :** Madhya Pradesh & Chhattisgarh form part of the Central Zone Water Partnership;
6. **North-East Zone Water Partnership :** North-East Zone Water Partnership consists of States like Arunachal Pradesh, Assam, Meghalaya, Manipur, Nagaland, Sikkim & Tripura;

However, actions like these are also not powerful enough to complete lt eliminate the serious threat India is facing. Organizational attempts must not simply end in reports. Such organizations must come forward to carry out the demonstration ofthe implementation of the project, instead of merely compiling reports and construction of knowledge products with modelling and simulation study. Such organizations must develop an approapriate approach for Water Mining and develop scientific sustainable water resource development rules, water reserve estimation and water mining regulations.

The following list elaborates of the issues that require urgent actions :

1. Developing national inventory of thestatus deterioration of all surface and ground water resources.

2. Protecting, enhancing and restoring all bodies of surface and ground water complying with the aim of achieving good ecological status.
3. Developing a national registry of the present impacts of coal and metal mine drainage on stream water, sediment and ecology.
4. National level classification of streams and waterbodies that are currently receiving mine drainage for streamlining their remediation schemes through proper delegations of authority and institutional attempts.
5. Determining the environmental variables (water and sediments) affected by pollution from mine drainage.
6. Determining the impacts of abandoned mine drainages on the structure of the aquatic community in receiving streams.
7. National level assesments of the effects of water pollutions on the function of the aquatic community in streams receiving mine drainage.
8. Detecting the differences in an ecosystem in terms of the functional response to pollution by coal and metal mine drainage through institutional attempts.
9. Investigating ecological recovery of damaged water resources and establishing the corresponding time scale for such actions.
10. Developing mass awareness scheme and bringing water study into school and college curriculum with appropriate laboratory components without discremenating of study stream as science, commerce or arts.

Some documents and guidelines are now available for the mining industry are :
• Best practice environmental management in mining – EPA, Australia [55 Overview of Best Practice Environmental Management in Mining, EPA, Australia, 2002. [Google Scholar]].
• US EPA practices for water management in coal mining areas [56 Coal Re-mining Best Management Practices Guidance Manual, U.S., Environmental Protection Agency, Washington, DC, 2001. [Google Scholar]].
• Water policy and its management in India [44 National Water Policy, Ministry of Water Resources, Government of India, New Delhi, p. 9, 20, 2002. [Google Scholar]].
• Global Acid Rock Drainage (GARD) guide (www.GARDGuide.com).
• South African Best Practice Guideline H4: Water Treatment [57P. Jacobs and W. Pulles, Best Practice Guideline H4 : Water Treatment, Department of Water Affairs and Forestry, Pretoria, 2007. [Google Scholar]].
• Berlin Guidelines of United Nations [25–27 Berlin II Guidelines for Mining and Sustainable Development, United Nations Department of Economic and Social Affairs [UNDESA], United Nations Environment Programme Industry and Environment [UNEP], United Nations, 2002. Berlin II Guidelines for Mining and Sustainable Development – Appendices, United Nations Department of Economic and Social Affairs [UNDESA], United Nations Environment Programme Industry and Environment [UNEP], United Nations, 2002. Mining and the Environment – The Berlin Guidelines – A Study Based on an International Round Table held in June 1991, United Nations Department of Technical Co-operation for Development (UNDTCD) and Development Policy Forum of the German Foundation for International Development, Mining Journal Books, London, 1992.].
• Equator Principles [28,29 The Equator Principles – A Financial Industry Benchmark for Determining, Assessing and Managing Social and Environmental Risk in Project Financing, Equator Principles Association, London, 2006. J.M. Conley and C.A. Williams, Global Banks as Global Sustainability Regulators? – The Equator Principles, Law & Policy 33 (2011), pp. 542–575.].
• NMA's and SME's Hard rock Mining and Beneficiation Environmental Management System Guide [58Hardrock Mining and Beneficiation Environmental Management System Guide, National Mining Association (NMA), Society for Mining Metallurgy and Exploration, SME, 2012. [Google Scholar]].

PRESIDENTIAL ADDRESS

Dr NK Nanda*

Good Afternoon!

Dignitaries on the dias and off the dias, dear members, participants, guests, ladies and gentlemen.

Minerals are valuable natural resources which forms the raw material for many basic industries and are a major resource for development. The history of mineral extraction in India dates back to the days of the Harappan civilization. The wide availability of the minerals provides a base for the growth and development of the mining sector in India.

The country is endowed with huge resources of many metallic and non-metallic minerals. Mining sector is an important segment of the Indian economy. Since independence, there has been a pronounced growth in the mineral production both in terms of quantity and value. India produces as many as 95 minerals, which includes 4 fuel, 10 metallic, 23 non-metallic, 3 atomic and 55 minor minerals (including building and other materials).

The total value of mineral production (excluding atomic & fuel minerals) during 2017-18 has been estimated at Rs 1,13,541 crore, which shows an increase of about 13% over that of the previous year. During 2017-18, estimated value for metallic minerals is Rs 53,029 crore or 47.7% of the total value and non-metallic minerals including minor minerals is Rs 60,512 crore or 53.3% of the total value.

During 2017-18, mineral production was reported from 32 States/Union Territories (actual reporting of MCDR from 22 states and estimation of minor minerals for all 32 States/Union Territories) of which the bulk of value of mineral production (excluding fuel and atomic minerals) of about 93.65% was confined to 10 States.

Auction of concessions for major minerals (other than coal, petroleum and natural gas) was done for the first time in the history of mineral administration in the country. 33 blocks were successfully allocated. However, 60 auction attempts failed during this period. The consensus emerged that the Mineral Auction Rules need to be amended and have been done on 30/11/2017.

Making an economic mineral discovery is the goal of geologists and geo-scientist around the world, but these efforts can also be extremely difficult, costly, and time-consuming, and most companies engaged in exploration end up walking away empty-handed.

With auction and up front commitment, even at the best of times, mining can be expensive, risky, and tricky. That's why investors and miners will want you to source even more data to see a clearer picture of the deposit, and see how it could take shape as a mine.

Exploration data, codified resource reporting, metallurgical tests, environmental assessments, 3d models, and mine designs can increase confidence in the project with an in-depth Feasibility Study and help in appropriate decision.

---

* Presidential Address delivered on 29th September 2018 at the 112th Annual General Meeting at Biswa Bangla Convention Centre, Rajarhat, Kolkata, President, MGMI and Director (Technical), NMDC

The other area which has come to occupy the central stage is “Corporate Governance”. ‘Board should govern not manage’. ‘Board should show the right path, it is management which should actually work on the path’. ‘Board ought to be transparent and vigilant in protecting shareholders interest’. Board should be independent of management etc’. These are now the buzz words. Bankruptcy and collapse of big Corporates have taught the Corporate World a lesson and Corporate governance has been ushered in to boost credibility and step up the sagging morale of Directors. While the seminal ideas on Corporate Governance can be traced to Barle and Means study of modern corporations and its ownership and control in 1932 in the context of Corporate scandals in USA, it was in the 90s that Corporate governance emerged as a powerful idea for reforming listed companies and for expanding capital markets. This also coincided with the globalization of financial markets and reduced international barriers for industry and trade. The effort, in sum, appears to be towards more efficient regulation through amendments to listing agreements and company laws as well as updated standards of accounting, reporting and disclosures. Thus, corporate governance became an important agenda for the multilateral organizations such as World Bank, IMF, BIS, UN System, Comsec. and the OECD.

In India, Corporate body are either State owned or privately owned, of which some of them are listed in the Stock Exchanges and bulk of it still continue to be with State.

In Private Sectors, there are yet a number of corporate bodies which are closely held and the issues of corporate governance in these enterprises have been agitating the mind of the policy makers in private as well as government sectors as these Corporates have tremendous power and resource and its mal-governance will be disastrous for the society, nation and democratic world. Misdeeds of East India Company in India during 18th and first part of 19th century, bankruptcy of many Corporates viz. Enron, ASEAN Tiger are pointer.

Recognizing the importance of corporate governance, SEBI (Stock Exchange Board of India) had constituted a Committee to develop guidelines on Corporate Governance.

We at MGMI have been maintaining a very high standards of Corporate governance with an elected council which remains the mainstay of this professional body for more than 100 years.

Corporate bodies are the engines of growth of the society. The makes the Corporate Sector grow and the society at large moves on. In this context it is quite apt to quote Archimedis ‘Give me a Lever long enough and a fulcrum strong enough and single handed I can move the World’. Yes, Corporate Governance can be the fulcrum with Board as the ‘Lever long enough’, the whole Corporate world can move on, as never before.

It is therefore, necessary that MGMI may re-engineer itself from a knowledge sharing organization to take the leadership of the mineral industry and professionally elevate the industry into a high pedestal of Indian Economy that if rightfully deserves.

As awareness and resultant competition increases, only the fittest and the fastest amongst the provider organizations will survive. It is, therefore, be imperative for the MGMI to look beyond the present horizons and find out how the mineral industries are being developed to meet national objectives. More importantly why and how the developed countries, are ensuring competitiveness in productivity, price, quality and marketability of their mineral resources and products.

Having an age-old tradition is well but at the same time embracing new changes to remain relevant with a world-class quality of professionals is equally important. There is no reason why MGMI cannot become a pan India and globally accepted professional body. What is needed is positive mind sets and conviction in fighting the cause of mineral industry at all fronts.

Let us hope, we can make it.

Thank You

60th HOLLAND MEMORIAL LECTURE

Dr Kirit Shantilal Parikh*

Dr Kirit Shantilal Parikh is one of the most eminent experts on energy policy and economics in India and internationally. Currently, he is the Chairman of the Integrated Research and Action for Development (IRADe), an organization he founded with Dr Manmohan Singh, Dr RA Mashelkar, Mr Adi Godrej and other distinguished Indian leaders. He holds a Doctoral degree in Civil Engineering and a Masters degree in Economics from the Massachusetts Institute of Technology (MIT), USA. Dr Parikh was Member of the Planning Commission, Government of India and the Chairman of its Integrated Energy Policy Committee. He was a Member of the Economic Advisory Council (EAC) of the Prime Ministers of India, S/Shri Atal Behari Vajpayee, PV Narasimha Rao, Chandra Shekhar, VP Singh and Rajiv Gandhi. He also founded the Indira Gandhi Institute of Development Research as the Director. Other key positions on which he has served include :

- Member of the Board of Directors, State Bank of India, LIC, IDBI and IPCL
- Senior Economic Adviser to the Administrator, UNDP, New York
- Programme Leader of the Food and Agricultural Programme, and later Chairman of the Indian National Committee at the International Institute for Applied Systems Analysis (IIASA), Austria
- Director of Programme Analysis Group (PAG), Department of Atomic Energy, Government of India
- Professor and Head of the Department of Economics, Indian Statistical Institute
- Member of the National Committee for Environmental Planning and Coordination
- Member of the National Committee on Science and Technology
- Member of the Fuel Policy Committee

He has been awarded the Padma Bhushan, the third highest civilian honours conferred by the President of India. Dr. Parikh has been the President of the Indian Econometric Society and Gujarat Economic Association. He was felicitated as one of the engineering personalities by Indian Engineering Congress, December 2006. He was honoured as the most distinguished and illustrious alumni of the decade from India by the Massachusetts Institute of Technology (MIT), USA in September, 2007. He was conferred the Distinguished Alumnus Award by Indian Institute of Technology (IIT), Kharagpur in September, 2007. Dr Parikh is also an elected Fellow of the National Academy of Sciences, India. Dr Parikh has authored and edited 29 books, including editorship of the India Development Report, which provides a non-governmental assessment of India's development and policy options. He has also been Review Editor to the most-recent 5th Assessment Report of the Intergovernmental Panel on Climate Change (IPCC).

FUTURE OF COAL IN POWER GENERATION*

Dr Kirit Shantilal Parikh

I am honoured to have been invited to give Holland Memorial Lecture and join the ranks of many illustrious persons who have given this lecture before.

Indians have an ambivalent attitude about the legacy of British rule in India. The railways and the steel frame helped unite India, though many feel that the steel frame is too rigid and has kept us backward. They created many research and development institutions, which helped India in its industrial and technical growth. Among these is the one created by Sir TH Holland, Mining, Geological and Metallurgical Institute of India (MGMI).

On the other hand, India was one of the richest countries of the world when Robert Clive landed in India and one of the poorest when India became independent. The worst part was that the British rule created among Indians a sense of diffidence.

However, there were many Britishers who nurtured a sense of inquiry and scientific attitude among Indians and we must be grateful Britishers like Sir TH Holland for their contribution to India's scientific development.

---

* Chairman, Integrated Research and Action for Development (IRADe)

* This is largely based on the final report of the study by IRADe for the Global Technology Watch Group set up by the Department of Science and Technology, Coal Road Map for India (2018)

COAL IN INDIA'S ECONOMY

Coal has been the major energy resource of India. India is short of oil and gas but coal reserves are relatively abundant. Coal has been the mainstay of our energy use. Table 1 shows the energy resources of India.

Table 1 : India's Hydrocarbon Reserves

Resources	Unit	Proved	Inferred	Indicated	Production in 2016-17	Net Imports in 2016-17	Reserve/ Production Ratio	
		(P)	(I)		(Q)	(M)	P/Q	(P+I) / Q
Coal (as on 31.03.2017)	Mtoe	58655	13440	57113				
Extractable Coal**	Mtoe	20882	6860-12685		271.7	77.6	77	102-123
Lignite (as on 31.3.2017)	Mtoe	1874	3478	7452				
Extractable Lignite	Mtoe	1874			13.0		145	
Oil (2005)	Mt	604.1			36.01	214	17	17
Gas (2005)	Mtoe	1161			29	17	40	40
Coal Bed Methane	Mtoe	96			0.52			

* Balance Recoverable Reserves

1 Indicated Gas resource includes 320 Mtoe claimed by Reliance Energy. In addition, GSPC has indicated about 360 Mtoe of reserves, which have not yet been certified by DGH.

2 From deep seated coal (not included in extractable coal reserves)

** Extractable coal from proved reserves has been calculated by considering 90% of geological reserve as mineable and dividing mineable reserve by Reserve to Production ratio (2.543 has been used in 'Coal Vision 2025' for CIL blocks); and range for extractable coal from prognosticated reserves has been arrived at by taking 70% of indicated and 40% of Inferred reserve as mineable and dividing mineable reserve by R:P ratios (2.543 for CIL blocks and 4.7 for non-CIL blocks as per 'Coal Vision 2025').

Sources :
http://petroleum.nic.in/sites/default/files/ipngs1718.pdf
Energy Statistics 2018 "Indian Petroleum & Natural Gas Statistics 2016-17"

Note :

Conversion factors : 1 Million Tonne of Coal
= 0.41 Mtoe
1 Million Tonne of Lignite
= 0.2865 Mtoe
1 Billion Cubic Meter of Gas
= 0.9 Mtoe
1 Million Tonnes of LNG
= 1.23 Mtoe

Extractable coal can last for 77 years at the rate of production of 2017-18. However, if the coal production keeps growing at 5% per year, then we can run out of coal including that from indicated and inferred reserves in less than 40 years.

Coal use in different sectors is given in Table 2.

Table 2 : Industry wise Consumption of Thermal / Non Coking Coal in India 2016-17 (Million Tonnes)

Industries	In Million Tonnes	Percentage Share
Power	527.26	67%
Industry	16.96	2%
Others	246.83	31%
Total	791.05	100%

Source : http://mospi.nic.in/sites/default/files/publication_reports/Energy_Statistics_2018.pdf

We see that power sector is the major user of coal consuming 67% of thermal coal used in the country. I will therefore look at the power sector.

Projection of requirement of coal in the power sector without any consideration of environmental concerns give us an upper bound of how much coal power sector would need in the future. Table 3 shows projection we have made with a multi-sectoral inter-temporal activity analysis optimizing model. In this coal efficiency improvement has been assumed at 1% per year. Also all new coal plants are to be super critical.

Table 3 : Coal Requirement for Power Sector (MT)

Year	Capacity (GW)	Generation (Billion Kwh)	Coal Requirement (MT)
2015	143	999	680
2020	216	1511	1022
2030	440	3081	2071
2040	836	5862	3930
2050	1398	9799	6557

The projected requirement is huge and would involve substantial import of coal. Can we absorb this level of coal use?

Coal faces severe challenges from environmental considerations. Local air pollution due to emissions of particulates and SOx, emissions of CO_2, displacement of people and land degradation due to mining are growing concerns. What role can clean coal technologies play here?

Major use of coal in India is for power plants. What are the implications for coal of dramatic reduction in cost of solar power and battery technology that is expected by many? Would it make coal power generation economically less attractive?

Role of Clean Coal Technologies in Controlling Local Air Pollution

The government already requires that coal plants have modern electro-static precipitators. One needs to make sure that these trap particulates of 2.5 micron size. This should involve some retrofitting of old plants and additional investment in new plants.

Controlling SOx NOx emissions requires FGD, flue gas desulfurization. Also selective catalytic reduction (SCR) can clean up the plant further. This is somewhat more expensive. Yet, coal power may still remain competitive with other alternatives. We have explored the role that FGD can play in a multi-sectoral inter-temporal optimizing model that considers various alternative power technologies and optimizes power production with a 40 year horizon. It considers the investment required as well as the operating costs of different types of plants. Table 4 shows the characteristics of different plants considered.

Table 4 : Characteristics of Different Coal Based Power Plants

Technology	Sub critical PC Boiler with ESP	Super-critical PC Boiler with ESP	Ultra-Super Critical PC Boiler with ESP	Sub-critical PC Boiler with ESP, FGD, SCR	Super-critica PC Boiler with ESP, FGD, SCR	Ultra Super-critical PC Boiler with ESP, FGD, SCR
Net Plant efficiency (%)	34.38%	35.92%	37.19%	33.18%	34.73%	35.96%
Auxiliary power (%)	7.27%	7.18%	9.92%	10.50%	10.27%	12.88%
S.F.C. (Kg/kWh) coal	0.89	0.85	0.83	0.93	0.88	0.85
Capital Cost# INR Cr/MW	5.90	6.30	7.01	9.28	9.69	9.96
O&M# INR Lakh/MW	97	96	104	121	122	125
LCOE (INR/kWh)	2.35	2.4	2.62	3.23	3.28	3.38
CO_2 emission (kg/Wh)	1015	971	938	1059	1010	977
SO_2 emission (kg/MWh)	10.1	9.6	9.3	0.3	0.3	0.3
NOx emission (kg/MWh)	4.5	4.2	4.1	0.5	0.5	0.5
Particulate emission (kg/MWh)	1	1	0.9	0.1	0.1	0.1

Source : GTWG Report (2018)

Cost in 2016 prices Source : IRADe Analysis, and Chapter 5 prepared by IIT-B and IIT-M

It is seen that plants with ESP, FGD and SCR have higher initial capital cost over plants with only ESP. The costs are 57%, 54% and 42% higher for sub-critical, super-critical and ultra-super-critical plants respectively. However, the CO_2 emissions are higher per kWh. The emissions of particulates, SOx and NOx are 85 to 95% lower.

What is of interest is to see what it would cost in terms of foregone growth in GDP or consumer income. Also what is the economically justifiable level of use of these technologies?

We generate two scenarios, one with all plants have ESP and another in which all plants have ESP, FGD and SCR. We call the scenarios as follows :

- **DAUPM :** Dynamics as usual with ESP that controls Particulate Matter emissions. Economical choice of technology no restrictions except as per government policy no new subcritical plants.
- **PMSOxNOx :** Only new plants with all pollution control technologies (ESP, FGD+SCR) are permitted The results are summarized for 2030 and 2050 in table 5.

The results are summarized for 2030 and 2050 in table 5.

Table 5 : Generation in bkWh by Different Technologies

Scenario Technologies	DAUPM		PMSOxNOx	
Coal	2030	2050	2030	2050
Sub Critical	700	453	703	694
Super Critical	2363	9337	48	58
Sub Critical FGD	3	1	356	196
Super Critical FGD	3	1	1972	8865
Total Coal	**3081**	**9799**	**3079**	**9813**
Gas	47	5	54	10
Diesel	0	0	0	0
Nuclear	15	7	15	7
Hydro	54	19	54	19
Renewable	27	14	27	14
Total Generation	**3224**	**9844**	**3229**	**9863**
Share of Coal Generation (Per Cent)	**96**	**100**	**95**	**99**

Source : Chapter 6, GTWG report

What is interesting to see is that the share of generation from coal based plants exceeds 95% in both the scenarios. The emissions under the two scenarios are summarized in table 6 :

Table 6 : Emissions under the Two Scenarios

Scenario	DAUPM		PMSOxNOx			
Year	**SOx**	**NOx**	**CO_2**	**SOx**	**NOx**	**CO_2**
2010	7	3	673	7	3	673
2020	15	6	1493	8	4	1547
2030	30	13	3017	8	4	3135
2040	57	25	5716	9	6	5940
2050	**94**	**41**	**9530**	**10**	**8**	**9932**
2010-50 (MT)	1534	672	155042	346	197	161034
2010-50 from the whole economy (GT CO_2)			298			303

The reductions in SOx and NOx emissions in PMSOxNOx scenario are substantial but seem much less than what one would have expected from the emission coefficients in table 4. This is because the existing sub-critical coal plants in 2017, after which no sub-critical plants are built, continue to operate for many years and have not been retrofitted with SOx NOx control devices. In fact from the cumulated emissions over 2010-50 of these sub-critical plants are 289 MT of SOx out of total 346 MT and 129 MT of NOx out of total 197 Mt.

With the PMSOxNOx scenario the emissions of SOx and NOx come down substantially. This suggests that if we want to control local air pollution, end of the pipe measures should be adequate. The question is how much do they cost?

We measure this in terms of the impact on Gross Domestic Product and on private consumption, which is an important element of consumer welfare. Table 7 shows these.

Table 7 : Macro Impact of SOx and NOx Control

Year	GDP Trillion 2007-08 Rs		Per capita consumption '000 2007-08 Rs/year	
	DAUPM	PMSOxNOx	DAUPM	PMSOxNOx
2010	53	53	21	21
2020	110	110	30	29
2030	242	240	69	68
2040	546	542	164	162
2050	1078	1068	399	394
CAGR 2010-30	7.91	7.88	6.17	6.09
CAGR 2010-50	7.83	7.81	7.67	7.63

Table 7 shows that there is very little difference in the growth rates of GDP and per capita consumption. Thus SOx, NOx and particulate emissions control does not involve any significant cost to the economy.

However, if you look at CO_2 emissions in table 6, there is no reduction in it, if anything there is a small increase. For this we need to explore carbon capture and storage (CCS).

ROLE OF CCS IN CONTROLLING CO_2 EMISSIONS

We consider two alternative technologies of CCS.

- Supercritical Pulverized Coal (PC) boiler with MEA-based CCS
- Supercritical PC boiler with oxy-fuel combustion (OFC)-based CCS

"Post-combustion technology means that the CO_2 is captured after the combustion of the coal (or other fossil fuel) has taken place. This can be done using various processes such as adsorption, absorption and membrane separation. Generally, in absorption, CO_2 is absorbed over a solvent such as Mono-ethanolamine (MEA) (Johnsson, 2011) and is then exposed to higher temperatures where CO_2 is stripped off from the solvent. Other solvents such as ammonia may also be used for such a process.

Post-combustion processes are the most matured ones at this point of time. However, solvent regeneration is an energy-intensive process and leads to significant losses in the energy output of the plant. The energy penalty here is thus, mainly due to the solvent generation (Johnsson, 2011).

Oxy-fuel combustion systems use pure oxygen or a nitrogen-free gas mixture instead of air for the combustion of a hydrocarbon fuel to produce a flue gas that consists primarily of water vapor and CO_2. This produces a flue gas stream with CO_2 concentrations greater than 80% by volume. The water vapor is then removed by cooling and compressing the flue gas stream. Oxy-fuel combustion requires an upstream air separation unit (ASU) to produce oxygen stream with a purity of 95-99%. Further treatment of the flue gas may be needed to remove air pollutants and non-condensed gases (such as argon and nitrogen) from the flue gas before the CO_2 is sent to storage." (Sreenivas Jayanti et al, 2018)

Table 8 gives the technological and cost details of the two technologies.

Table 8 : CCS technologies Costs and Emissions

Technology	Supercritical PC with MEA based CCS	Supercritical PC with CCS + OFC
Net Plant efficiency (%)	29.05%	26.44%
Auxiliary power (%)	24.93%	31.69%
S.F.C. (Kg/kWh) coal GCV 2800 Kcal/kg	1.06	1.16
Capital Cost# INR Cr/M	19	23
O&M# INR Lakh/MW	246	221
LCOE (INR/kWh)	6.61	6.76
CO2 emission (kg/MWh)	121	132
SO2 emission (kg/MWh)	0	0
NOx emission (kg/MWh)	0.6	0.7
Particulate emission (kg/MWh)	0.1	0
Net Plant efficiency (%)	29.05%	26.44%
Auxiliary power (%)	24.93%	31.69%
S.F.C. (Kg/kWh) coal GCV 2800 Kcal/kg	1.06	1.16
Capital Cost# INR Cr/MW	19	23
O&M# INR Lakh/MW	246	221
LCOE (INR/kWh)	6.61	6.76
CO_2 emission (kg/MWh)	121	132
SO_2 emission (kg/MWh)	0	0
NOx emission (kg/MWh)	0.6	0.7
Particulate emission (kg/MWh)	0.1	0

We develop two scenarios, where the total CO_2 emissions over the period 2010 to 2050 that India can make are given by 133 GT and 156 GT. These limits are imposed in the scenarios. These are arrived at looking at the global carbon budget and allocating it to different countries giving each country the same per capita allocation based on their population in 1990 and 2010. The two scenarios with carbon budget (CB) are as follows :

- **CB156 :** a carbon budget of 156 GT from 2010-2050 imposed
- **CB133 :** a carbon budget of 133 GT from 2010-2050 imposed

Table 9 : shows power generation in the different scenarios

Scenario	DAUPM		CB156		CB133	
Technologies	**2030**	**2050**	**2030**	**2050**	**2030**	**2050**
Coal						
Sub Critical	700	453	446	54	96	12
Super Critical	2363	9337	34	4	5	1
Ultra Super Critica	3	4	2	0	0	0
Sub Critical FGD	3	1	2	0	0	0
Super Critical FGD	3	1	2	0	0	0
Ultra Super Critical FGD	3	1	2	0	0	0
Super Critical PC with MEA CCS	3	1	469	6120	154	1005
Super Critical CCS OFC	3	1	3	1	1	1
Total Coal	**3081**	**9799**	**960**	**6179**	**256**	**1019**
Gas	5	5	47	10	22	3
Diesel	0	0	0	0	0	0
Nuclear	7	7	1806	1968	1968	1968
Hydro	19	19	292	600	376	600
Renewable	14	14	73	724	382	5129
Total Generatio	**3224**	**9844**	**3178**	**9481**	**3004**	**8719**
Share of coal (percent)	96	100	30	65	9	12

With a carbon budget of 156 GT, there is still 65% generation is from coal in 2050. It may also be noted that MEA CCS is selected and not CCSOFC. However, with a tighter budget of 133 GT, coal power generation is only 12%. It shows it is cheaper to go for nuclear, hydroelectricity and renewables.

The macro-economic impact carbon constraint on GDP and per capita consumption is shown in table 10. The impact is not very large on GDP but some what larger on private per capita consumption, which is 4% lower in CB156 and 11% lower in CB133 in 2050. The cumulative loss will be substantial as can be seen in table 11.

Table 10 : Macro Impact of Carbon Constraint

Scenario	GDP Trillion 2007-08 Rs/year			Per capita consumption Thousand 2007-08 Rs/year		
Year	**DAUPM**	**CB156**	**CB133**	**DAUPM**	**CB156**	**CB133**
2010	53	53	53	21	21	21
2020	110	111	110	30	28	27
2030	242	239	233	69	66	62
2040	546	534	524	164	158	149
2050	1078	1058	1015	399	384	359
CAGR 2010-30 (%)	7.91	7.85	7.72	6.17	5.96	5.66
CAGR 2010-50 (%)	7.83	7.78	7.67	7.67	7.57	7.38

Table 11 : Reduction in cumulated GDP and Consumption (Trillion 2007-08 Rs) Compared to DAUPM (DAUPM value - Scenario Value)

Year	GDP		Consumption	
	CB156	CB133	CB156	CB133
2010-20	-3	3	6	15
2010-30	10	50	33	80
2010-40	80	195	101	246
2010-50	212	554	277	684

IMPACT OF STEEPER DECLINE IN RENEWABLE COSTS

The significant increase in renewable generation with the tighter carbon budget of 133 GT has assumed fall in renewable technologies costs is modest. There are many however, who expect a much steeper decline in renewable costs and rapid increase in their efficiency.

REFERENCES

- Sreenivas Jayanti, Anand B Rao, DK Sharma, Sreedevi Upadhyayula, Preeti Aghalayam, Munish Chandel, (2018), "Technologies for Coal-based Power Generation" in Global Technology Watch Group, Coal Road Map for India, final report
- Johnsson F, (2011), Perspectives on CO_2 capture and storage, Greenhouse Gases : Science and Technology, vol. 1, pp. 119-133, 2011
- GTWG (global Technology Watch group), (2018), Coal Road Map for India
- Probal Ghosh, Kirit Parikh, Vinay Kumar Saini, Jyoti Parikh, (2018), "Model-based Assessment of Technology Options : Sustainability Analysis" in GTWG final report

TECHNICAL ARTICLES

RELIABILITY AND AVAILABILITY ANALYSIS OF A CONTINUOUS MINER MACHINE IN AN INDIAN UNDERGROUND COAL MINE

Sumit Banerjee[1], Prof NC Dey[2]

ABSTRACT

Continuous Miner (CM) is a globally renowned machine for effective extraction of underground coal seams. Here an analysis of reliability and availability of a CM machine has been carried out. For the ease of analysis the overall CM based system was divided into several subsystems. From the analysis it was found that the electrical and traction system associated with CM based working are contributing to slightly higher trend of unavailability. Possible reasons behind this unavailability are discussed with experienced mine personnel and primarily improper maintenance of the equipment is found to be the cause of this. Here few possible recommendations to overcome this situation is discussed, where mainly the design of proper preventive maintenance programme and adopting Mean Time Between Failures concept for spare replacement is important.

Key words : Continuous Miner, Availability, Reliability, Preventive maintenance

INTRODUCTION

Mining in India is still one of the leading industries as coal is the major source of power throughout the globe. India ranked third in annual coal production globally, just after China and USA, with an annual coal production of 639.23 Mt in 2015-2016[1]. However, India needs implementation of new cutting edge technologies to boost the overall production to meet the indigenous demand of coal. The government has taken initiative to convert the semi mechanized mines to mechanized mines by implementation of Long wall and Continuous Miner (CM) technology. CM has already proven its high productivity while working with other major coal producers throughout the world. In India analysis of geo-mining and other conditions is a prerequisite for implementation of CM technology, which necessitates extensive research.

Implementation of CM technology requires sufficient reserve, proper gradient and other suitable geo-mining conditions; to favour the high productivity trend. Few of the panels are already identified and implemented with CM technology; in few of those panels the performance is not meeting the expectations of the equipment manufacturer. There are specific reasons behind this hindrance in overall productivity; improper selection of equipment fleet and implementation under incompatible geo-mining condition are the main reasons.

Basically CM technology is the integration of few machines together to produce coal at higher rate successfully. The CM demands few specified range of geo-mining conditions; such as; the gallery width should be 6 m, which violates the rules of CMR 2017, approval from the specified authority is the pre-requisite for the purpose. The gradient should not be very steep for CM based system to work.

The OMS of underground mines in India is considerably low as compared to the globally renowned mining countries who are working with CM system for years.

2. DETAILS OF CM BASED SYSTEM

CM works with specifically designed coal cutting machine with other compatible fleet of machines such as coal haulers, feeder breakers and conveyor assembly.

Here for the purpose of study the overall CM based system is divided into few of the following subsystems. The subsystems are as follows:

2.1. Electrical : All the electrical components cables, power packs etc, failure of which directly affects the performance of CM based system operation.

2.2. Cutter : This is the cutting arrangement fixed in the front edge of the machine. This is dedicated for the cutting of coal. It consists of a drum which carries numbers of Tungsten carbide picks to shear the coal face.

2.3. Gathering arm : This is the arrangement provided at the bottom of CM machine to gather the produced coal and guide it to the shuttle car through the integrated chain conveyor fitted to the CM machine.

*Research Scholar [1], **Professor[2], Department of Mining Engineering, Indian Institute of Engineering Science and Technology, Shibpur

2.4. Traction : This includes the components which help in movement and tramming of the machine.

2.5. Hydraulic : This includes all hydraulic ram-cylinder arrangements, hoses etc. The lifting arrangements of different parts of the CM have important hydraulic components.

2.6. Coal haulers : These are basically low height underground truck dedicated for coal hauling from the CM to the feeder breaker.

2.7. Feeder Breaker : It is the coal crushing unit comes along with CM package and is dedicated to crush oversized coals.

2.8. CM Conveyor : It is the integral part of CM dedicated to guide the produced coal to the shuttle car.

2.9. Mine Conveyor : It conveys the coal from feeder breaker to surface.

3. DESCRIPTION OF THE MINE SITE

This coal mine belongs to one of the major coal producing company in India. There are total four seams among which three are workable seams, within which one is thick seam, and working with blasting gallery method, which is rare in current mining scenario in India. For other two seams, one is working with continuous miner and the other one with conventional room and pillar method. The continuous miner working in this project was also engaged in depillaring operation during the tenure of visit.

The geo-mining condition of this project is as follows :

The thickness of seam of the CM panel is 5.92m and gradient is 1 in 17 these are favourable for implementation of CM, depth of cover is 194 m and pillar size is 32m × 32 m.

4. METHODOLOGY

The study was conducted for 120 shifts of working in above mentioned CM based underground mine site. The availability analysis of the subsystems along with recommendations for improvement for the subsystems with lower availability was done through this paper.

The downtime and working time data are the prerequisite for this purpose; which are collected directly from field observations. These data are useful to calculate Mean Time Between Failure (MTBF), Mean Time To Repair (MTTR) and availability[2.],[3],[4].

$$\text{MTRF} = \frac{\text{Total actual woking time}}{\text{Total numbers of failures}}$$

$$\text{MTTR} = \frac{\text{Total time to repair}}{\text{Total numbers of repairs}}$$

$$\text{Availability} = \frac{\text{MTBF}}{\text{MTBF+MTTR}}$$

The TBF data is the key to evaluate the availability and reliability of equipment. Trend test and serial correlation test are the prerequisites for the implementation of proper statistical distribution. Data sets free from any trend and serial correlation are suitable for implementation of conventional statistical distributions. Here the serial correlation test an trend tests performed for all subsystems and all are found suitable to workout with conventional statistical distributions. Trend test is the line plot between the Cumulative Failure Number and Cumulative Time Between Failure and serial correlation test is the scatter plot between the ith Time Between Failure and (i-1)th Time Between Failure[4].

Here the serial correlation test plot for electrical system and traction is shown in figure. 1 and figure. 2,

The serial correlation plot of electrical system and traction are depicted here :

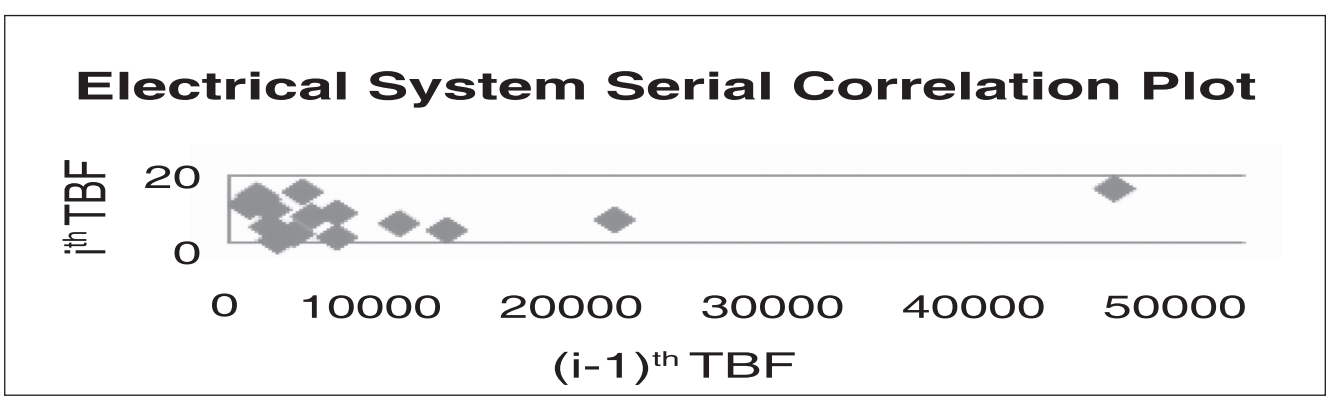

Fig. 1 : Serial correlation plot of electrical system

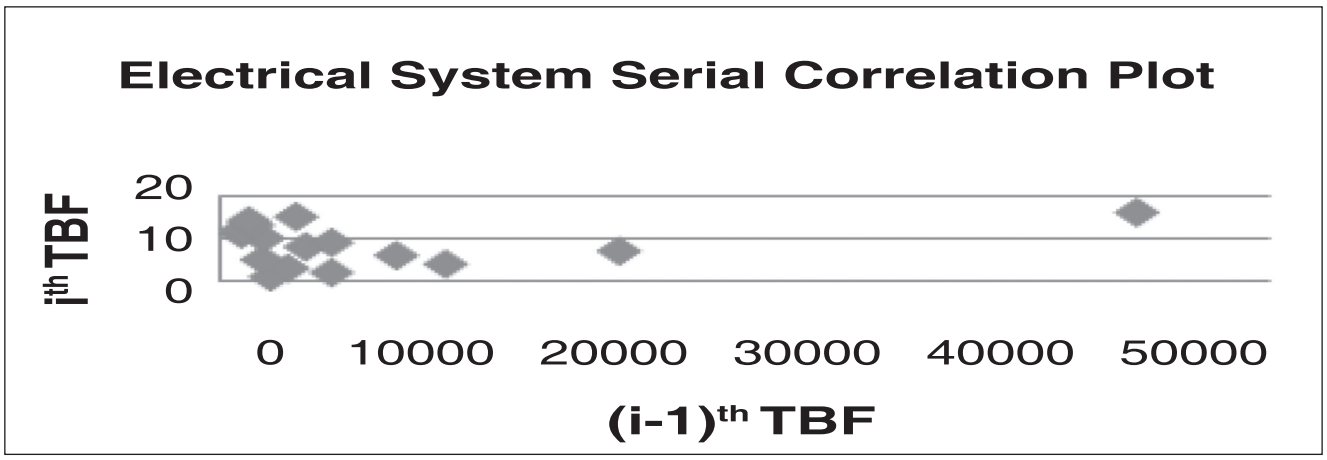

Fig. 2. Serial correlation plot of traction

From serial correlation test and trend test of data sets it is found that the data sets are free from any trend and serial correlation and hence suitable with conventional statistical distributions.

5. ANALYSIS AND OBSERVATION

The reliability plots for different subsystems are depicted hereunder :

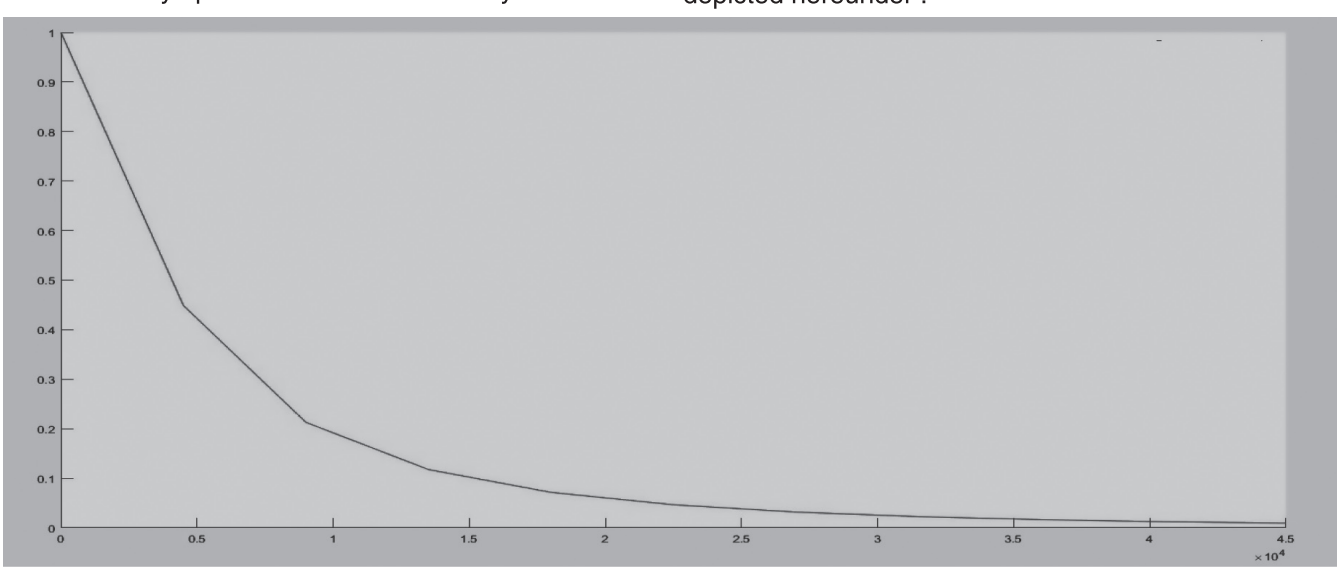

(a)

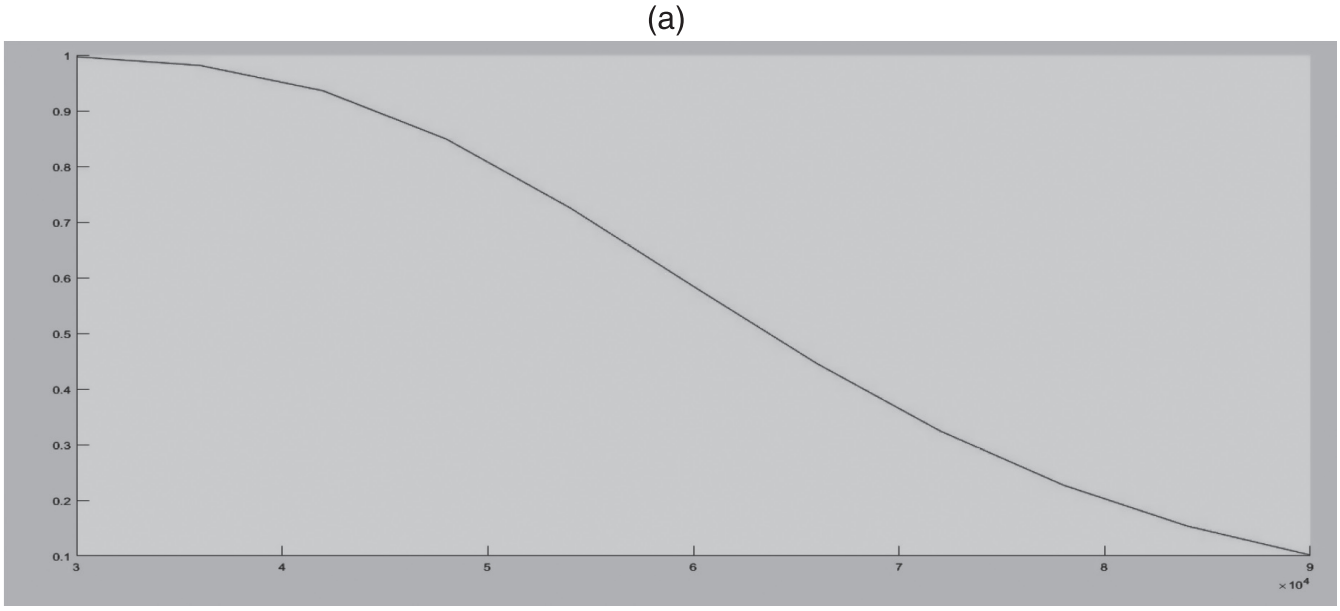

(b)

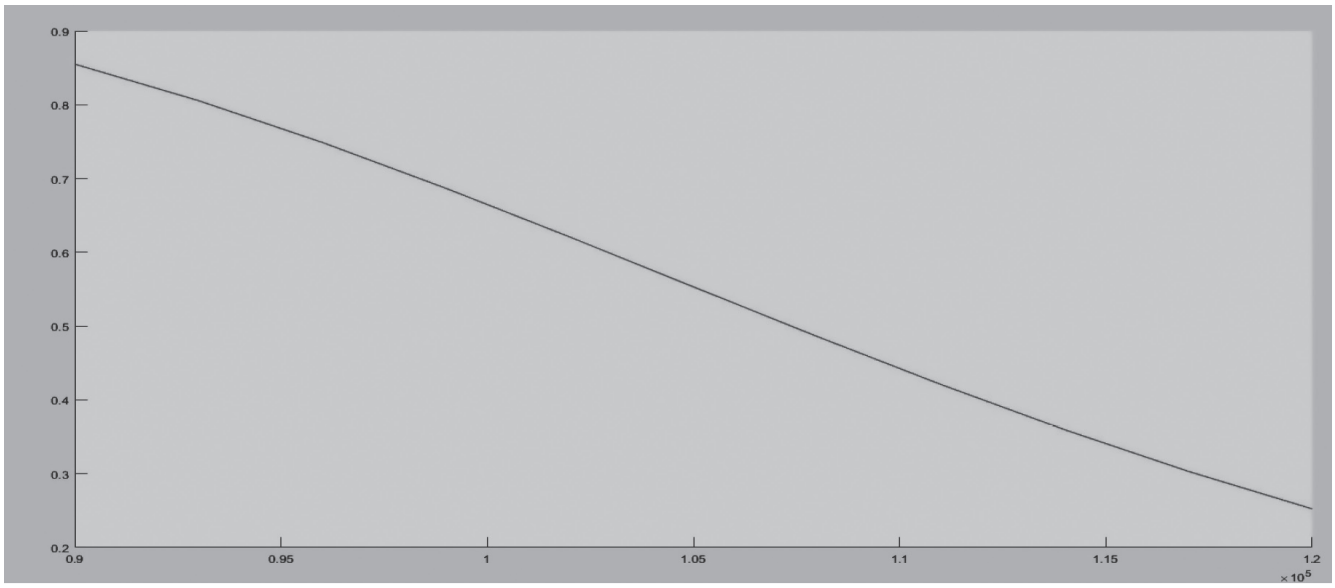
0.9
0.8
0.7
0.6
0.5
0.4
0.3
0.2
0.9
0.95
1
1.05
1.1
1.15
1.2
×10^5

(c)

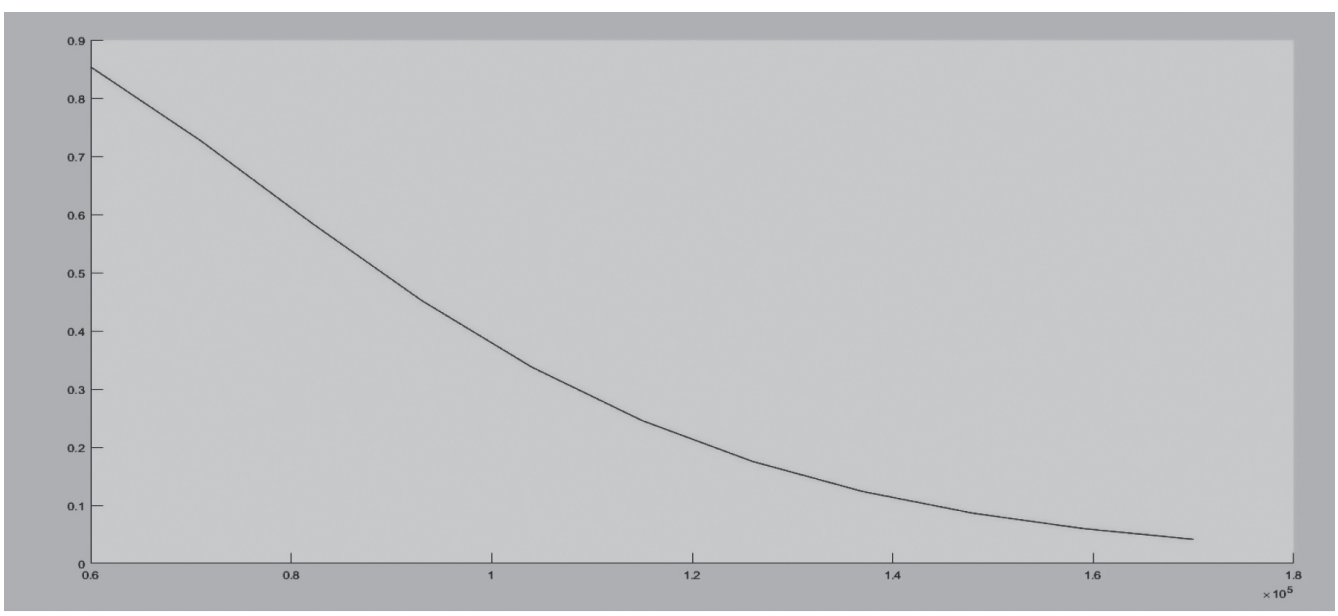
0.9
0.8
0.7
0.6
0.5
0.4
0.3
0.2
0.1
0
0.6
0.8
1
1.2
1.4
1.6
1.8
×10^5

(d)

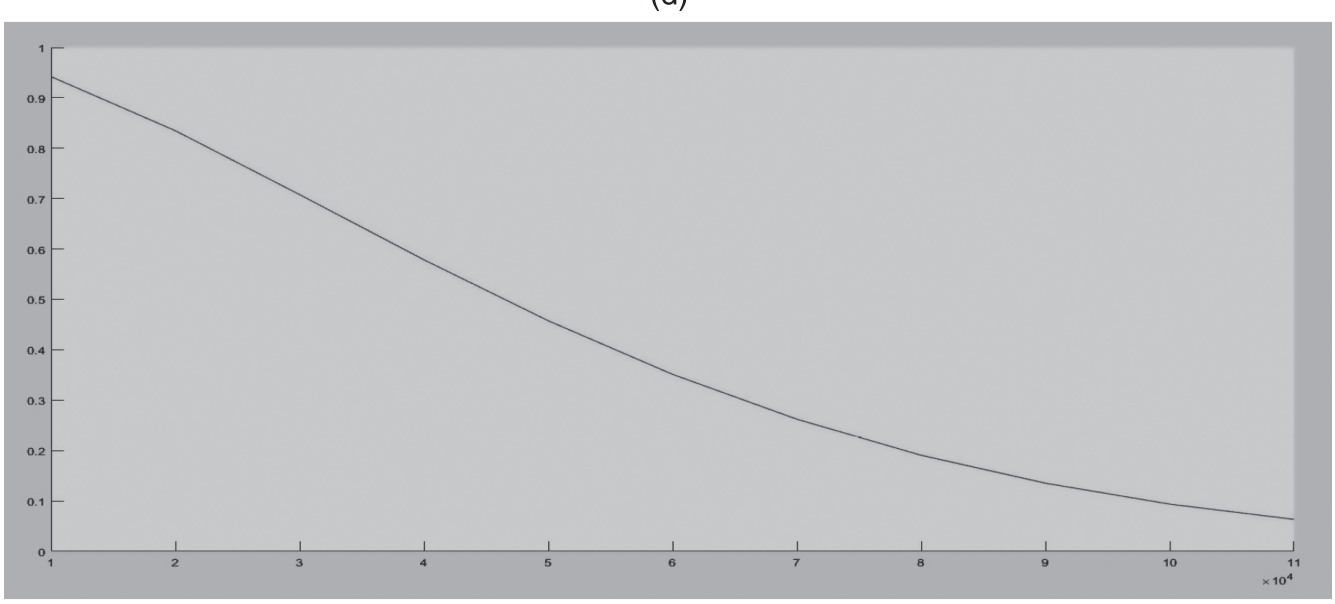
1
0.9
0.8
0.7
0.6
0.5
0.4
0.3
0.2
0.1
0
1
2
3
4
5
6
7
8
9
10
11
×10^4

(e)

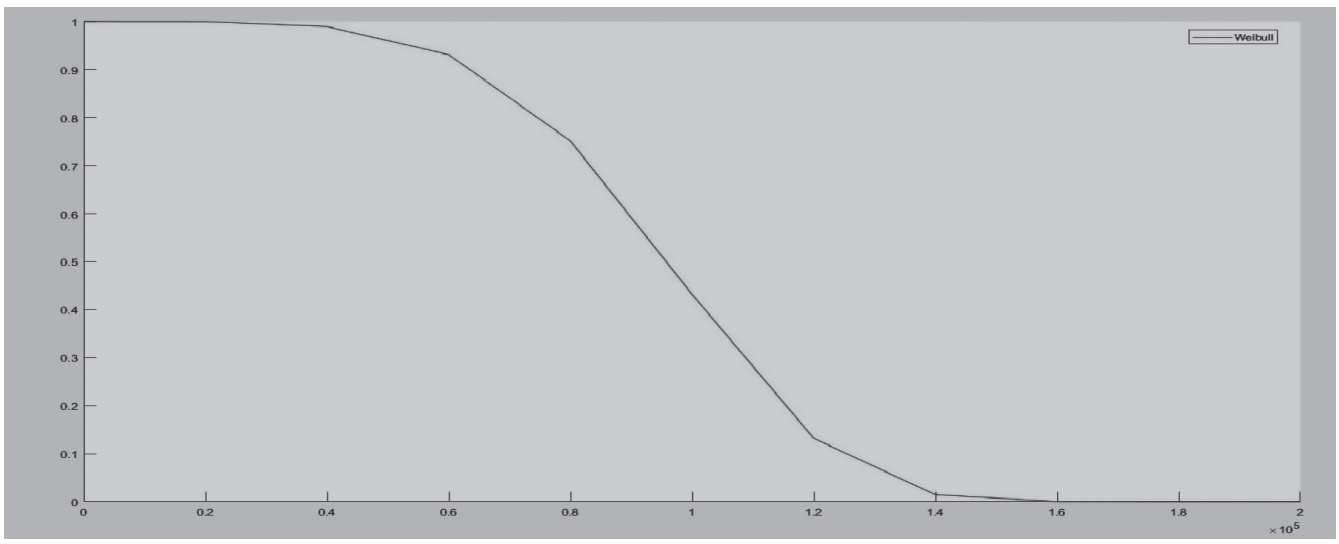

(f)

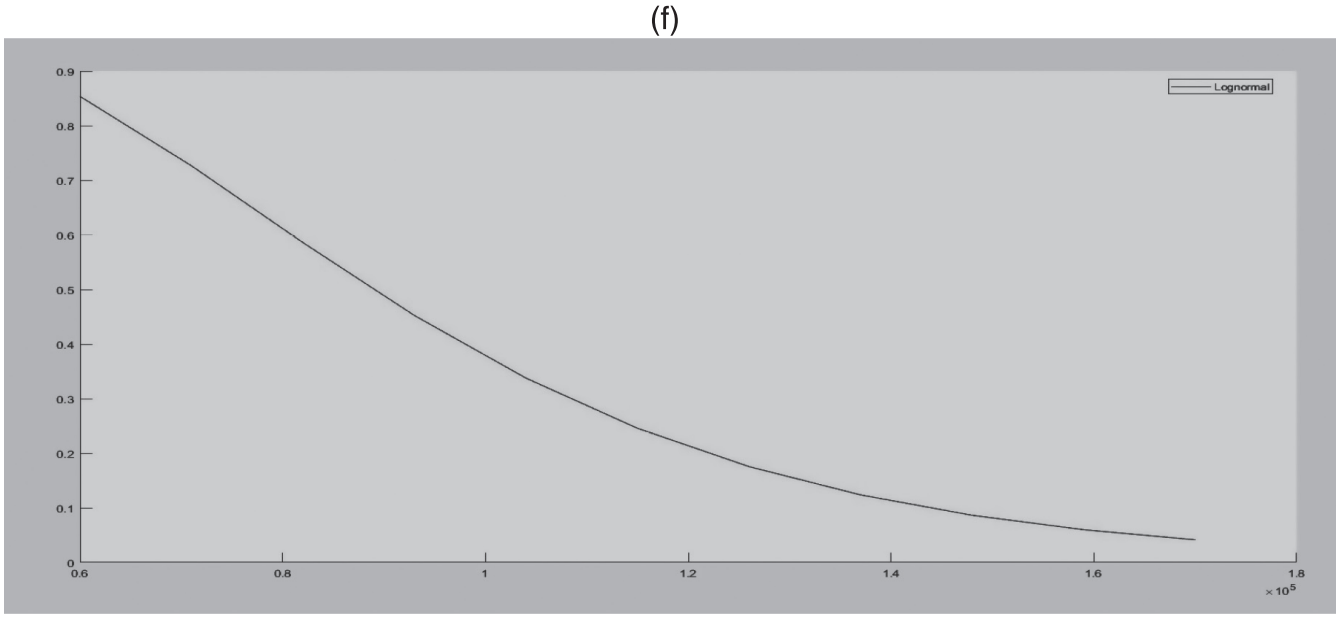

(g)

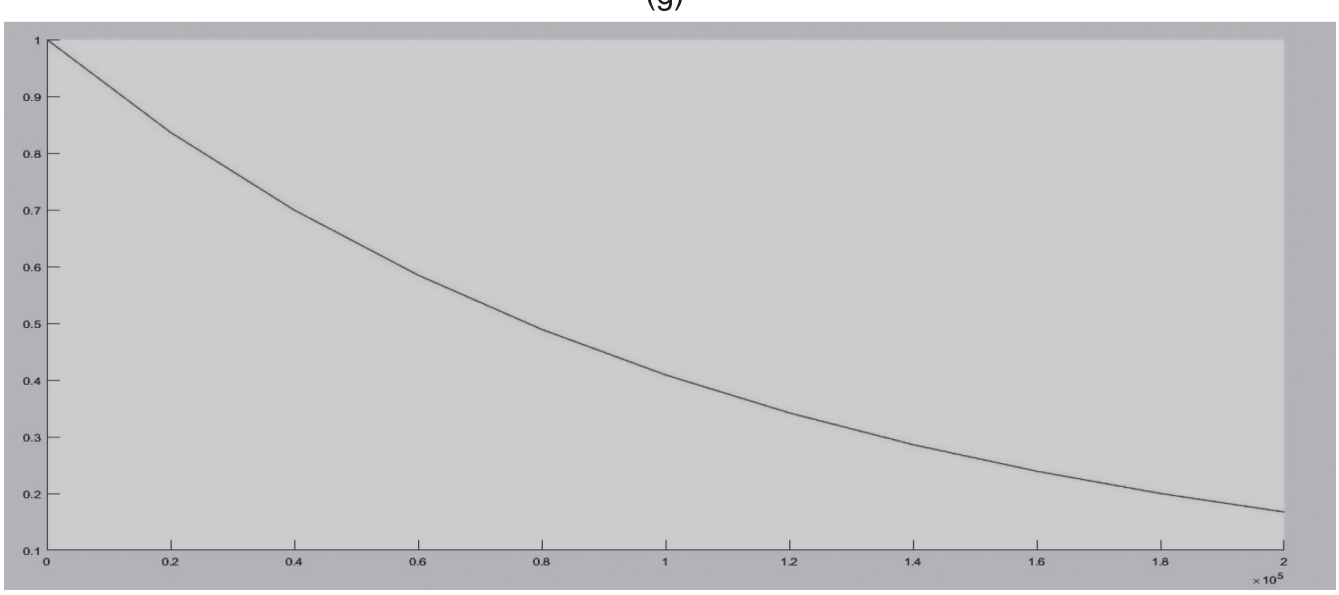

(h)

Fig. 3. Reliability plot of (a) Electrical, (b) Hydraulic, (c) Conveyor, (d) CM Conveyor (e) Traction (f) Shuttle Car (g) Feeder Breaker (h) Gathering

From the reliability plot generated through MATLAB 2013a it can be seen that the reliability of electrical system reaches to fifty percent after 50000 minutes of operation as depicted in figure 3. (a), figure 3(b) depicts the reliability trend of hydraulic system which reaches fifty percent reliability after 63000 minutes of operation. Conveyor and CM conveyor reaches half of the reliability after 100000 minutes and 90000 minutes of operation respectively and depicted on figure 3(c) and 3(d). Traction reaches to fifty percent reliability after 40000 minutes and shuttle car reaches fifty percent reliability after 100000 minutes of operation which is depicted through figure 3(e) and 3(f). Feeder breaker reaches half of its reliability after 90000 minutes of operation and depicted through figure 3.(g). Whereas, gathering system of CM reaches fifty percent reliability after 70000 minutes of operation and depicted through fig. 3 (h). Therefore, traction, electrical systems and hydraulic systems are the three least reliable systems within the CM package.

The availability of all the subsystems are depicted through a bar chart depicted in fig. 4.

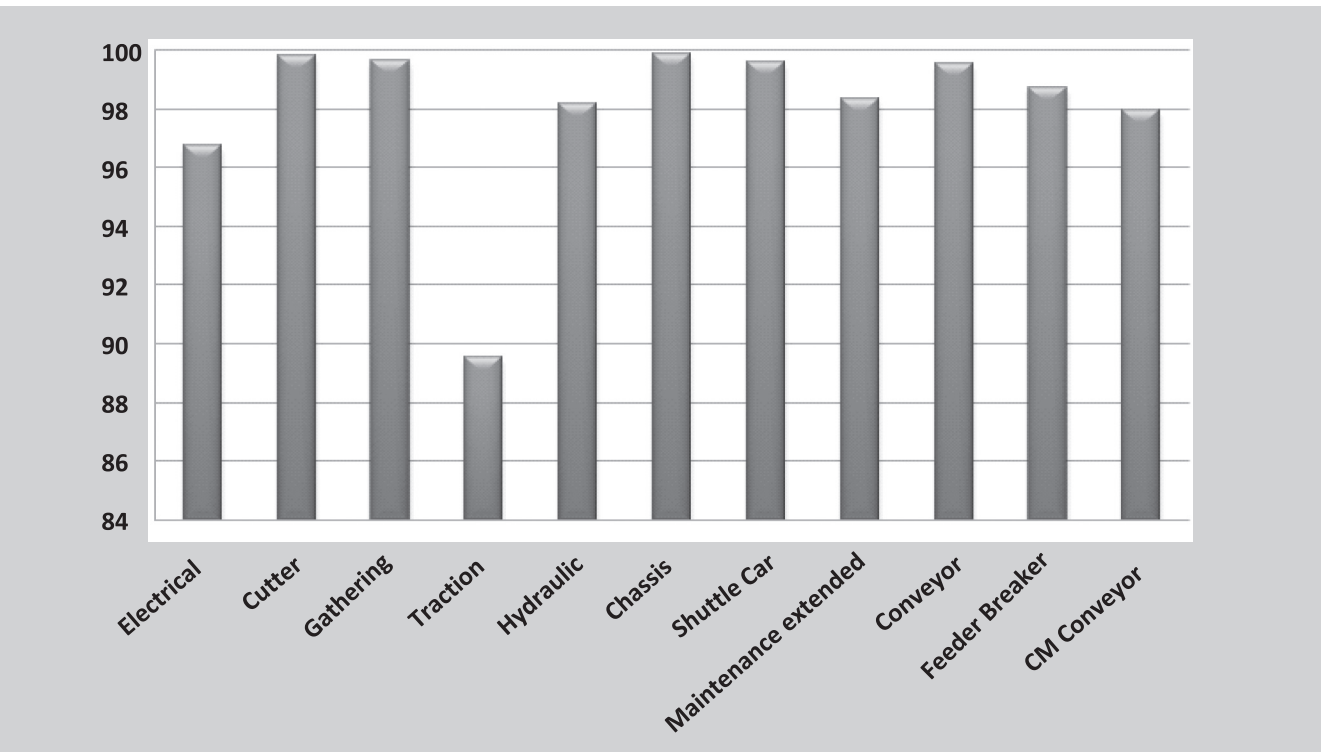

Fig. 4 : Availability percentage of different subsystems of the CM based production system

From Fig. 4. it can be concluded that the traction and electrical subsystems are the subsystems with lower availability trend.

The reasons behind this low availability trend was discussed with experienced personnel from the mine site. From a properly designed investigation it was found that the handling of cable needs to be more careful and maintenance of all electrical components including power-packs, cable and other components requires more care.

Traction failure in this site is due to the floor strata characteristics; proper measure should be taken to improve the floor strata characteristics and condition.

6. POSSIBLE REMEDIES TO THE CONDITION

- Proper pumping arrangement to remove excess water and control the slurry formation which helps in better manoeuvrability of the vehicles.
- Better cable handling to reduce cable faults.
- Proper maintenance of the traction arrangements.
- Replacement of spares before calculated MTBF
- Design of a proper preventive maintenance programme.

7. CONCLUSION

Here in this paper a detailed analysis of availability and reliability of a CM machine deployed in a project belonging to one of the leading coal producing company in India has been presented. From the analysis it was found that among all the subsystems traction and electrical are the one with moderately lower reliability trend. From analysis it was found that the maintenance programme followed in this mine site requires slight modification for betterment of overall equipment availability and utilisation.

Sturdiness of ay equipment is decided with the help of availability and reliability of that equipment. The reliability and availability depends majorly on maintenance practice. Here in this mine site the maintenance programme of electric subsystem and traction system of CM requires slight modification.

8. REFERENCES

1) Annual Coal Report 2016-17, Chapter - 6. [online] Available at: http://coal.nic.in/sites/upload_files/coal/files/coalupload/chap6AnnualReport1617en.pdf [Accessed 14 Jul. 2017].

2) Rahimdel, Mohammad Javad, et al. "The reliability and maintainability analysis of pneumatic system of rotary drilling machines." Journal of The Institution of Engineers (India): Series D 94.2 (2013) : 105-111.

3) Rohani, Hoda, and Azad Kamali Roosta. "Calculating Total System Availability." (2014).

4) Vagenas, Nick, Neil Runciman, and Serge R. Clément. "A methodology for maintenance analysis of mining equipment." International Journal o/Surface Mining, Reclamation and Environment 11.1 (1997) : 33-40.

GEOMORPHIC INDICATOR MODEL FOR IDENTIFYING MANGANESE MINERALIZATION

Shaurav Kumar[1*], Asim Chatterjee[2], Dr. Rajesh Mukherjee[3], Rajib Deb[4], Subhashbabu Ainampudi[5]

ABSTRACT

Economically important manganese and iron ore deposits were not formed evenly in Earth's history. The formation of sedimentary and residual deposits of manganese and iron, is determined by complex interactions in the ocean atmosphere-lithosphere-biosphere system. Most prominent is the example of banded iron and manganese formations formed in the late Archean and Early Proterozoic. Manganese ores in India are being exploited since the past hundred years. Continuous exploitation of shallower and larger deposits already taken place to a greater extent and search for deeper and more complex deposit has necessitated for unconventional methods of exploration like use of advance geophysics, remote sensing etc., helping in more focused approach in search for the mineral and in-turn save time and money potentially.

The objective of developing Geomorphic Indicator model for manganese mineralization was to establish the control of geomorphology, lithology, drainage, structure, slope in localization of manganese mineralization, which in turn help in identification of unknown potential manganese bearing zone.

Keywords : Manganese, Geomorphic Indicator Model, Satellite Imagery, Geomorphology

1. INTRODUCTION

Manganese deposits are of diverse genetic type occurs in terrestrial geological record (Roy, 1981). These were produced by direct hydrothermal activity, sedimentary processes may be interrelated, each involving distinct mechanism that place the deposit into specific genetic types. Some of these processes are best understood in preset-day depositional site (Supriya Roy, 2012). The formation of manganese deposit in Bonai-Keonjhar belt (study area is part of this belt) is considered to be of volcano-sedimentary in nature, where transgressive shale unit along with manganiferous shale is deposited in early stage of transgression or during low stand, overlain by ferruginous shale and finally iron formation deposited during maximum flooding (Beukes et. al., 2008). The depositional and localization of manganese mineralization, in the present context seems to be geomorphologically and structurally controlled. Therefore, study was intended to establish the correlation of various aspects like geomorphology/ landforms, drainage, lithology, structure (lineaments), slope, etc. if any, with known manganese occurrences and develop "Geomorphic Indicator Model", which may further lead to identification of undiscovered potential target zones for manganese mineralization.

2. DETAILS OF STUDY AREA

The study area covers iron and manganese leases of Tata Steel Limited (TSL) in and around Joda and Noamundi area, in the Indian states of Jharkhand and Odisha. The study area was delineated by taking a buffer zone of 10 km in all sides from the periphery of iron and manganese leases of TSL. The study area mostly comprises of structural hills with varying altitudes rising from 340 m to 1110 m above MSL. Majority of the study area (80%) falls within 1-15° slope category, showing overall gentle slope in the area. The study area is highly undulating and rugged with valleys and lowlands.

3. CONCEPTUALIZING GEOMORPHIC INDICATOR MODEL

An attempt has been made to develop a Geomorphic Indicator Model for identifying possibility of unknown manganese occurrences in and around Joda-Noamundi area. Geomorphology and other parameters viz., geology, structure, lineament density, drainage density and slope have been studied with reference to the known manganese occurrences within TSL leasehold and effort has been put to establish a relationship of these parameters with the known manganese occurrences and thus to develop an 'Indicator Model'.

1. Tata Steel Limited, Natural Resources Division, General Office, 3rd Floor, Jamshedpur-1, India.
2. RMSI, Hyderabad, India
* Corresponding author e-mail: shaurav.kumar@tatasteel.com

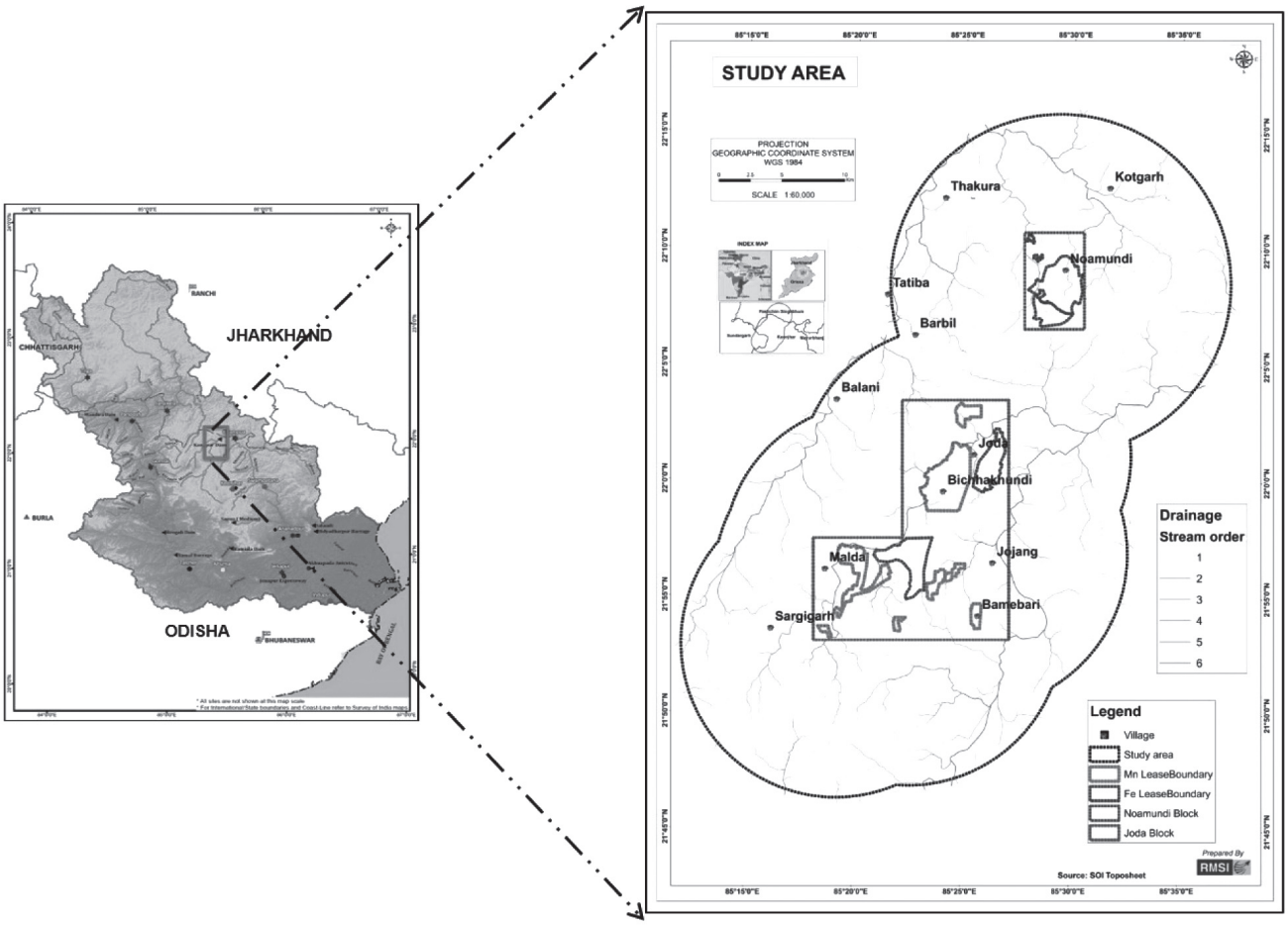

Figure 1: Location Map of the Study Area

Initial model (Figure 2) was a conceptual idea, which includes 4 sub models with a view to analyze each criterion i.e., geomorphology, geology, structure, drainage density, lineament density and slope for the known manganese occurrences in TSL lease areas. Sub model 1 shows the landform and quality of known manganese occurrences, Sub model 2 shows the slope of landform and structural conditions and Sub model 3 shows the specific lithology in which known manganese mineralization occurs. Combination of Model 1, 2 and 3 leads to generation of Sub model 4 having all the information related to geomorphology, geology, structure and slope for known manganese occurrences. Sub model 4along with drainage and geochemical data of known manganese occurrences lead to generation of a “Geomorphic Indicator Model”. Later-on, with improved understanding, this model was a bit modified and depicted in the form of a refined flowchart (Figure 3), covering all relevant aspects like geomorphology, geology, structure, drainage density, lineament density, slope and quality of the known manganese occurrences.

DATA USED:

Data pertaining to different thematic layers viz. geomorphology, geology, structure, drainage density, lineament density and slope of the study area were collected through various sources. Geomorphology map was prepared with the reference of SRTM DEM (30m) and GSI district resource map consisting of generalized geomorphology and were used as a base map which have been further updated using LISS IV (2014) satellite imagery and field observations. Structural features were also updated using LISS IV satellite imagery and with reference to the structures in the existing GSI geology map of the study area. These structures/lineaments were used to generate lineament density map of the study area. Slope and drainage density maps were prepared using SRTM DEM and SOI Toposheets (1:50,000) of the study area.

The favorable set up for manganese mineralization in terms of geology, geomorphology, slope, lineament and drainage density was analyzed and a probabilistic Indicator Model has been developed. Various data

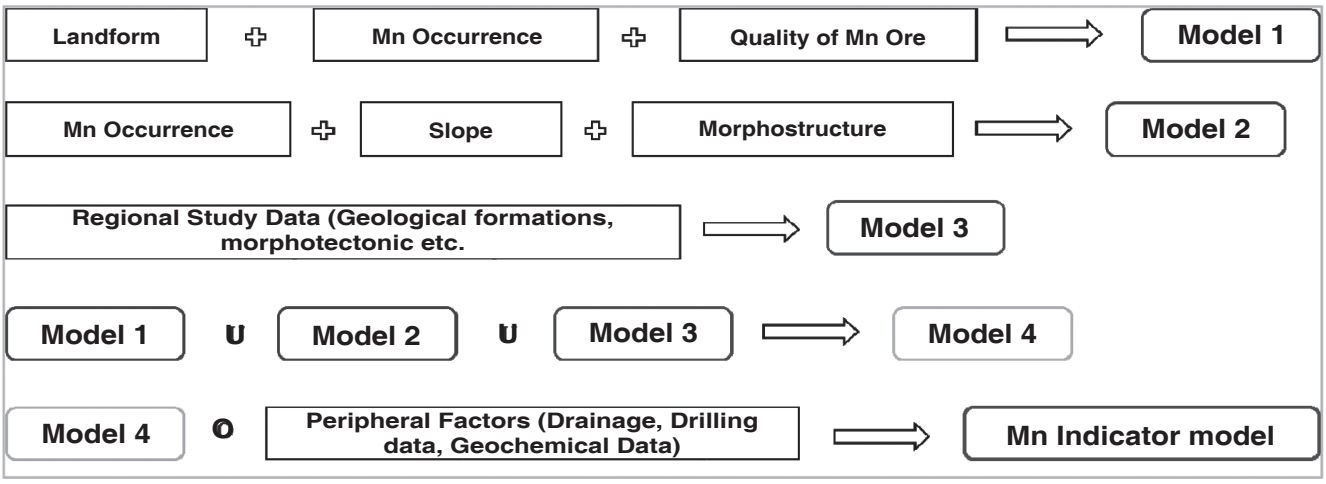

Figure 2 : Conceptual flow chart (Initial idea) for generating "Geomorphic Indicator Model"

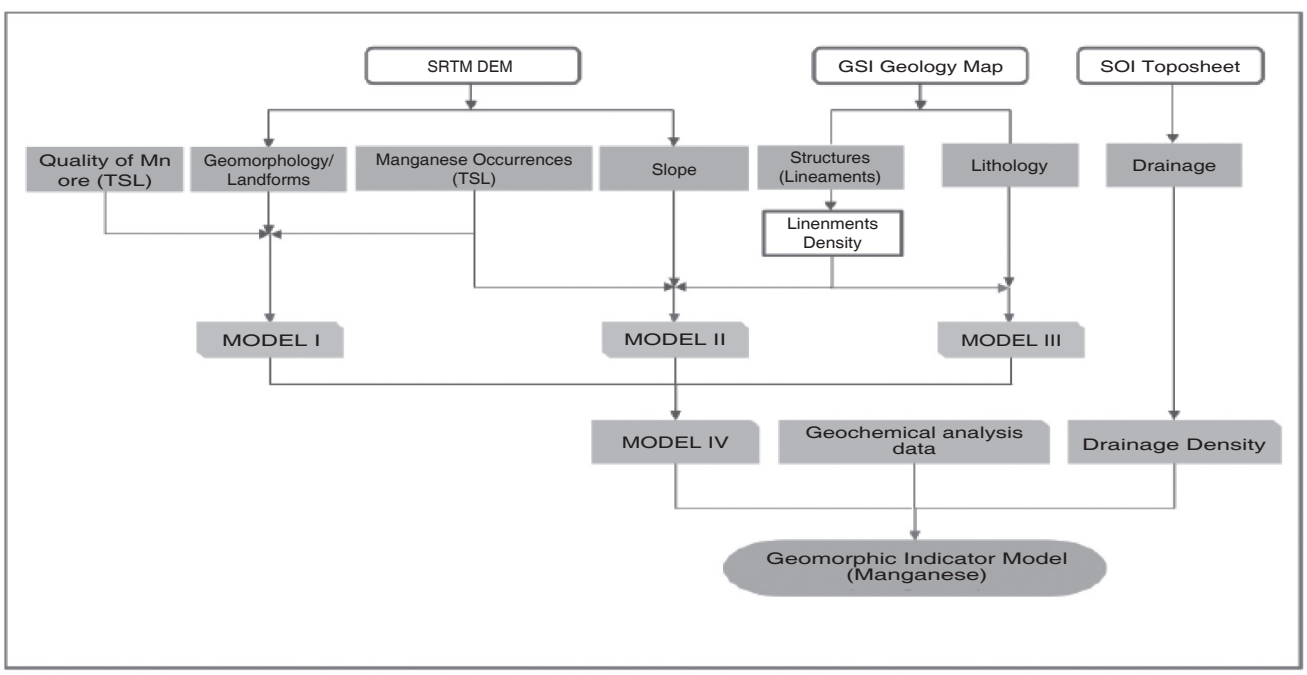

Figure 3 : Flowchart shows the enhanced methodology adopted for "Geomorphic Indicator Model"

related to known manganese occurrences from the leases of TSL were analyzed with respect to the "Geomorphic Indicator Model". Geological and geomorphological set up of known manganese occurrences along with the ranges of various other parameters like lineament density, drainage density and slope were also given due consideration.

FIELD VALIDATION:

Based on the correlation of different thematic layers viz. geomorphology, geology, structure, drainage density, lineament density and slope of the study area with the known/already reported locations of manganese mineralization, an indicator model was developed. This model was again run through in the entire study area to identify the unknown manganese bearing areas. Based on the same, 14 unknown manganese mineralization zones (Figure 4) were delineated as target areas for field validation. Field work of all the target areas were done in two phases. The main objective of the field observations and their analysis is to understand the relations of the model parameters and their correlative features at the locations of manganese occurring areas within the identified probable zones. During field validation, GPS locations along with the information on geomorphology, lithology, drainage, slope, structural data and surrounding drainage features were collected for further analysis, interpretation and refinement of the

manganese indicator model. Representative samples of manganese ore and other associated rocks were also collected from the surface outcrops and were analyzed. Out of fourteen (14) zones, nine (9) zones were proved to have indication of manganese mineralization while the other five (5) zones were categorizedunder least probable zones.

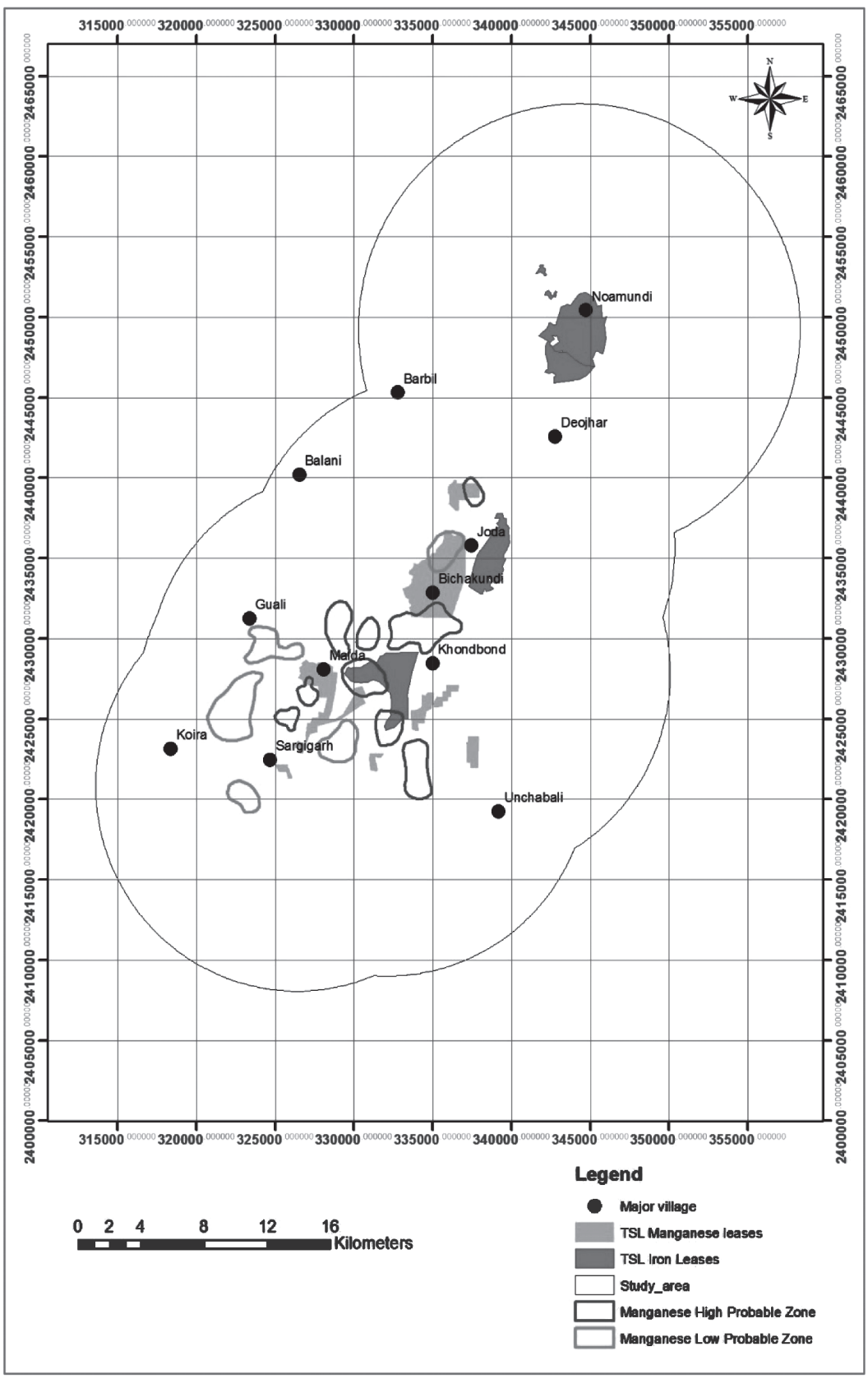

Figure 4 : Location of 14 identified manganese mineralization zone

The study and analysis of the known manganese location has helped in developing the initial model and based on which 14 probable manganese locations were identified and their field validation has helped in strengthening the model. Accordingly, the parameters for the Geomorphic Indicator model for manganese mineralization were established (Figure 5).

1. The geomorphological features, where manganese mineralization is occurring are pediments /buried pediments. The locations of buried pediments are in negligible count when compared to the pediment areas.
2. The pediment/buried pediment features will not alone indicate the probability of manganese occurrence. In addition to that, its geology also plays a major role in the localization of the manganese mineralization. In the present geological conditions, the lower shales / manganiferous shales are the source lithology for the manganese mineralization. This has been proved by the study of all the geological cross sections for known locations of manganese mineralization in TSL lease areas.
3. In addition to the lithology, the structural controls also play a major role in localization of the manganese mineralization (Acharya 2008). In the present study, the structural features which were taken to create lineament density are ranging 0.5-2.1 km/km². favors the probable locations of manganese mineralization.
4. In geomorphology, drainage patterns are governed by the topography of the land, whether a particular region is dominated by hard or soft rocks. With this as a reason the derived parameter of the drainage pattern, in the form of drainage density, was considered as a parameter. As per the study the drainage density favors localization of manganese ore where its ranges are between from 1.1 to 4.1 km/km².
5. Since the pediments and buried pediments are being formed at slope areas, slope is also proved as one of the relative parameter, which has a relation to localization of manganese mineralization. The slope ranges for manganese mineralization are varies from 5° to 15°

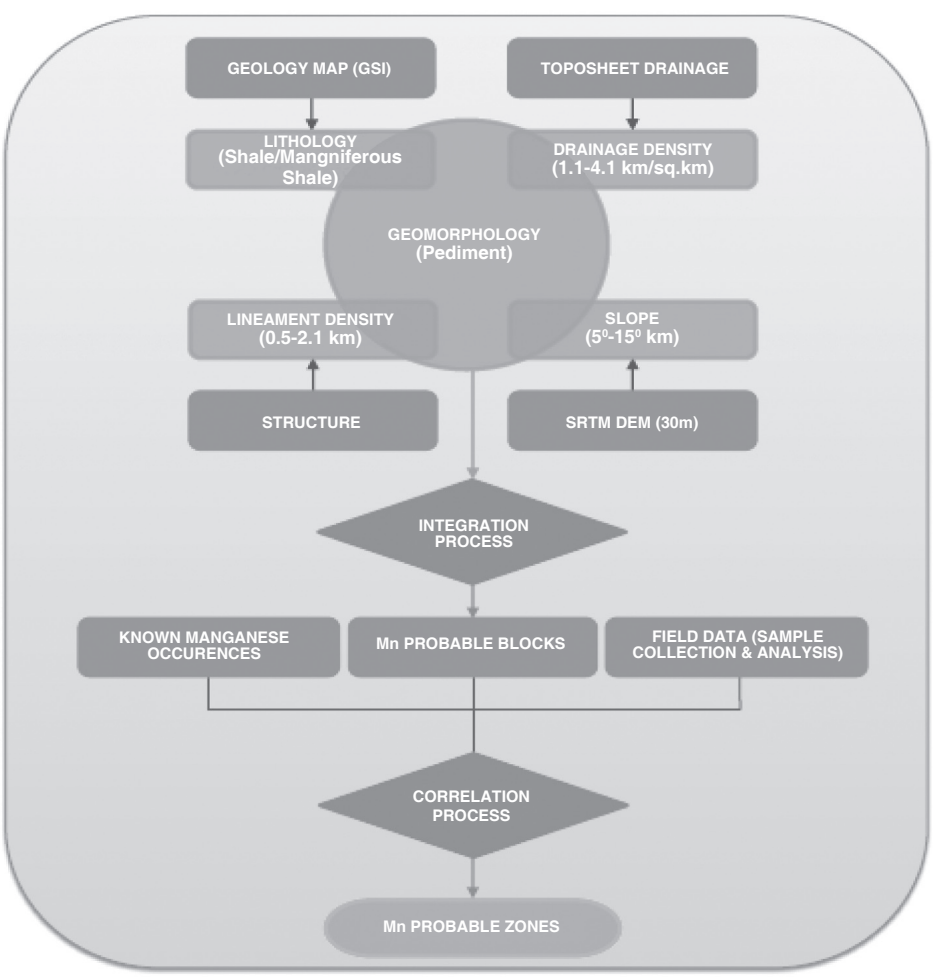

Figure 5 : Manganese Geomorphic Model

4. TESTING OF GEOMORPHIC INDICATOR MODEL

Any scientific model should be supported by multiple independent lines of evidences. With this concept, the geomorphic model thus developed, based on the results of known manganese occurrences and the field observations, has been tested with manganese occurrences reported by various agencies within the study area. The manganese occurrences were reported by GSI through District Resource Map, published by IBM (Indian Mineral Year Book 2013 on Manganese Ore) and reported in a publication by IMMT, Bhubaneswar. Analysis has been done for all the characteristic parameters of the model and described in the following sections.

District Resource Map - GSI

An attempt has been made for testing of the geomorphic model parameters by analysis of the 21 (twenty-one) manganese occurrences shown in the District Resource Map of GSI within the study area. The locations of manganese occurrences were overlaid on different thematic layers viz. geomorphology, geology and structure, drainage density, lineament density and slope of the study area and analyzed.

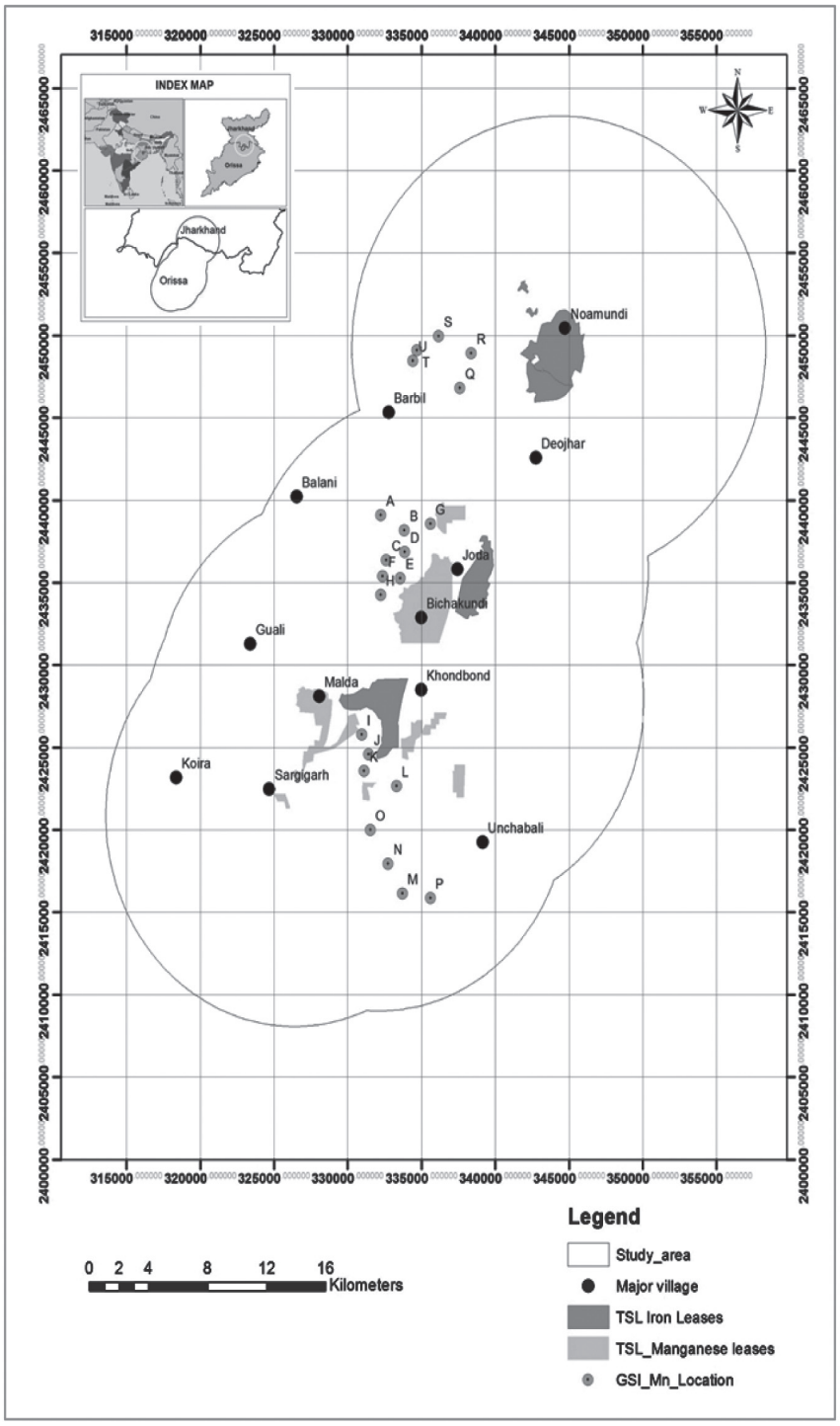

Figure 6 : Manganese location as shown in District Resource Map

The analyzed results of the model parameters from the DRM map have been correlated with the parameters of the established model developed based on the known manganese occurrences of TSL and the observations from the field validation. Eventually it can be concluded that out of 21 manganese occurrences reported by DRM (GSI), 18 occurrences have been found to be positive and matching the parameters of the established model while three locations are differing in geomorphology but fulfilling all the other parameters.

Manganese Ore Reported by IBM

Further to strengthen the developed geomorphic model, the characteristic parameters of the model have been tested with locations of manganese occurrences published by IBM in their Indian Mineral year book 2013 of Manganese Ore. A total of three (3) locations, falling within study area, were overlaid on all the thematic layers (geomorphology, geology, slope, lineament

density and drainage density) and analyzed in order to know the response of model parameters. After analysis, it was concluded that only one location seems to be promising while other two zones do not fulfill the criteria for indicator model.

Technical Publication - IMMT, Bhubaneswar

From Geological map of Precambrian IOG rocks in horseshoe-shaped synclinorium, north Odisha, India, manganese occurrences are located in Koira-Noamundi province as reported by IMMT. Therewere twenty-one (21) locations which were overlaid and analyzed on different thematic layers viz. geomorphology, geology and structure, drainagedensity, lineament density and slope of the study area. These locations were also validated in the field. Subsequently, it can be concluded that out of 21 locations of manganese occurrence reported by IMMTa total of 19locations were found to be positive with respect to the "Geomorphic Indicator Model

5. SUMMARY

This model is an indirect method in deciphering the target areas for manganese mineralization. Geomorphic indicator model was initially developed based on the known mineral occurrences and field validation of probable identified manganese locations. This model was further strengthened by testing all the parameters with manganese occurring areas shown in the map and published reports of IBM, GSI and IMMT. The parameters finalized for the model are

a) Geomorphology - Pediments/mounds surrounded by pediments

b) Lithology - Shale/Manganiferous Shale

c) Slope - 5 to 15°
(gentle slope/slopes of BHJ/BHQ)

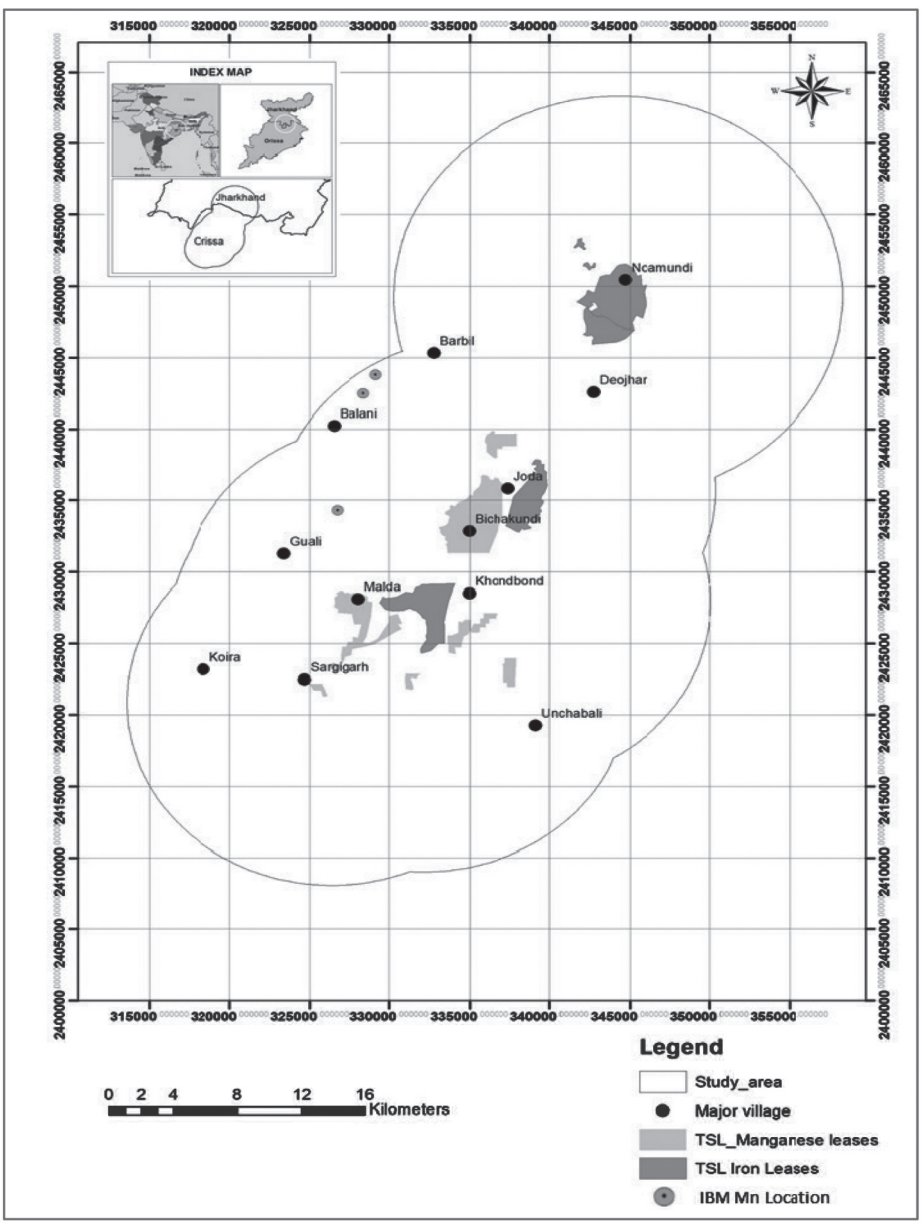

Figure 7 : Manganese location in study area published by IBM

d) Lineament density - 0.5 to 2.1 km/sq.km

e) Drainage density - 1.1 to 4.1 km/sq.km

The success rate of the geomorphic indicator model based on various analysis and testing comes out to be

- The success rate of geomorphic model based on District resource map of GSI is 85.71%.
- The success rate of geomorphic model based on manganese occurring Locations reported by IBM is 33.33%.
- The success rate of geomorphic model based on from the publication of IMMT, Bhubaneswar is 90.48%.

Since the manganese mineralization in the study areas are in discontinuous form and occur as lenses, therefore exploration is very challenging. An integrated approach of using such geomorphic model along with detailed geological & geochemical mapping in the anomaly zone can help in increasing the confidence of target areas and the success rate of exploration there by reducing the time and cost for exploring manganese deposits.

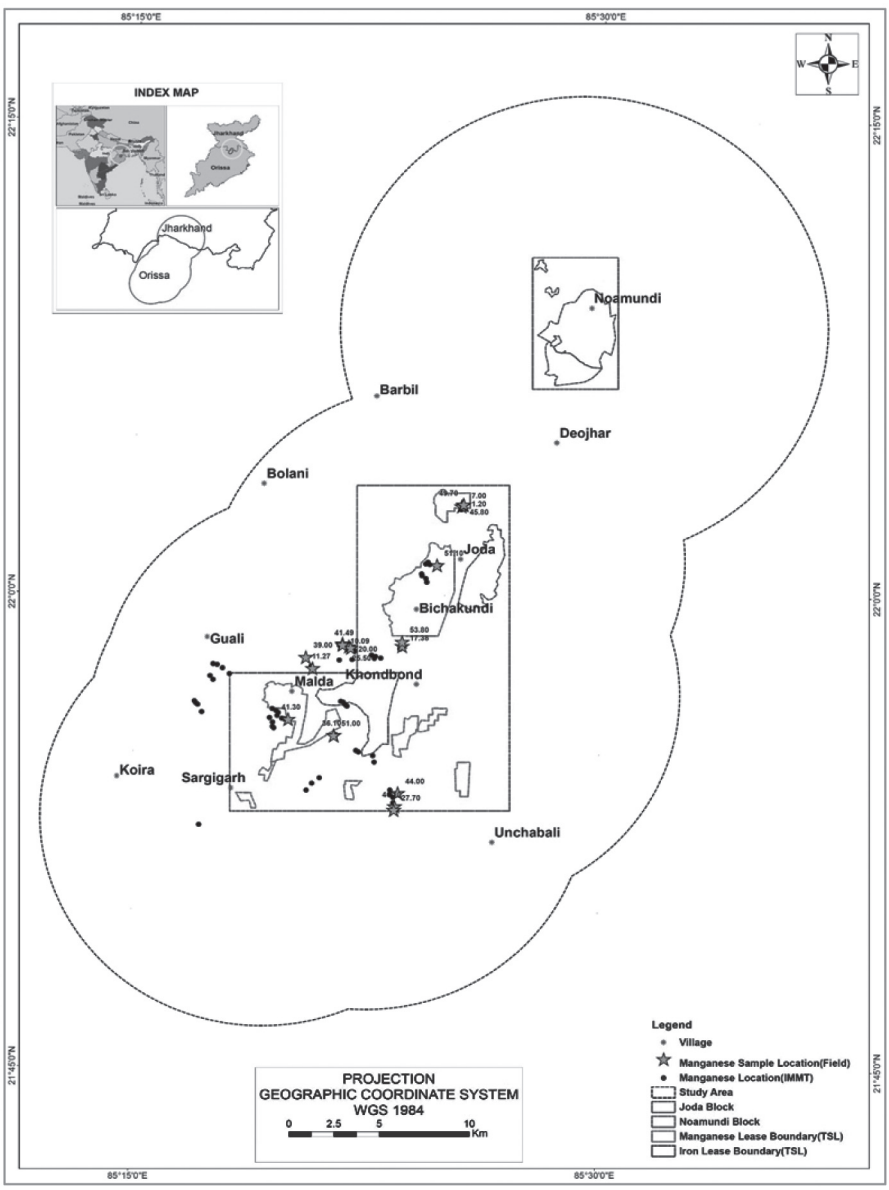

Figure 8 : Manganese location reported by IMMT, Bhubaneshwar

ACKNOWLEDGEMENTS

We gratefully acknowledge Tata Steel Ltd for granting approval and providing all the resources to conduct the study. Special thanks to Prof. Joydip Mukhopadhyay (Dept of Geology, Presidency College, Kolkata) for giving concepts on geomorphological control of manganese mineralization. We extend our sincere thanks to the geologists of FAMD division of Tata Steel for providing the data and support during the field validation.

REFERENCE

1. Acharya, S. (1984). "Stratigraphic and structural evolution of the rocks of Iron ore basin In Singhbhum-Orissa iron ore province. Crustal evolution of the Indian shield and its bearing on Metallogeny", Indian journal of Earth Science, 19-28.
2. Acharya, S. (2000). "Some observation on parts of the Banded Iron Formations of Eastern India. Presidential Address"., 87th session Indian Science Congress: section of Earth System Sciences, 1-34.
3. Banerjee AK (1977). "On the Precambrian banded iron formation and the manganese ores on the Singhbhum Region, Eastern India
4. Bukes et al, (2008). "Genesis of high-grade iron ores of the Archean Iron ore group around Noamundi, India.
5. Mohakul JP, and Bhutia SP, (2015) Regional Structural analysis And Reinterpretation In The Bonai–Keonjhar Belt, Singhbhum Craton:

Implication For Revision Of The Lithostratigraphic succession, Journal of Geological Society of India, 85, 26-36

6. Mcmillan R.A and Shary P.A (2009); “Landforms and Landform Elements in Geomorphometry”, Developments in Soil Science, 33, 227–254.

7. Sarkar, S.N. and Saha, A.K. (1977);” The present status of the Precambrian stratigraphy, tectonics and geochronology of Singhbhum-Keonjhar-Mayurbhanj region”, Eastern India, Indian J. Earth Sciences, S. Ray volume, 37-66.

8. Detailed Information Dossier (DID) on Iron Ores in India (2006); Geological Survey of India

9. Indian Minerals Year Book, IBM (2013)

LABORATORY MEASUREMENT OF PERMEABILITY OF ARGON AND CARBON-DI-OXIDE IN COAL

T Bakshi[1], Dr K Pathak[2], Prof BK Prusty[3], Prof SK Pal[4], AK Patra[5]

ABSTRACT

A laboratory-scale coal permeability measurement study was done to assess the permeability variation trend in different directions with respect to the bedding plane. Samples were collected from Moonidih coal mine of Jharia basin and Argon and CO_2 were used as purging gases. The experimental results showed that the average permeability of Argon varies from 0.79 mD to 1.92 mD along the bedding plane and 0.52 mD to 0.65 mD across the bedding plane. Similarly CO_2 permeability varies from 0.49 mD to 1.29 mD, when measured parallel to bedding plane, and 0.18 mD to 0.35 mD when measured perpendicular to it. It is evident from the experimental result that permeability is higher along the bedding plane than across it. Experimental studies have further confirmed that the studied coal sample has high CO_2 sorption capacity (19.2 cc/g). The higher permeability values of Ar than that of CO_2 is attributed to the sorptive nature of CO_2 in coal.

1. INTRODUCTION

Due to gas outbursts and explosions, coal mine methane (CMM) was considered a severe hazard in underground coal mining operations. But with introduction of coalbed methane (CBM) and coal mine methane (CMM) as a commercially viable energy resource, scientists started looking into coal as an unconventional reservoir. With increased energy demand and technological advances in the CBM industry in the United States, CBM has become a resource of global significance, with emergence of active CBM plays in China, Canada, Australia and India. With increased CBM exploitation, it has become clear that the permeability of coal is an important parameter that affects production.

However, CBM exploitation or its enhanced recovery, or CO_2 sequestration in coal seams mainly depend upon coal permeability. Permeability is one of the most important parameters that controls gas production and well performance. The permeability of coal not only determines the overall recovery performance during primary development but also has an important effect on CO_2 injectivity during ECBM operations.

The permeability of coal depends on the fracture/ cleats, the effect of sorption, stress etc. Coal reservoirs are complex geologic systems that require innovative exploration and completions strategies to produce natural gas economically.

Although the field study of permeability gives more realistic results than laboratory study, the latter is sometimes preferred because in most cases laboratory study can give a quick estimation of permeability. However, evaluation of permeability co-efficients does not present the complete account of the flow of fluids through rocks. Values measured using gas and liquid differ as their flow behaviour is different. Permeability co-efficients are also influenced by certain parameters of the medium, such as, grain size distribution, shape of pores, pore size distribution etc. The present study evaluates the gas permeability co-efficients in different directions to understand the nature of flow with respect to the bedding plane. Finally an attempt has been made to understand the difference of flow behaviour between a sorbing gas and inert gas.

2. BACKGROUND

2.1. Structure of Coal

Coal is a dual porosity rock, containing both macropore and micropore systems, as shown in Fig.1

a. (Jahediesfanjani & Civan, 2005; Warren and Root, 1963). The macropore system is comprised of fractures and cleats that act as the main paths for gas movement. Microporosity on the other hand, occurs within the coal matrix blocks, and consists of a number of interconnected pores that also store methane in adsorbed state. In earlier works of CBM reservoirs, a matchstick geometry was considered for coal (Harpalani & Schraufnagel, 1990; Gray, 1987). According to the model, as shown in Fig.

[1,2,3,4,5]Department of Mining Engineering, Indian Institute of Technology, Kharagpur

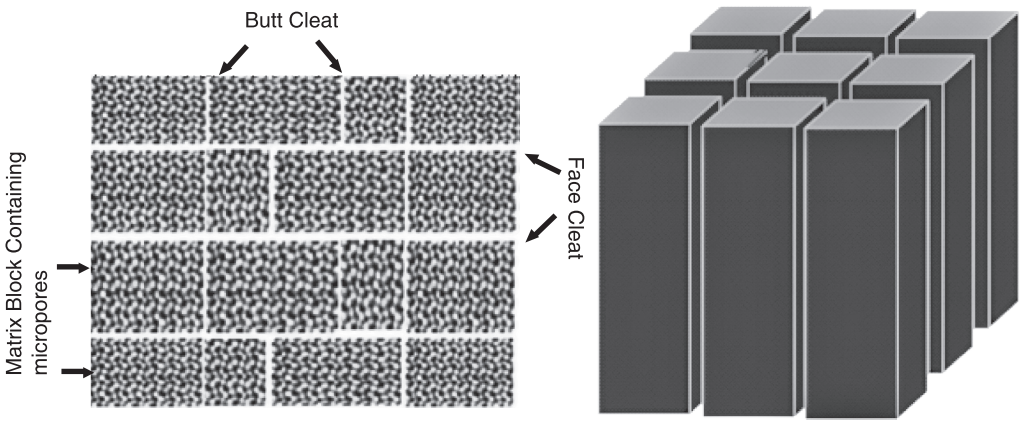

Figure 1. Physical structure and conceptual matchstick model of coal.

b. Each matchstick denotes a block of coal matrix, and the void space between them represents the cleats (Reiss, 1980; Seidle,1992).

2.2. Gas transport incoal

Generally the cleats inside coals are filled with water, and that water pressure holds the methane in place. When the water is pumped out, de-pressurization occurs which finally results in desorption of methane. Afterwards, the released gas moves to the depressurized zone. Usually, gas transport occurs indifferent phases :

a. In the first step, free gas is depleted from the high permeability fracture network and then from coal matrix.

b. After the depletion of free gas, desorption of adsorbed gas present in the micropores of the matrix initiates.

c. The desorbed gas diffuses to the matrix surface and reaches the fracture network. d) In the fractures, the gas is carried towards the production well because of the prevailing pressure gradient following the Darcy's law (Harpalani and Chen 1997). The general process of gas transport in coal is schematically shown in Fig.2.

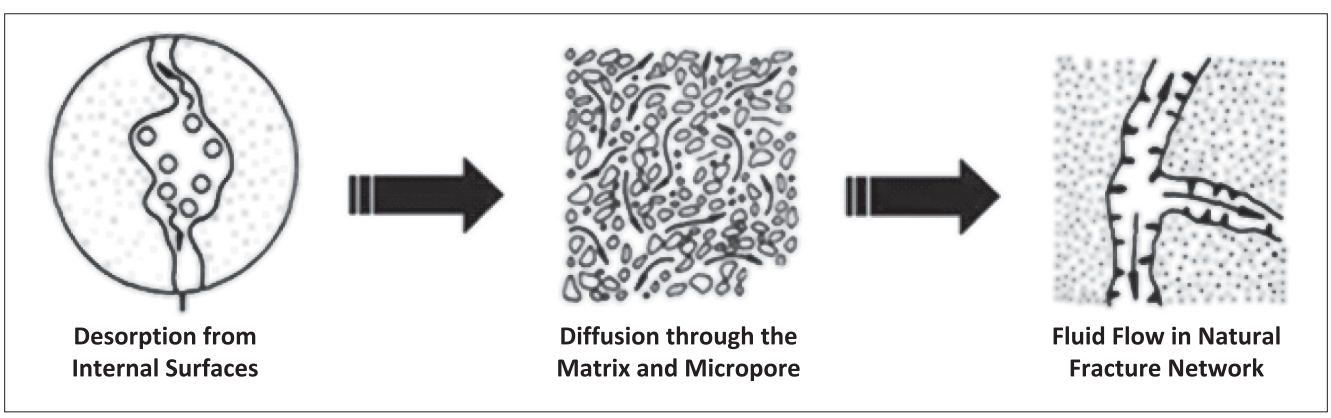

Figure 2. Transport Mechanism in Coal (King, 1985)

2.3. Permeability

Earlier investigations on flow of fluids through porous media is due to Darcy. Darcy's finding can be stated mathematically as :

$$q = -\frac{k}{u}\frac{dp}{dl} = Q/A \quad (1)\ (\text{Dullien., 1992})$$

Where q = filter velocity = Q/A, Q = rate off low

A = cross-sectional area
k = co-efficient of permeability
μ = viscosity of flowing fluid
dp/dl = pressure gradient

From the above equation permeability of a medium can be easily be found out by assuming a linear flow model.

The permeability of rocks with air as flowing fluid, in general, will be different from that of the water as flowing fluid. Klinkenberg observed that permeability of a core sample measured by flowing air is always greater than the permeability obtained when a liquid

is flown. He postulated on the basis of laboratory experiments that liquid had a zero velocity at the sand grain surface while gases exhibit some finite velocity at the sand grain surface, that is to say, the gases exhibit slippage at the sand grain surface. The amount is proportional to frequency of molecular collision and hence to the mean free path. He also found that for a given porous medium, as the mean pressure in creased, the calculated permeability decreased.

Attempts were made by Thomas and Ward (1972) to study the effect of overburden pressure and water saturation on gas permeability of tight sandstone cores. They reported that the overburden pressure reduced the porosity of sandstone cores by 5% of original porosity, thereby reducing gas permeability by 14 to 37% for unfractured sandstone cores. The initial permeability was, however, calculated considering klinkenberg's effect. The effect of over burden pressure on permeability of sandstone cores when saturated with water, on the other hand, had been found to be small or non – existent.

Air permeability of compacted cohesive soils was determined experimentally in the laboratory by Langfelder and Justice (1968). Darcy's law was used for incompressible fluid and the following empirical equation was obtained for compressible fluid.

$$Q = K_c \frac{\Delta pA}{\mu l} p_1^{(1+m1)} - p_2^{(1+m1)} / (1+ m_1) (p_1 - p_2) p_2^{m1} (2)$$

Where K_c = permeability co – efficient for compressible fluid,

m_1 = a constant determined by thermodynamic character of flow,

p_2 = exit pressure of gas,

p_1 = entrance pressure of gas.

Because the flow velocity considered was not high, isothermal flow was assumed to exist in which case m1 becomes equal to 1 and writing p1+ p2 / 2 = pm = average pressure, and interposing we get

$$K_c = \frac{\mu Q l p2}{Apm\Delta p} (3)$$

3. SAMPLE COLLECTION AND GENERAL GEOLOGY

The samples used in the experiments were cored from the coal block samples of XVI seam of Moonidih mines of BCCL.

The Moonidih mine is located in the eastern part of Jharia basin. The location of the mine is illustrated in Figure 1. The Jharia Basin is part of the east-west trending Damodar-Koel group of Gondwanan basins in India. Structurally the basin is a westerly plunging synform with its southern limb faulted. Late Permian Raniganj Formation forms the core of this syncline while the coal bearing early Permian Barakar Formation occupies

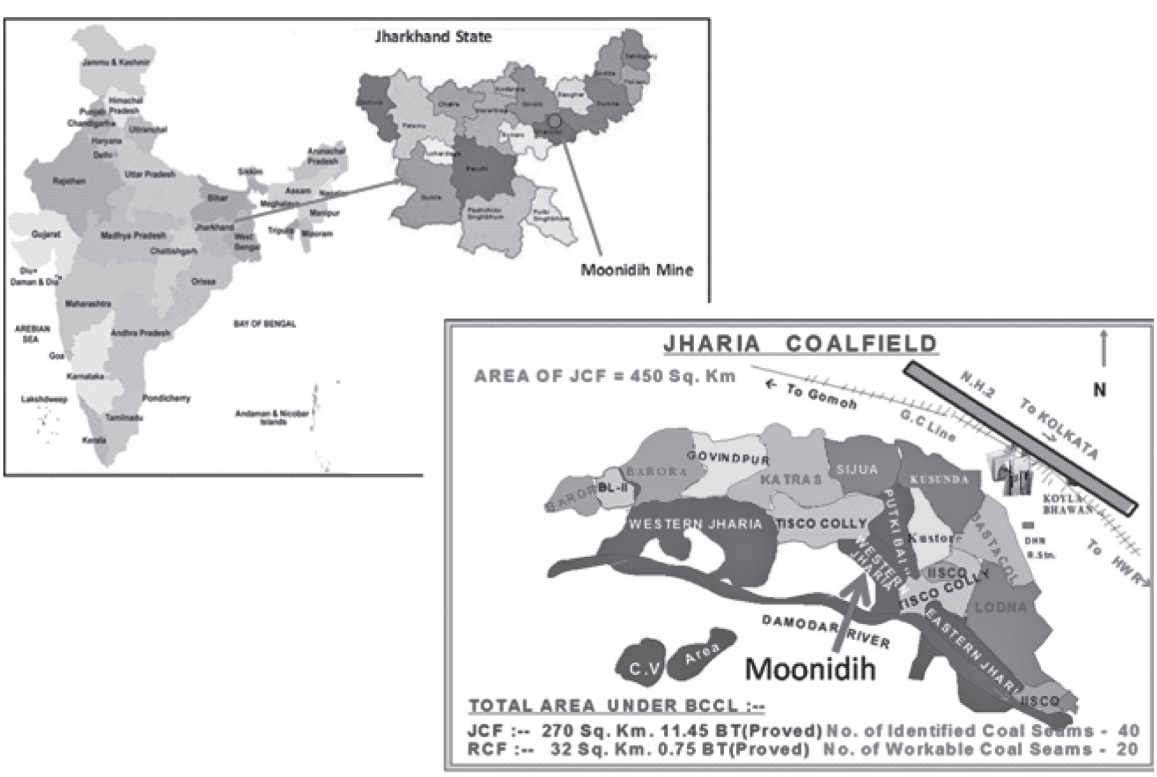

Figure 3. Location of Moonidih Coal Block

about 60% of the basin area in the entire northern and eastern flanks. The mine are a is cut across by two sets of intersecting normal faults. These faults and their associated fractures possibly have increased the permeability of the CBM reservoir. In the vicinity of the intrusives, the coal seams are often rendered as burnt out seam, locally known as Jhama. Barakar coals have very large vertical development with 18 major coal seams. Barakar coals are high rank (HVA to MV bituminous). The vitrinite reflectance ranges from 0.9-1.3%.

4. EXPERIMENTAL SET UP

A gas cylinder is connected to a sample holder through a high pressure tube of thin bore. The joints are standard high pressure joints. A pressure gauge is connected in between the holder and the cylinder and this indicates the pressure of the flowing area. Other end of the sample holder is connected to a graduated 100 cm3 glass burette through a flexible polyethylene tube. Atwoway stop cock is in serted before the burette to divert the flowing gas when the measurements are not being taken. The other end of the burette is connected to a special shaped glass funnel named

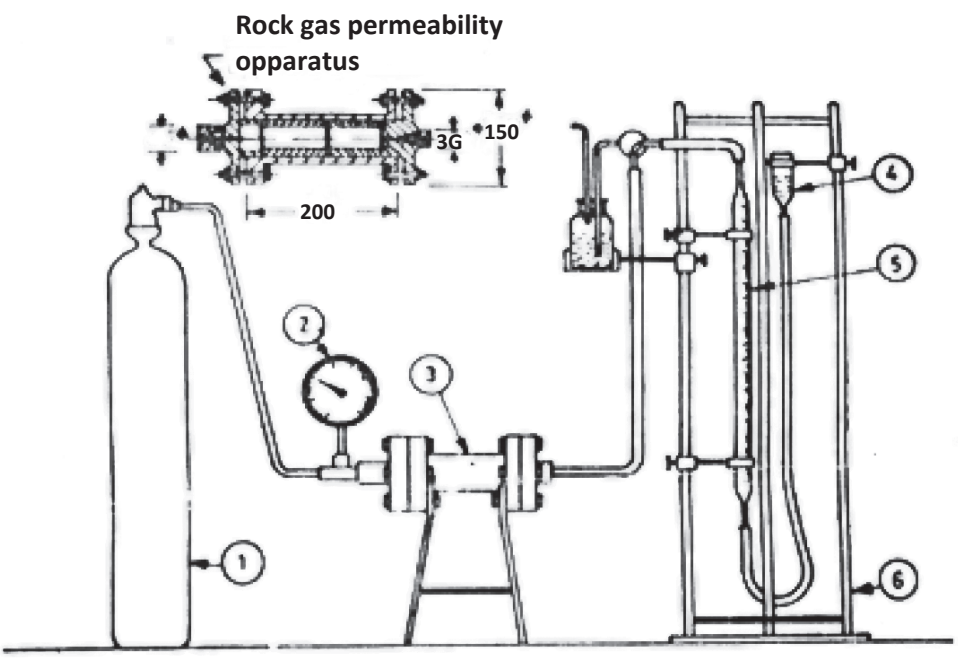

1. N_2 CYLINDER; 2. PRESSURE GAGE; 3. ROCK SAMPLE HOLDER; 4. LEVELLING BOTTLE; 5. BURETTE; 6. STAND

Figure 4. Schematic diagram of gas permeability apparatus (After S.K.Pal., 1986)

'levelling bottle' through a flexible polyethylene tube. A schematic diagram of the experimental set up is given in Fig 4.

The sample holder is made up of chromium steel. It consists of three parts. The middle part is a hollow cylinder having flanges on either side and has a hole of 60 mm diameter. In this hole, a cylindrical chromium steel sleeve which holds the sample core can slide smoothly. There is another length adjusting sleeve placed beside the core holdings leeve. Both the sleeves have circular V - notches on either side and a smooth lead washer is placed between them. The other two parts of the sample holder have flanges which can be connected with the flange soft he middle part by six steel nuts and bolts. A small hole of 3 mm diameter is provided in these two parts of the holder for inflow and out flow of gas. When the three parts areas sembled the projecting portions of the front and rear parts sit firmly onto the lead washers on either side of the sleeves. Circular V-notches are also present in these projecting portions. The adsorption capacity was measured in an adsorption isotherm (AI) instrument. The diagram of instrument given in Figure 5. The details of the adsorption analysis have been already discussed in Bakshi et al., 2017b.

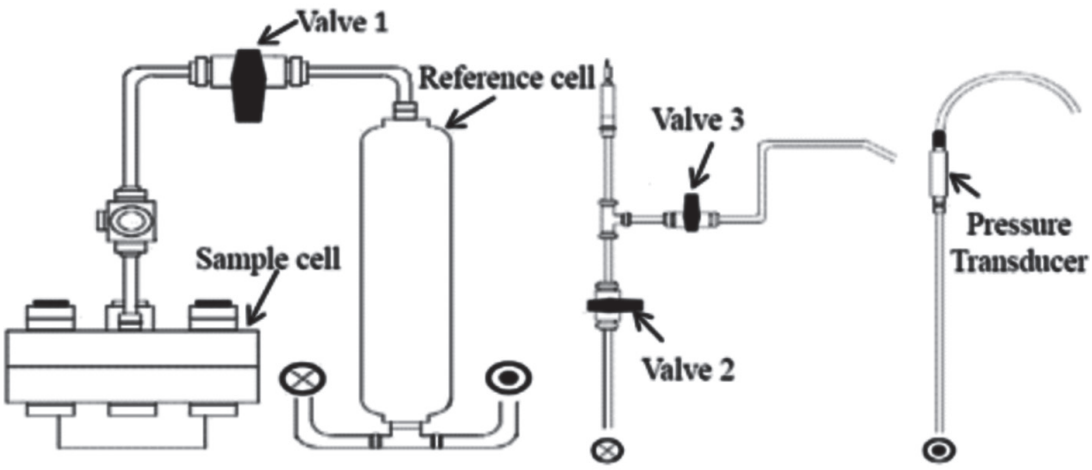

Figure 5. Schematic diagram showing experimental apparatus

5. METHODOLOGY

The permeability of coal samples was measured in the laboratory. Since permeability is an anisotropic property, it was measured in two directions; one in the horizontal direction and the other in the vertical direction. Coal blocks of XVI seam were collected from the Moonidih mine. Coring was done in two directions, that is, horizontal and vertical direction. The coredia meter was 57 mm and height was ~ 61 mm (Figure 6).

The cylindrical cores prepared are placed centrally inside hollow, cylindrical chromium steel sleeves of 60 mm outer diameter and 30 mm inner diameter. Then for each specimen, the an nular space between the curved surface of the sample core and the inner surface of the sleeve is filled with liquid 'Araldite' and 24 hours are allowed for the araldite to settle. Then the steel sleeve is held in the chuck of a lathe machine and two faces of the casted sample are made parallel. The Argon cylinder is connected to one end of a sample holder through high pressure tube soft hinbore. The pressure gauge between the sample holder and the cylinder indicates the inlet pressure of the flowing gas. The other end of the sample holder is connected to a graduated 25 cm3 glass burette through a flexible polyethylene tube. A 2-way stop cock is inserted before the burette to divert the flowing gas when measurements are not taken. The other end of the burette is connected to a leveling bottle through a flexible polyethylene tube. Each sample was cast inside the hollow cylindrical chromium steel sleeve by araldite. Argon/CO_2 gas at different pressures was passed through the sample. With each inlet pressure, the time required to collect 25 cm3 of gas in the measuring burette under atmospheric condition is noted. The barometric pressure and room temperature are also noted during the experiment.

Adsorption capacity of coal is one critical parameter for determining the extractability or recovery percentage of CBM/CMM. Adsorption capacity of coal was determined by conducting adsorption experiment in a high pressure adsorption is other mexperiment under reservoir simulated conditions. A schematic of the adsorption isotherm setup is shown in Figure 5. Coal

(a) (b)

Figure 6. (a) Sample coal block with directions 1 & 2; (b). Core obtained from the sample coal in the direction 1

blocks were collected from XVI seam of Moonidih mine. First powdered coal samples were prepared as per ASTM standards D 1412 and 2013. About 30-40 g of moisture equilibrated samples was used for the adsorption experiment. Helium gas was used for determination of the void volume of the setup.

6. RESULTS AND DISCUSSION

Argon and CO_2 were taken to assess the permeability of coal. The measurements were done along the bedding plane and across the bedding plane and are presented in table 2, 3, 4 and 5. The gas permeability Kg is calculated as equation 4 below.

$$Kg = \frac{2Q\mu LP_2}{A(P_1^2 - P_2^2)} \qquad (4)$$

Where, Q = measured flow rate of gas, μ = dynamic viscosity off lowing gas, L = length of sample, A = cross-sectional area of the sample, P1 = inlet gas pressure, and P2 = outlet or atmospheric gas pressure.

The coefficients of gas permeability Kg of the samples are calculated by rearranging Eqn. 4

$$Kg = 2Q\mu Lp2/A(p1^2 - p2^2) \qquad (5)$$

Table 2. Data for Ar permeability measurements perpendicular to the bedding plane.

Pressure(bar)	Volume (ml)	Av. Time	Avg. Q	$P_i^2 - P_o^2$	K_g $_mD$
0.15	100				
0.15	100	52.5	1.91	0.32	0.5232
0.15	100				
0.20	100				
0.20	100	37.36	2.68	0.43	0.5384
0.20	100				
0.25	100				
0.25	100	28.80	1.47	0.56	0.5462
0.25	100				
0.30	100				
0.30	100	22.56	4.43	0.68	0.5684
0.30	100				
0.35	100				
0.35	100	18.23	5.48	0.81	0.5898
0.35	100				
0.40	100				
0.40	100	15.00	6.67	0.95	0.6140
0.40	100				
0.45	100				
0.45	100	12.16	8.22	1.09	0.6593
0.45	100				

Table 3. Data for CO_2 permeability measurements perpendicular to the bedding plane.

Pressure (bar)	Volume (ml)	Time (s)	Av. Time	Avg. Q	$P_i^2 - P_o^2$	K_g $_mD$
0.31	100	66.70				
0.31	100	67.55	67.1	1.49	.71	0.1839
0.31	100	67.20				
0.40	100	34.06				
0.40	100	34.80	34.65	2.89	0.95	0.2658
0.40	100	35.10				
0.50	100	24.79				
0.50	100	25.24	25.04	3.99	1.24	0.2823
0.50	100	25.10				
0.58	100	19.21				
0.58	100	19.75	19.52	5.12	1.48	0.3025
0.58	100	19.6				
0..66	100	15.32				
0.66	100	15.20	15.31	6.53	1.74	0.3287
0.66	100	15.40				
0.72	100	12.69				
0.72	100	12.75	12.65	7.91	1.94	0.3566
0.72	100	12.5				

Table 4 and 5 shows results of the measurements done along the bedding plane for carbon-di-oxide and argon respectively. It is observed that, values of flow rate (Q) and permeability coefficient (Kg), measured alongthe bedding plane are higher in argon than that of carbon di oxide.

Table 4. Data for CO_2 permeability measurements along to the bedding plane.

Pressure (bar)	Volume (ml)	Time (s)	Av. Time	Avg.Q ml/s)	$P_i^2 - P_o^2$	$K_g D_m$
0.08	100	95.42				
0.08	100	95.18	95.33	1.05	0.19	0.49402
0.08	100	95.38				
0.10	100	45.12				
0.10	100	45.45	45.32	2.21	0.21	0.93077
0.10	100	45.38				
0.12	100	31.45				
0.12	100	31.40	31.51	3.17	.025	1.10497
0.12	100	31.67				
0.14	100	25.03				
0.14	100	25.11	25.2	3.98	0.30	1.17497
0.14	100	25.33				
0.18	100	17.23				
0.18	100	17.55	17.39	5.75	0.39	1.29721
0.18	100	17.40				

Table 5. Data for Arpermeability measurements along to the bedding plane.

Pressure (bar)	Volume (ml)	Time (s)	Av. Time	Avg.Q (ml/s)	$P_i^2 - P_o^2$	$K_g D_m$
0.05	100	27.18				
0.05	100	27.11	27.1	0.92	0.10	0.796
0.05	100	27.14				
0.09	25.00	14.70				
0.09	25.00	14.94	14.82	1.69	0.19	0.794
0.09	25.00	14.82				
0.12	25.00	9.78				
0.12	25.00	9.81	9.77	2.56	0.25	0.891
0.12	25.00	9.71				
0.19	25.00	4.03				
0.19	25.00	4.02	4.04	6.19	0.41	1.317
0.19	25.00	4.06				
0.24	25.00	2.12				
0.24	25.00	2.13	2.14	11.68	0.53	1.923
0.24	25.00	2.17				

The permeability coefficient values are calculated for different pressure differentials in each sample and then averaged and presented in Table 6. It has been found that the permeability co-efficients have higher value in perpendicular direction to the bedding plane. This implies that the fracture encountered in this direction of flow is more than in the direction of bedding plane by the gas. Similar studies have been found by Pan et al., 2014, where he has experimentally proved that gas permeability is highest along the bedding plane and lowest, perpendicular to it.

It can also be noted that the co-efficient values in case of Argon are higher than Carbon Dioxide. This might be due to the non-adsorbing nature of Argon and adsorbing nature of CO_2. This claim is further verified by the CO_2 adsorption experiments done on the same coal sample. The experiment showed that the coal sample is highly sorptive of CO_2 with maximum sorption capacity or VL being 19.2 cc/gm. The isotherm curves of CO_2 adsorption is shown in figure 7. This high sorption capacity is resulting in reduced permeability value of CO_2 while travelling through coal cores.

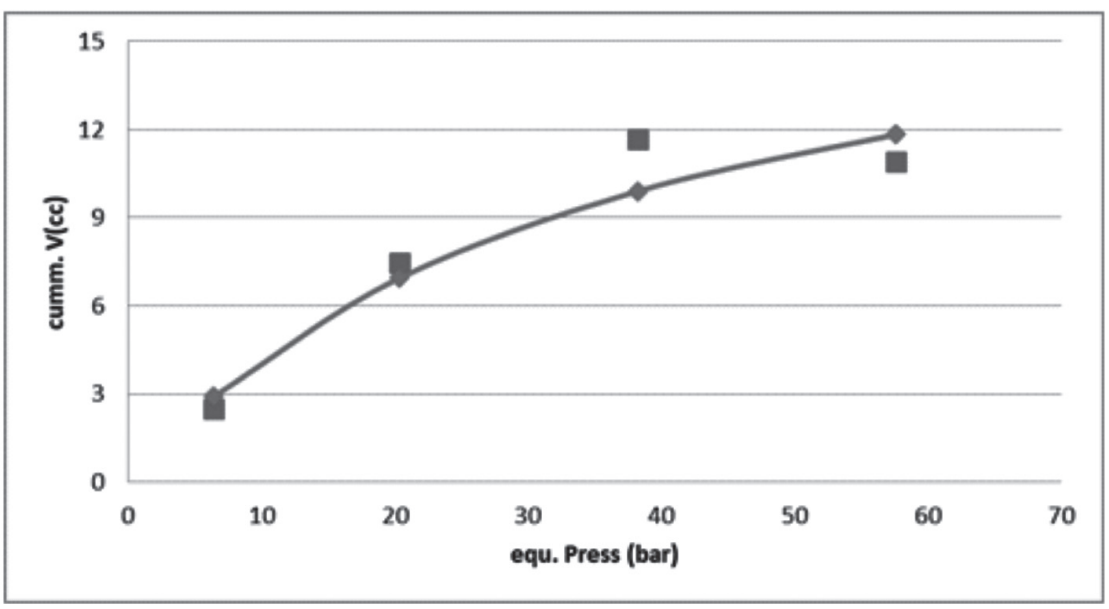

Figure 7. Carbon-di-oxide adsorption isotherm on Moonidih coal sample (XVI seam)

Table 6. Final permeability coefficient values for CO_2 and Ar.

Sample Orientation	Gas used	Kg (milidarcy)
Perpendicular to bedding plane	Argon	0.577
Along bedding plane	Argon	1.15
Perpendicular to bedding plane	CO_2	0.28671
Along bedding plane	CO_2	.000388

7. Conclusion

From the gas permeability and adsorption studies of the samples of Moonidih mine, the following conclusion can be drawn :

1. The carbondioxide sorption capacity is very high in the coal sample
2. The permeability co-efficent values in case of Argon are higher than Carbon Di oxide which is due to the high adsorbability CO_2 in studied coal sample.
3. It has been found that the permeability co-efficients have higher value in perpendicular

direction to the bedding plane. This implies that the fracture encountered in this direction of flow is more than in the direction of bedding plane by the gas.

ACKNOWLEDGEMENTS

This work was carried out with funding from the European Union project “Greenhouse gas recovery from coal mines and unmineable coal beds and conversion to energy”. The authors wish to thank Prof Sevket Durucan for providing the necessary support. They also wish to thank there viewers and editors for their constructive comments and suggestions in improving the manuscript

REFERENCES

D. Thomas, Rex & C. Ward, Don. (1972). Effect of Overburden Pressure and Water Saturation on Gas Permeability of Tight Sandstone Cores. Journal of Petroleum Technology - J PETROL TECHNOL. 24. 120-124.

Dullien, F.A.L., 1992, Porous Media : Fluid Transport and Pore Structure. Academic Press, New York.

Gray I. Reservoir engineering in coal seams : Part 1 - The physical process of gas storage and movement in coal seams. SPE Res Eng 1987; 2 : 28–34.

Harpalani S, Schraufnagel RA. Influence of matrix shrinkage and compressibility on gas production from coalbed methane reservoirs. In : SPE annual technical conference and exhibition. Society of Petroleum Engineers; 1990.

Harpalani, S., Chen, G., 1997. Influence of gas production induced volumetric strain on permeability of coal. Geotech. Geol. Eng. 15, 303–325.

Jahediesfanjani H, Civan F. Damage tolerance of well-completion and stimulation techniques in coalbed methane reservoirs. J Energy Res Technol 2005; 127 : 248–56.

King, G.R., 1985, Numerical Simulation of the Simultaneous Flow of Methane and Water through Dual Porosity Coal Seams during the Degasification Process, Ph.D. Dissertation, Pennsylvania State University.

Langfelder, L.J, C.F. Chen, J.A. Justice 1968. Air Permeability of Compacted Cohesive Soils. Journal of Soil Mech. And Found. Div. ASCE, vol. 94, No. SM4, July, p. 981-1001.

Pal., S.K. (1986). M.Tech thesis, submitted in IIT Kharagpur

Pan, R., Cheng, Y., Yuan, L.,& Yu, M.,2014. Effect of bedding structural diversity of coalon permeability evolution and gas disasters control with coal mining. Natural Hazards. 73. 10.1007/s11069-014-1086-7.

Reiss LH. The reservoir engineering aspects of fracturedformations. France: Editions Technip; 1980.

Seidle JP, Jeansonne MW, Erickson DJ. Application of matchstick geometry to stress dependent permeability in coals. In : SPE rocky mountain regional meeting. Society of Petroleum Engineers; 1992.

T. Bakshi, B.K. Prusty, K. Pathak, S.K. Pal, 2017, Pore characteristics of Damodar valley shale and their effect on gas storage potential. Journal of Petroleum Science and Engineering, 162, 725-735.

Warren, J.E., Root, P.J., 1963. The behavior of naturally fractured reservoirs. SPE 426, 245–255.

ASSESSMENT OF OCCUPATIONAL STRESS VARIABILITY (OSV) OF DEEP UNDERGROUND MINERS INCLUDING ESTIMATION OF SKELETAL MUSCLE FORCE, FATIGUE, AND ITS RECOVERY TESTING BY HAND-GRIP DYNAMOMETRY (HGD)

Shibaji Ch. Dey[1]; Prof NC Dey[2]

ABSTRACT

This study aims to measure the effects of mine depth of cover (DOC) and working environment on occupational stress variability (OSV), muscle force and fatigue sustainability rate (FSR) of side discharge loader (SDL) operators in four selected Indian mines. Methodology adopted here has three phases. The first phase comprises of measurement of working heart rate, other physiological, environmental and psychological parameters. Second phase comprises of measurement of muscle force at different exposure time during the whole shift hours by the help of hand grip dynamometry (HGD) and third is dealing with measurement of FSR once at the surface and again at the underground workplace during SDL operation. The result shows OSV under heat stress in different mine DOC. Physiological strain index and average working heart rate have been recorded 26.1% and 23% higher in deepest mine. Muscle force has decreased 25% at the end of working shift. FSR has also gone down 17.01% in deepest mine compared to the surface. It was observed that heat stress indices WBGT is mine DOC dependent while effects on OSV and muscle force (MF) mainly depends on the time of exposure for a specific operation. Environmental stressors present down the mines are key contributing factors behind alteration of FSR.

Keywords : Occupational Stress Variability (OSV); Depth of Cover (DOC), Average working Heart rate (AWHR); Fatigue Sustainability Rate (FSR); Muscle force; Hand grip dynamometry (HGD).

1. INTRODUCTION

As the upper crop of coal is getting exhausted quickly, the future of coal mining will be shifted towards deeper mines. However, human stress growth behavioral pattern and muscle force (MF) as a response to varied stress factors in deeper mines is nearly unknown. Meanwhile, the causative outcomes of mineral extraction in the form of occupational injuries and disorders (Dey, 2015a) have been measured with high loss of working days (Hull, 1996; Coleman, 2007; Groves, 2007) in some coal mine sectors which contributes huge social and economic impact for individuals, their families and communities as a whole. A cross-section of various research studies in mining sectors also reveals that there are reference of occupational injuries (Kalkowsky, 2006; Bandyopadhyay, 2012) among the miners with high energy expenditure and cardio-pulmonary stress (Dey, 2006, 2013, 2017; Saha, 2008; Dey, 2015b). There are very insignificant works done specifically on psychological and muscle fatigue sustainability (FS) related issues responsible for improvement in working efficiency in deeper mines. Moreover, modern occupational health and safety (OHS) legislation states the requirement of detailed risk assessment of industry's work procedures to ensure that it is aptly designed, manufactured, supplied, installed and used having no possibility of significant risks to the health, safety, and comfort of workers associated with it (Quinlan, 2007). Significant emphasis has been given in two different provisions (126 and 215) stipulated in current coal mine regulation (CMR, 2017). The basic requirement is aimed at application of ergonomics in seat and cabin design for underground mining machine such that operators while on work suffer from negligible strain.

Mining in India is a very back breaking work process which is dynamic in nature (Dey, 2014) and not being carried out solely by mechanization. A vigorous and varied change in dynamic working postures (Morrissey, 1983; Mandal, 2010), repetitiveness (Dey, 2018) and environmental factors create a potential of increasing occupational disorders (McPhee, 2004; Sharma, 2016). However, energy consumption in environmental heat stress (EHS) exposure is also a critical and prime factor in muscle fatigue analysis. Studies have also shown that energy consumption may increase rapidly when it

Ergonomist & Research Fellow[1];
Professor[2], Department of Mining Engineering, Indian Institute of Engineering Science and Technology, IIEST Shibpur. W.B., India.
Corresponding Email:deyshibaji@gmail.com[1]

is moving from resting condition to the highest working intensity (Sahlin, 1998). In the Indian mining industry, there is almost no work found related to muscle force alteration with respect to increase in depth of mining and related environmental stress factors.

There are different EHS factors present at Indian mines, therefore; effect of environment and mine depth on muscle efficiency in deeper mines is a core area of concern in terms of overall efficiency, work output and productivity of miners. In this connection, the measurement of occupational stress variability (OSV) can be used to forecast the responses of environmental stressors on miner's efficiency in deeper mines. On the other hand, hand grip dynamometry (HGD) is a measure of muscular strength or the maximum force/tension generated by muscles. Therefore, to measure effect of environment and mine DOC on muscle efficiency, HGD is a classic tool to assess muscle force (Luna-Heredia, 2005; Bohannon, 2001) alteration. It can be used as a screening tool for the measurement of upper body strength and muscle fatigue. Measurement of HGD is performed using dynamometers, which estimate the muscle strength primarily generated by the flexor muscles of the hand and the forearm. In the present research study, it is aimed to assess the OSV of the operators along with determine the skeletal muscle force, its' fatigue, and recovery in deeper mines.

2. WORKING METHODOLOGY

2.1. Selection Basis :

(a) Mine selection : In this study the main focus has been given on depth of working from surface. The depth of working of majority of underground coal mines in Eastern Coalfield Limited is found to be within 90 meter - 220 meter range. But the study is designed to observe the effect of increasing depth on physiological and other allied factors. Accordingly, some more mines are required to be selected having depth of more than 220m. These mines having working at greater depth are available in Singareni Collieries Company limited. Total four number of mines (Mine A, B, C, and D) from different subsidiaries of Coal India Limited (CIL) and depth of cover (DOC) have been selected for the study where depth of Mine A is 90 m, Mine B 130m, Mine C 160m and Mine D 320m respectively. The study can be done more effectively if air velocity in all mines selected under study is almost same.

(b) Selection of Workforces: Total 30 (N=30) side discharge loader (SDL) operators are selected from four mines. SDL operators are selected as because they devote at least 4 working spells each of around 30-35 minute in the underground with continuous exposure to machine vibration and altered postures. Workforces are selected on the basis of measured physical fitness (BMI, BSA, and resting ECG etc.) where rejection criteria decided taking views of all concerned OHS supervisors including information as received from the mines. Afterwards, it has been again processed through physiological data sampling and willingness criteria to get downsized sample of 24 (N=24, taking 6 from each mine) as subjects. Only those subjects having BMI range of 18.5-25 kg/m^2 (WHO, 2000), BSA up to 1.9 m^2 (Medicinenet.Com 2016) and normal Resting Electrocardiograph (RECG) (Dale, 2000; Ganong, 2001) before work with no past illness record are selected.

2.2. Design of experiment :

As part of the process, the first stage comprises of recording of OSV i.e. physiological and psychological [Rate of Perceived Exertion (RPE)] parameters (Borg, 1982). Physiological parameters i.e. heart rate and metabolic demand (M) [Eq. 1] parameters are measured through direct measurement of heart rate with portable heart rate monitor (HRM) RS 400 (FS Finland) continuously during work exposure. Scientists Yokata and Moran studied on the context of metabolic rate and physiological strain index respectively. Work established on MR is well represented by following equation –

$$M = [0.68 + 4.69(\text{HRratio} - 1) - 0.052 (\text{HRratio} - 1)(Ta - 20)]58.1AD \text{---------- (1)}$$

(Yokata, 2008)

Where,

HR ratio-observed HR given at the time/resting HR of the individual, and

T_a - ambient temperature in ^{O}C

AD - body surface area (m^2).

Measurement of perceived discomfort (PD) or RPE is done by a simple observational method (questionnaire for RPE). Average working heart rate (AWHR) is measured every 5 seconds interval throughout the

whole working shift where average data of every hour is considered for the analysis. OSV is estimated by the help of gathered heart rate and working body temperature data from underground mines. Derived stress parameter named physiological strain index (PSI) [Eq. 2] is fixed as the indicator of OSV measurement. Work established on PSI is well represented in following equation –

$$PSI = 5(Tcore_t - Tcore_o) \times (39.5 - Tcore_o)^{-1} + 5(HR_t - HR_o) \times (MHR - HR_o)^{-1} \text{------}(2)$$

(Moran, 1998)

Where,

$Tcore_t$ = Core temperature during work exposure.

$Tcore_o$ = Core temperature at resting or base.

HR_t = Heart rate during work exposure.

HR_O = Heart rate at resting or base.

MHR = Maximal heart rate.

Resting heart rate (RHR) is measured both at surface and mines for 5 minute in sitting condition before starting their job. Environmental parameters like globe temperature (T_g), ambient temperature (T_a), wet bulb temperature (T_w) have been measured directly with the Environmental Parameters....help of black globe thermometer and Assman hygrometer. Derived environmental stress parameters like discomfort index (DI), operating temperature (T_O), wet bulb globe temperature (WBGT), and mean radiant temperature (MRT) have been estimated by different scientific formula (Epstein, 2006) while, digital anemometer is used to measure the air velocity (V). Air vapor pressure (AV_p) is calculated from gathered environmental data by using derived formula bar of National Weather Service (NWS), America (Brice, 2019).

Subsequently, muscle force or strength analysis and fatigue recovery are measured through HGD every 60 minute throughout the whole working shift of each subject. Each 60 minute is divided in 40 minute working and 20 minute of rest allowance to get back the muscle force into normal condition. Total 330 minutes of exposure time (E) from the deepest mine (Mine D) is taken into consideration where total 7 experiments (1 in surface and rest 6 at mine with 60 minutes as an interval) of HGD have been carried out. The workers were seated in 60^0 flexion and the sidearm was rested at 90^0 angle with the floor measured with the help of a Goniometer. Since flexor and extensor muscles of the dominant hand are involved in testing and in every 60 minute of an interval the strength is measured. In every measurement, maximal grip strength (MGS) and alteration or decrease in % MGS is measured. It was also recorded that how much time the worker was taking for muscle fatigue recovery after each rest between the working spells.

In the third and the last part of the study was devoted to measuring fatigue sustainability of miners where same subjects (N=24, 6 subjects from each mine) were tested once on the surface and again at workplace in resting condition after performing some light job. As per Brouha's fatigue assessment technique (Biswas, 2006) resting pulse of recovery period i.e. from 30 second to 1 minute after work is considered as recovery pulse 1 (RP1), from 1½ to 2 minute as recovery pulse 2 (RP2) and again from 2½ to 3 minute as recovery pulse 3 (RP3). A difference of third pulse and first pulse (RP3-RP1) is considered as fatigue sustainability rate.

2.3. Statistical analysis : Difference between mean values have been estimated from two different sets of data which are tested by one and two tail paired 't' test (homoscedastic) with a significance level of 'α' = 0.05. Null hypothesis (H_0) is proposed here that there is no significant difference between the group means.

One way ANOVA is done to test whether there is an interrelationship between dependent and independent variables and differences between the means of three or more groups along with an assessment of F, $F_{critical}$ and p-value (α<0.05 is considered as significance level).

3. RESULTS

3.1. Mine environment : It is found that the mean WBGT values of mine (average value of 4 mines taken) and the surface is higher than the action TLVs (Threshold limit values) of the National Institute for Occupational Safety and Health (NIOSH, 1986) for moderate to very heavy kind of work category.

Table1: Environmental parameters of different DOC mines

Parameters	Mine A	Mine B	Mine C	Mine D	Surface
T_w (° C)	26.63±0.47 (26-27.5)	27.13±0.5 (26-28)	27.44±0.6 (26-28)	29.97±0.53 (29-31)	26.9±0.6 (27-29.5)
T_a (° C)	27.94±0.63 (27-29)	28.75±0.66 (27.5-29.5)	28.8±0.7 (27.5-29.8)	31.72±0.63 (31.5-33)	27.2±0.4 (26-28.5)
T_g (° C)	28.56±0.51 (28-29.5)	29.31±0.7 (28-30)	29.5±0.81 (28-30.5)	32.4±0.62 (32-34)	28±0.8 (28-30.5)
T_o (° C)	28.02±0.56 (27.54-29.27)	28.9±0.68 (27.8-29.8)	28.92±0.8 (27.8-30.04)	31.9±0.61 (31.76-33.8)	27.35±0.6 (27.6-29.9)
AV_p (kPa)	3.19±0.06 (3.124-3.275)	3.38±0.03 (3.323-3.443)	3.514±0.04 (3.402-3.566)	3.68±0.08 (3.566-3.821)	3.174±0.1 (3.12-3.2)
MRT (° C)	28.61±0.5 (28.05-29.54)	29.36±0.71 (28.04-30.1)	29.51±0.82 (28.04-30.6)	32.41±0.62 (32.04-34.06)	29.3±0.9 (27.9-30.8)
WBGT(° C)	27.1±0.45 (26.6-27.95)	27.7±0.51 (26.6-28.6)	27.9±0.65 (26.6-28.75)	30.6±0.52 (29.5-31.9)	27±0.4 (26.6-27.8)
DI	28.45±0.48 (26.77-28.14)	29.09±0.54 (27.9-29.9)	29.3±0.66 (27.9-30.02)	31.52±0.54 (30.4-32.38)	28.3±0.4 (27.8-29.3)
V(ft/min)	0.14±0.06 (0.1-0.3)	0.16±0.08 (0.1-0.4)	0.1±0.04 (0-0.2)	0.09±0.03 (0-0.1)	0.81±0.2 (0.6-1.1)

- **Legends:** T_w = wet bulb temperature, T_a = ambient temperature, T_g = globe temperature, T_O = operative temperature, AV_p = Air vapor pressure, MRT = Mean radiant temperature, WBGT = wet bulb globe temperature, DI = Discomfort index and V = air velocity.

It is seen that; in respect of Mine A, Mine D is having higher environmental data values (table 1). The value of WBGT is found 12.9% higher with 230 meter of increase in mine DOC. If it is considered that the air velocity (V) is near about same or having no significant differences (P>0.05; Not significant) between mines then, another important derived parameter like DI has gone up to 11.3% where MRT and AV_p are increasing 16.77% and 15.3% respectively (table 1).

In every case, it is seen that with increasing DOC some of the important environmental variables (WBGT and DI) are increasing significantly (p<0.05). Moreover, in comparison with the reference value of different national and international agencies like NIOSH, OSHA, and other valid national agencies, current mines are showing heat stress condition at workplace.

3.2 OSV in mines :

Continuous measurement of heart rate variability (HRV) is considered as one of the important indicator of occupational stress and fatigue. Effect of job stress mostly comes through the cardiopulmonary system of an individual. Therefore, heart rate which is continuously measured has been categorized as moderate-heavy for Mine A and B. Similarly, the workloads were identified as heavy to very heavy for Mine C and D using reference values from Astrand (Astrand, 2003). It is further observed (figure 1, table 2) that the AWHR (figure 1) and other physiological stress factors like metabolic rate (MR) is increasing significantly with the increase in depth (Mine A vs Mine D; p<0.05). Effects of environmental and other stress factor were found to be critical during operation since parameters like HR ratio, AWHR, Peak HR, and MR were much above the normal values.

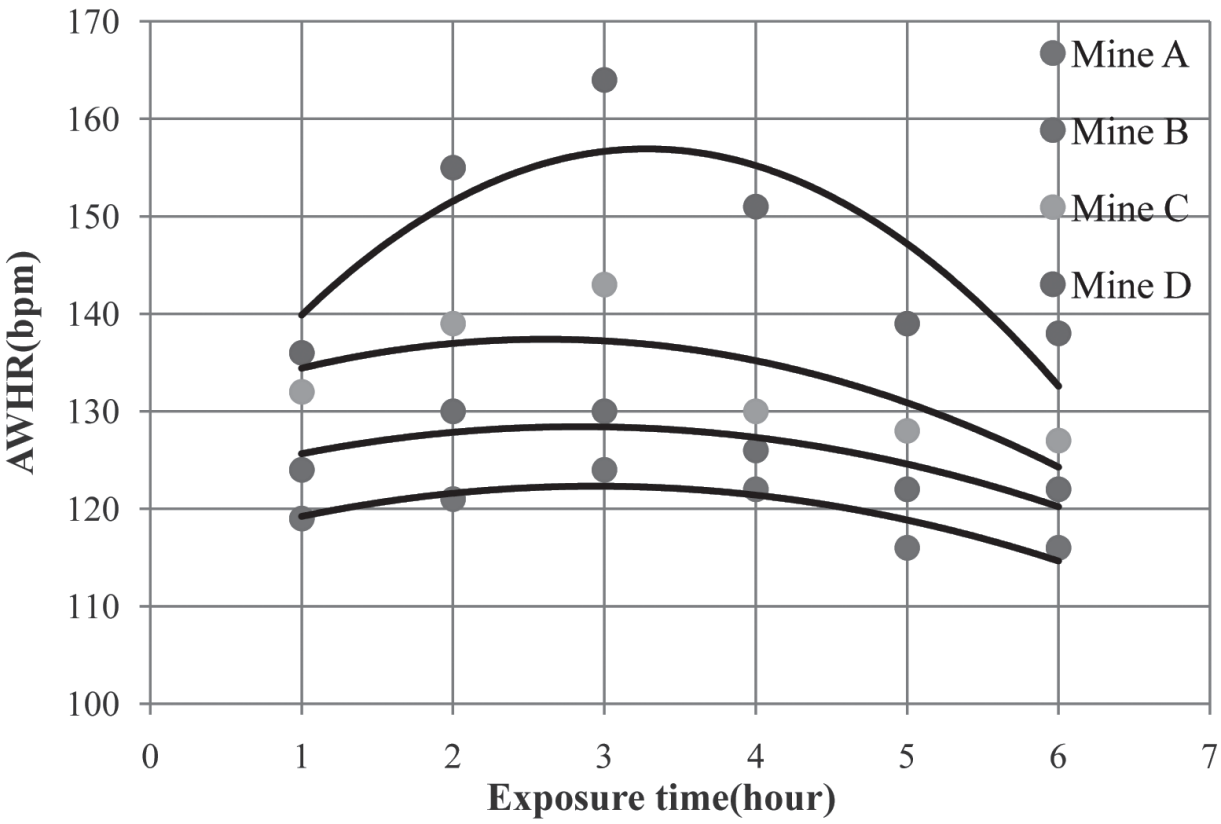

Figure 1 : Plotting of AWHR data against exposure time

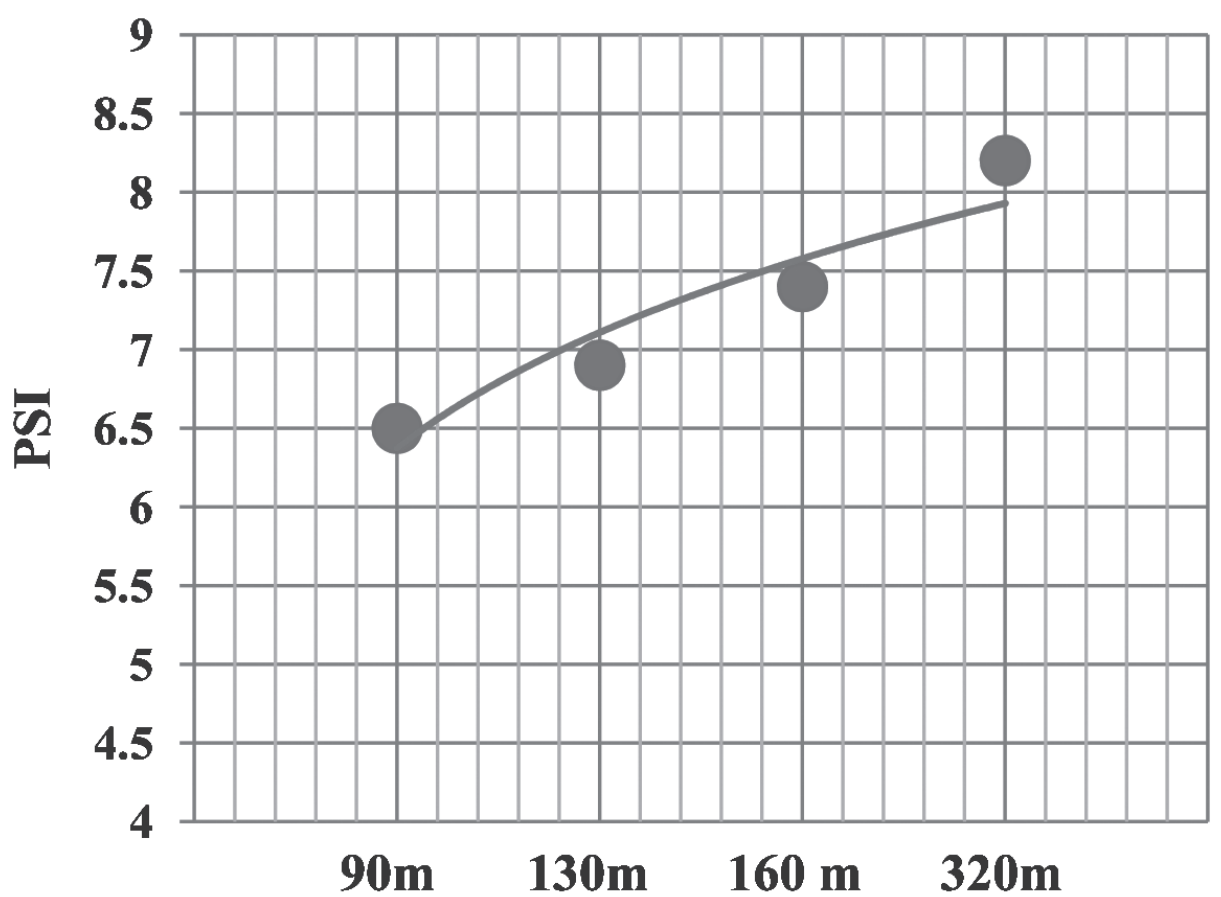

Figure 2 : Physiological strain index in mines

Table 2 : Physiological stress variables.

Physiological Parameters	Underground mines [N=24; Average ± Mean (Range)]			
	Mine A (N=6)	Mine B (N=6)	Mine C (N=6)	Mine D (N=6)
AWHR ($bmin^{-1}$)	119.66±4.92 (114-118)	125.66±7.50 (115-134)	133.16±5.30 (125-141)	147.2±6.8 (140-160)
RHR (bmin-1)	70.5±2.07 (67-75)	72.6±2.7 (67-76)	70.5±2.1 (67-75)	72.5±2.33 (68-76)
MHR ($bmin^{-1}$)	177±4.33 (170-184)	178.9±3.6 (172-185)	177±4.33 (170-184)	178.9±3.6 (172-185)
PD (RPE)	14.2±1.1 (13-17)	14.5±1.09 (13-17)	13.9±0.9 (12-16)	14.3±1.0 (12-16)
% MHR	65.4±4.9 (58.4-77.4)	66.5±4.3 (58.2-73.8)	65.3±4.6 (58.8-76.7)	66.4±4.2 (58.2-73.1)
MR ($Watt/m^2$)	271.0±24 (242.10-313.14)	291.81±13.73 (268.75-305.22)	322.23±23 (288.13-341.54)	335.6±25.5 (302.70-370.2)

Only cardiac frequencies of Mine A and Mine D are depicted as Mine A and Mine D represents the lowest and highest DOC respectively. Cardiac frequencies have been found in the range of 100-110 bpm^{-1} (25%), 110-120 bpm^{-1} (30%), 120-130 bpm^{-1} (20%), 130-140 bpm^{-1} (15%),140-150 bpm^{-1} (9%) and > 150 bpm^{-1} (1%) for Mine A whereas frequencies of 100-110 bpm^{-1} (8%), 110-120 bpm^{-1} (14%), 120-130 bpm^{-1} (25%), 130-140 bpm^{-1} (34%), 140-150 bpm^{-1} (9%) and > 150 bpm^{-1} (10%) were recorded for Mine D respectively. Additionally, PSI of different mines (figure 2) is also found in the range of moderate-very heavy workload category.

3.3 Alteration of muscle force at different mines:

It is found from hand grip dynamometry that maximal grip strength during an operational shift is highly dependent upon exposure time, environmental stressors and most importantly metabolic demand of an individual. A positive correlation (r= 0.99; R^2 = 0.98; P<0.05) between exposure time and %

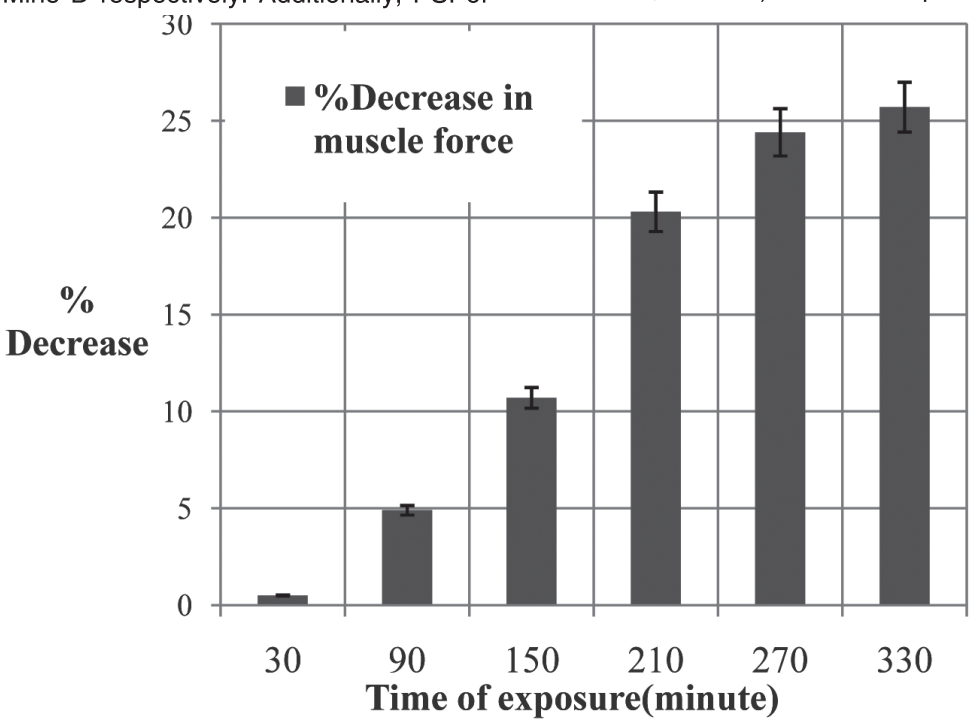

Figure 3 : muscle force vs. time of work exposure.

decrease in muscle force is seen. Muscle force alteration can be seen (table 3) as a serious concern as about 25% (figure 3) of muscle force loss has been observed in deepest mine during 6 hours of operation. Subsequently, the recovery time for gaining muscle force during the experiment in mines has been found critical and time-consuming as the exposure time was increasing towards the end of the working shift. The recovery time of muscle at the end of the shift was thrice as compared to that at the start of the operation (table 3).

Table 3: measurement of muscle force during the mining operation

Parameters	Surface	During operation (Mine D) (SDL operator; N=6)					
Experiment	Experiment time 1 (surface)	Experiment time 2 (E=30m)	Experiment time 3 (E=90m)	Experiment time 4 (E=150m)	Experiment time 5 (E=210m)	Experiment time 6 (E=270m)	Experiment time 7 (E=330m)
MGS (kg)	40.05±1.65 (38.32-41.77)	39.83±1.69 (38.05-41.61)	38.08±1.77 (36.22-39.94)	35.75±1.94 (33.71-37.78)	31.75±2.58 (29.03-34.46)	30.25+2.25 (27.88-32.61)	29.75+2.19 (27.45-32.04)
Recovery time (min)	5.42±0.5 (4.90-5.93)	6.62±1.0 (5.53-7.69)	7.20±1.0 (6.18-8.21)	8.12±1.0 (7.08-9.14)	10.02±0.8 (9.21-10.81)	13.03+1.0 (11.99-14.07)	17.17+2.0 (15.10-19.23)

Legend: E= Exposure time.

3.4. Changes in Fatigue Sustainability Rate (FSR): FSR has been taken into consideration for analysis as per Brouha's fatigue assessment technique. For same subjects, it is found that FSR after some light job at the mine was 12.95% lower than that at the surface for Mine A and 15.7% for Mine B, 16.66% for Mine C and 17.01% for Mine D respectively (Table 4).

FS measurement as per Brouha's fatigue index indicates that the mine FSR is dependent on environmental stressors present at mines as well as their respective DOC. It is also partinent here to mention that an individual's ability to cope up with the environment is better at the surface and eliminates metabolic heat generation of the body in a smoother way than during mine operation.

Table 4 : Differences in Fatigue Sustainability Rate at Surface and Mine

Mines	HR_{Rec} at resting condition	SDL operator at surface (bpm^{-1}), N = 24; Mean + SD (Range)	SDL operator during operation (bpm^{-1}), N = 24; Mean + SD (Range)	Remarks
Mine A	RP3-RP1	-9±1.6 (-8-10)	-10.34±2.1 (-7-12)	12.95% loss in FS rate has been observed
Mine B	RP3-RP1	-10.2±2.2 (-8-12)	-12.1±2.1 (-8-15)	15.7% loss in FS rate has been observed
Mine C	RP3-RP1	-9.5 ±1.5 (-8-12)	-11.4±1.5 (-8-14)	16.66% loss in FS rate has been observed
Mine D	RP3-RP1	-9.90±1.5 (-6-12)	-11.93±1.8 (-6-14)	17.01% loss in FS rate has been observed

4. DISCUSSION

The primary goal of the study is to estimate the changes in muscle force and OSV with increasing DOC and environmental changes. From the study, it is established that there are several stressors (physiological, environmental and psychological) present in mine operation which affects the daily work stress pattern of miners. Different stress parameters have been measured throughout the working shift where except perceived discomfort (RPE); all physiological and environmental parameters have been found linked with mine DOC significantly. Heat stress variables (WBGT) are also found increasing significantly with mine DOC

and higher than the TLV of NIOSH. However, other environmental parameters like DI and T_O in mines are also found significantly higher than the value obtained from the surface. WBGT of Mine D is about 13.3% higher than the surface and 12.9% increase is seen over changes of 230 meter of mine depth (Mine A-Mine D). Other parameters like DI, MRT, AV_p, Ta, and T_g are also following the same trend. Increase in mine working temperature may not be the solitary effect of mine DOC but, the factor cannot be kept aside as air velocity has been considered for the study does not vary significantly. Subsequently, the effect of the working environment is seen through the value obtained for physiological parameters in mines. Physiological parameters like HR ratio, AWHR, MR, and PSI are found in the category of moderate-very heavy workload. Therefore, it cannot be ignored that increasing depth may have an impact over OSV.

In context with OSV and high PSI value of operators during operation, muscle force is also found a matter of concern. MGS or muscle force is significantly decreasing at end of the shift (Exp 1 vs Exp 7 and Exp. 2 vs Exp 7, $p<0.05$) compared to the value which measured at surface of the same subject prior to starting their operation. Muscle force alteration may be the phenomenon which is coming out of high environmental stressor value, unscientific rest break between spells during operation, engaging high dose of hand arm machine vibration exposure, excessive loss of fluid or over exhaustion and loss of sweat under heat stress. In this study, recovery time after performing HGD under different exposure periods (E) is found significantly higher than measured at surface which indicates fatigue of muscle due to long exposure to environmental heat stress ambiance. However, physical fatigue determination with Brouha's fatigue assessment technique has shown comparatively low FSR of operators at the resting condition in mines than on the surface. The low FSR at mines indicates significant interaction of mine environmental stressors with miners' physiological system. Low air current, high ambient temperature and high relative humidity may cause complication in FSR of miners at mines. After analysis of maximum grip strength and muscle force throughout the whole shift, it can be noted down that muscle force is decreasing more rapidly at last lap of working shift therefore, measures of fixing suitable environmental set up, providing suitable rest break and workload distribution, adequate ventilation, availability of cool air in surroundings of SDL operator may have better effect in getting desired metabolic heat loss, low PSI, low muscle fatigue and high FSR of operator during operation.

Additionally, the interrelationship between DOC and some physiological parameters like HR ratio ($F=15.2$; $p<0.05$), AWHR ($F=15.41$; $p<0.05$) and MR ($F=16.8$; $p<0.05$) have been established where no significant relation with psychological parameters has been found. However, muscle force during work is found associated with exposure duration ($p<0.05$, $R^2 = 0.97$, $r= -0.989$) of SDL operation while FSR has been found associated with environmental stressors present in underground workplaces in coal mines.

5. CONCLUSION

Occupational stress variability is closely linked with duration of exposure, effect of stressors having combined impact on PSI and WBGT which increases with mine depth. It is also true that other environmental and physiological parameters are equally important in managing stress in deeper mines. Muscle force is dependent upon the duration of operation in mine where effect of environmental stress factors is additional. It can be concluded that a suitable environment along with reasonable workload for each specific operation and scientific rest break between spells are essential not only to reduce occupational stress effects but also to increase muscle force. This will further increase work efficiency and provide better endurance during various underground machine operation.

6. ACKNOWLEDGMENT

Author(s) sincerely convey their heartfelt acknowledgment to the underground coal mine authority of Coal India Limited (CIL) for extending permission to undertake this study in underground. Besides this, co-operation and the hospitality provided by the colliery officials deserve a special mention for the successful completion of the study.

7. REFERENCE

- Åstrand P.O., Rodhal K., Dahl H.A., Stromme S.B. (2003). Text Book of Work Physiology. 4th ed. Human Kinetics: Canada.
- Bandyopadhyay A., Dev S., & Gangopadhyay S. (2012). A study on the prevalence of musculoskeletal disorders among the coal miners of Eastern Coalfields of India. International Journal of Occupational Safety and Health, 2(2), 34-7.

- Biswas R., & Samanta A. (2006). Assessment of physiological strain in inland fishing activity. Indian Journal of Occupational and Environmental Medicine, 10(1), 19-23.
- Bohannon R.W. (2001). Dynamometer measurements of hand-grip strength predict multiple outcomes. Perceptual and motor skills, 93(2), 323-328.
- Borg G.A.V. (1982). Psychophysical basis of perceived exertion. Medicine and Science in Sports and Exercise, 14(5), 377–381.
- Brice T., & Hall T. (2019). Vapor pressure calculator. National Weather Service. Retrieved from: https://www.weather.gov/epz/wxcalc_vaporpressure.(Accessed 20.02.18)
- Coleman P.J., & Kerkering J.C. (2007). Measuring mining safety with injury statistics: Lost workdays as indicators of risk. Journal of safety research, 38(5), 523-533.
- Definition of Body Surface Area. Medicinenet. Com, (2016). Retrieved from: http://www.medicinenet.com/script/main/art.asp?articlekey=39851. (Accessed 08.10.16)
- Dey N.C., Dey S.C. & Sharma GD. (2017). Importance of ergonomic application for the improvement of coal productivity in mines, Proceedings of the 17 th Coal Operators' Conference.2017, 306-313.
- Dey N.C., Nath S., Sharma G.D. & Dey S.C. (2015a). An Inventory Approach to Humanizing Work and Work Environment in Indian Underground Coal Mines. Research Updates in Medical Sciences (Rumes), 3(3), 10-18.
- Dey N.C., Nath S., Sharma G.D. & Mallick A. (2014). Environmental impact on physiological responses of underground coal miners in the eastern part of India. Journal of Human Ergology, 43(2),69-68.
- Dey N.C., Samanta A. & Saha R. (2006). A Study of the Workload of Underground Trammers in the Ranigang Coal Field Area of West Bengal, India. International Journal of Occupational Safety and Ergonomics (JOSE), 12(4), 399–407.
- Dey N.C., & Sharma G.D. (2013). A critical study on the underground environment of coal mines in India-An ergonomic approach. Journal of The Institution of Engineers (India): Series D, 94(1), 1-6.
- Dey N.C., Sharma G.D. & Dey S. (2015b). An Ergonomic Study of Health of Drillers Working In an Underground Coal Mine with Adverse Environmental Conditions. MGMI Transactions, 111 (March), 58-65.
- Dey S.C., Dey N.C. & Sharma G.D. (2018). Occupational Malfunctioning and Fatigue Related Work Stress Disorders (FRWSDs): An Emerging Issue in Indian Underground Mine (UGM) Operations. Journal of the Institution of Engineers (India): Series D, 99(1), 103-108.
- Dubin D. (2000). Rapid Interpretation of EKG's. 6th Edition. Cover publishing company. Florida USA.
- Epstein Y., & Moran D.S. (2006). Thermal comfort and the heat stress indices. Industrial health, 44(3), 388-398.
- Ganong W.F. (2001). Review of Medical Physiology: 20 th Edition. The McGraw-Hill Companies. USA.
- Groves W.A., Kecojevic V.J. & Komljenovic, D. (2007). Analysis of fatalities and injuries involving mining equipment. Journal of safety research, 38(4), 461-470.
- Hull B.P., Leigh J., Driscoll T.R. & Mandryk J. (1996). Factors associated with occupational injury severity in the New South Wales underground coal mining industry. Safety Science, 21(3), 191-204.
- Kalkowsky B. & Kampmann B. (2006). Physiological strain of miners at hot working places in German coal mines. Industrial health, 44(3), 465-473.
- Luna-Heredia E., Martín-Peña G. & Ruiz-Galiana J. (2005). Handgrip dynamometry in healthy adults. Clinical Nutrition, 24(2), 250-258.
- Mandal B.B. & Srivastava A.K. (2010). Musculoskeletal disorders in dumper operators exposed to whole body vibration at Indian mines. International Journal of Mining Reclamation and Environment, 24(3), 233-243.
- McPhee B. (2004). Ergonomics in mining. Occupational Medicine, 54(5),297–303 Retreived from: https://www.ncbi.nlm.nih.gov/pubmed/15289585 (Accessed 08.10.16)

- Moran D.S., Shitzer A. & Pandolf K.B. (1998). A physiological strain index to evaluate heat stress. American Journal of Physiology-Regulatory, Integrative and Comparative Physiology, 275(1), R129-R134.
- Morrissey S.J., Bethea N.J. & Ayoub M.M. (1983). Task demands for shovelling in non-erect postures. Ergonomics, 26(10), 947-951.
- Quinlan M. (2007). Organizational restructuring/downsizing, OHS regulation and worker health and wellbeing. International journal of law and psychiatry, 30(4-5), 385-399.
- Saha R., Dey N.C., Samanta A. & Biswas R. (2008). A comparison of cardiac strain among drillers of two different age groups in underground manual coal mines in India. Journal of occupational health, 50(6), 512-520.
- Sahlin K., Tonkonogi M. & Söderlund K. (1998). Energy supply and muscle fatigue in humans. Acta Physiologica Scandinavica, 162(3), 261-266.
- Sharma G.D., Dey S. & Dey N.C. (2016). Rationalising postural demand of side discharge loading machine operators with respect to musculoskeletal pain and discomfort in underground coal mines in India. International Journal of Human Factors and Ergonomics, 4(1), 60-72.
- The Coal Mine Regulation (2017). The Gazette of India : Extraordinary. Retrieved from : https://www.dgms.net/Coal % 20 Mines % 20 Regulation % 202017.pdf (Accessed 01.03.2019).
- The National Institute for Occupational Safety and Health (1986). Occupational Exposure to Hot Environment-Revised Criteria. Washington D. C : Department of Health and Human Services. Retrieved from : https:// www.cdc.gov/niosh/docs/86-113/86-113.pdf. pp 89-90 (Accessed 20.10.2018).
- World Health Organization (2000). Obesity : preventing and managing the global epidemic/. WHO Technical report series No. 894. WHO. Geneva. 8-9.
- Yokata M., Larry B., Cheuvront S., Santee W., Latzka W., Montain S., Kolka M. & Moran D. (2008). Thermoregulatory model to predict physiological status from ambient environment and heart rate. Computers in biology and medicine, 38 (11-12), 1187-1193.

DEVELOPMENT OF A GUI BASED SOFTWARE - TOOL FOR SURFACE DEFORMATION MAPPING THROUGH DinSAR PROCESSING : A CASE STUDY OVER JHARIA COAL FIELD

Tapas Kumar Dey[1], Prof Biswajit Manna[2], Debashish Chakravarty[3]
Biswajit Samanta[4], and Arundhati Misra[5]

ABSTRACT

Interferometric Synthetic Aperture Radar (InSAR) is considered to be one of the most efficient remote sensing techniques used to measure topography of the earth surface and it's change on a regular interval. The complexity associated with InSAR processing makes it not so popular unlike other remotely sensed geodetic techniques. To ease the complexity of InSAR processing flow and to process the SAR data without having much in-depth knowledge about all the sub-processing steps, a Graphical User Interface (GUI) based tool namely, 'InSAR Tool for Ground observation' (ITG-tool) has been developed at Indian Institute of Technology, Kharagpur. This can be used as an educational or research tool for Differential InSAR (DInSAR) processing to get the information about the surface change over any particular area. It has the ability to process from the raw SAR data and through some intermediate steps, finally, it generates a deformation map of the area imaged. This paper explains the practical application of this software toolkit by showing a deformation trend over an Indian coal mining area as Jharia coal field, Jharkhand where subsidence has been occurring due to underground mining activities in recent past. An attempt has been made to present InSAR processing technique in a nutshell way both in theory and implementation through ITG tool, and hence to extend the usefulness of the software as a utility tool for DInSAR processing.

Index Terms - GUI, DInSAR, ITG-tool, DEM, Interferogram, Deformation map.

I. INTRODUCTION

The unplanned extraction of the material from the subsurface weakens the adequate support from the overlying rocks. It creates a gradual or sudden sinking of earth surface to a lower level, even sometimes results in a complete surface collapse which poses huge risks to lives and property in and around the area concerned. These type of subsidence related phenomena are very common in mining industry[1]–[3]. During underground mining operations, subsidence may occur above any area where coal is being mined or has been removed. Proper understanding the dynamics of subsidence associated with underground mining activity requires accurate knowledge of mining system, layout, production rate, and geological formation etc.[4]–[7]. Along with those prior information, a precise & reliable measurement and monitoring of the surface above the mines are also required to study the subsidence pattern. Hence, the need for long-term deformation monitoring is very essential to minimize damage related to surface change phenomena (e.g., damage to structures, utilities, environment, etc.). In case of conventional field-based measurements, the total extent of deforming area is poorly understood due to point-based technique of measurement. The other drawbacks of field-based techniques are : labor intensive and expensive if large areas are to be monitored on a regular basis[8]–[11]. In addition to that, field-based measurements are usually made on some reasonable assumptions without going for actual readings or data in case of unreachable areas.[12],[13]. In order to overcome these limitations, Interferometric Synthetic Aperture Radar (InSAR) is considered to be one of the best geodetic techniques due to its ability to remotely monitor over a large area in a regular interval [8],[14]–[16].

InSAR is the synthesis of conventional Synthetic Aperture Radar (SAR) and interferometry techniques that have evolved over several years in radio astronomy [17]–[19]. One of the modern applications of InSAR lies in the extraction of the topographic

TK Dey[1], B Manna[2], D Chakravarty[3], and B Samanta[4] are in Indian Institute of Technology, Kharagpur, W.B., 721302 India
email : (tkd@iitkgp.ac.in; bmiitkgp@iitkgp.ac.in; dc@mining.iitkgp.ernet.in; samantab@mining.iitkgp.ernet.in).

A. Misra[5] is the group director of AMHTD, EPSA, Space Applications Center, Indian Space Research Organisation, Ahmedbad, Gujarat, 380015, India, e-mail : (arundhati@sac.isro.gov.in).

information as Digital Elevation Model (DEM) for monitoring ground surface change[20]. DEM generation from SAR images is not as simple as it is generated from optical satellite imagery because interferometric processing is associated with some complicated steps to be executed in course of InSAR processing[12]–[15]. SAR image consists of both the magnitudes (pixel intensity) and the phase values. The pixel intensity is dependent on size, shape and dielectric constant of the point target to be imaged. The phase in a complex SAR image is the coherent signal information about the distance between a ground point and the radar antenna as well as the information about texture of the terrain within a resolution cell[21]–[23]. Using differential InSAR (DInSAR) techniques, ground deformation can be monitored by quantifying phase differences of the same ground pixel at different time intervals.[19],[24].

The SAR platform transmits pulses at some Pulse Repetition Frequency (PRF) for each pulse to be back-scattered from the ground surface as echo pulse. Then the echoes are sampled and digitized in range at the rate of sampling frequency based on the principle of the Nyquist's sampling rate[25]. The radar signals are coherent in nature which means that frequency of all the pulses remain the same through out it's whole two-way journey. So, both the magnitude and phase of each echo signal are sampled depending on transmitted signal's frequency and phase characteristics[21]. The raw SAR data file is a 2-D array of complex pixel values where I (in-phase component) is the real part and Q (quadrature component) is the imaginary part. Then the two dimensional raw data set is to be processed to form a SAR image [26],[27]. In InSAR technique, two SAR images acquired with equal incidence angle (usually the former is regarded as master and the latter as slave) are combined to produce a phase interference image called interferogram. Using the phase information of the interferogram, it is possible to extract topographic information and also to measure any surface change which has happened in between the two image acquisitions.[14],[19],[21].

InSAR is becoming very popular among the remote sensing and geo-science community as it is considered to be one of the finest tools to quantify and monitor the surface deformation with highest accuracy. Most of the open source InSAR related software are involved with command based execution techniques for processing the SAR data. However, the complexity associated with command based steps makes the InSAR processing not so popular unlike the other remotely sensed geodetic techniques. To ease the complexity associated with InSAR processing or to process the SAR data without having much in-depth knowledge a graphical user interface (GUI) based software tool needs to be developed so that InSAR processing can be done in a most easy, understandable and interactive way. A GUI based software named, InSAR Tool for Ground observation (ITG-tool), has been developed at Indian Institute of Technology, Kharagpur with the help of Space Applications Center (SAC), Indian Space Research Organization (ISRO), Ahmedabad. This can be used as educational or research tool for Differential InSAR (DInSAR) processing. The objective of present investigation is to test the applicability of this software toolkit to measure surface deformation which is occurring due to mining activities over an Indian coal mining area.

II. BACKGROUND

A. Theory of Synthetic Aperture Radar

Being an active remote sensing system operating at microwave frequencies, Synthetic Aperture Radar

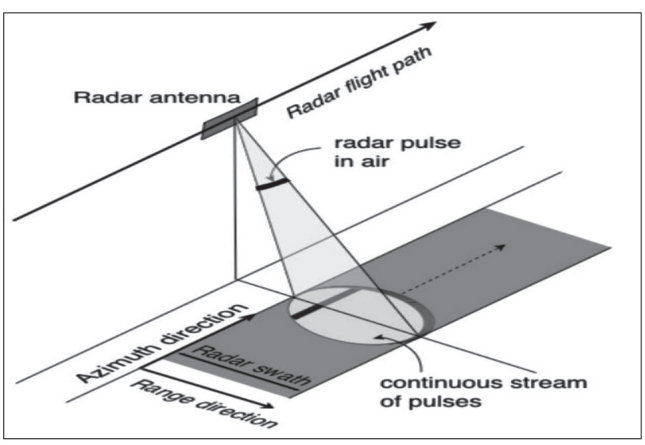

(a)

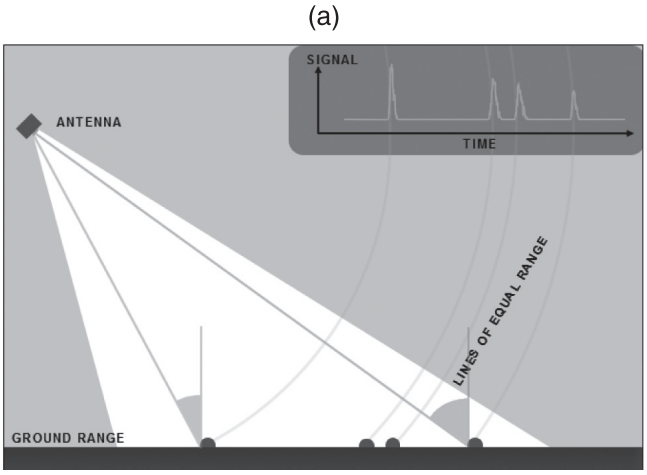

(b)

Fig. 1 : (a) : Mechanism of Synthetic Aperture Radar on a moving satellite; (b) : Image formation along range direction for each points and their corresponding incidence angle[28].

(SAR) system can capture images of earth surface in all type of weather conditions and also in day and night[14]. The name 'synthetic' comes because of a large virtual aperture or antenna which is formed by coherently combining the collection of echo pulses while the radar antenna moves along its flight path[13]. In real aperture radar (RAR), the physical length of the antenna can be the order of meters whereas in SAR, the synthesized aperture length can be the order of kilometers virtually [21],[16]. The SAR systems give unique images representing the electrical and geometrical properties of the area of the earth surface imaged[29]. The intensity of each pixel of a SAR image is dependent on the spatial orientation, roughness and dielectric constant of the imaging surface[30]. This systems are operated on air-borne or space-borne platforms around thousand kilometers above the earth surface and take the image of whole earth by following one by one specific linear path or track as shown in Fig. 1(a). The transmitting antenna of the SAR system transmits a series of coded pulse towards the ground swath that sweeps across the imaging swath and then the echo of the each pulse is recorded at the receiving antenna. The SAR system does not capture the area perpendicularly below the antenna rather it looks at a looking angle to avoid the left-right ambiguities in the image[31]. In other words, to distinguish all the image pixels by their distinct phase values along the range direction, antenna is kept with some look angle. In a particular scene, different pixels have their own incidence angle along the range (i.e. nearest point from the antenna has the smaller incidence angle than that of farthest point) as shown in Fig. 1(b). The transmitted pulse from the antenna is reflected back from different points at different time instant along the range while swiping the swath area. When the echo signal is received at the receiver, the 3-D earth is converted into two dimensions i.e. range (across the track) and azimuth (along the track) in the process of SAR image formation[27].

B. Principle of Interferometric SAR (InSAR)

SAR amplitude images were used widely for reconnaissance and environmental monitoring in remote sensing. However, the phase component recorded simultaneously with amplitude by SAR system was overlooked for a long time. In 1974, Graham L.C., first invented that a pair of SAR images of the same area taken from slightly different positions can be used to form an interferogram from which topographic information can be fetched[32]. After this

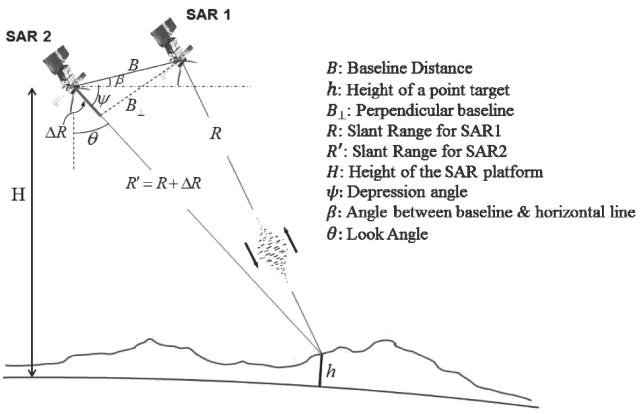

Fig. 2 : Schematic diagram of Interferometric Synthetic Aperture Radar (InSAR)

invention, interferometry comes into the picture in SAR signal and systems related research. Interferometric Synthetic Aperture Radar (InSAR) is the synthesis of conventional Synthetic Aperture Radar (SAR) and interferometry techniques that have been evolved over several years in radio astronomy[19],[21].

InSAR is one of the remotely sensed imaging techniques, where two images are taken either at the same time with the help of two radar receivers installed on board (one-pass flight) or at a different time using only one receiver (repeatpass flight) of the same area of interest[21],[22],[31]. Depending on the phase difference of two images taken either simultaneously (one pass) or sequentially (two pass), a digital elevation model (DEM) is generated. The geometry of InSAR can be interpreted with the help of Fig. 2, where SAR1 and SAR2 are two radar sensors which are separated by a baseline B oriented at an angle β with respect to local horizontal line, viewing the same earth point P of height h. The distance between SAR antenna and the point P on the ground is called the slant range. The aim of InSAR technique is used to determine the elevation h at each point in the SAR scene[16],[33]. A relationship between a change in the estimated height of point target (δh) with the change in difference in range is given as :

$$|\delta h| = \frac{cos\,\psi}{sin(\psi+\beta)}\left(\frac{R}{B}\right)|\delta(\Delta R)| \qquad (1)$$

From eqn.1, it can be derived that, the amount of error amount in height estimation is proportional to the error in slant range difference (ΔR) multiplied by the ratio (R/B). In other words, in order to measure the height of any point target accurately, the baseline needs to be large enough with the smallest possible value of slant range difference for the two pass. On the other hand,

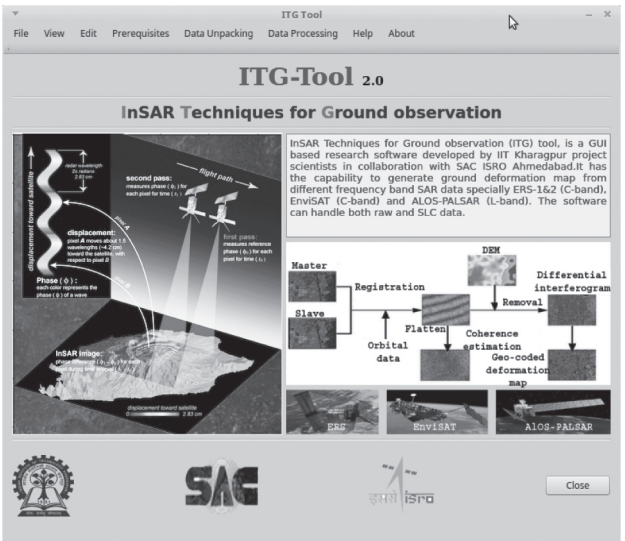

Fig. 3 : Screenshot of the main window in ITG tool.

baseline cant be too large to make the two images appeared to be quite different from each other. The more appropriate term of baseline is perpendicular baseline, i.e. the perpendicular distance from one satellite to the slant range of the other satellite. The upper limit of the baseline is termed as critical baseline. So, for choosing any InSAR pair for successful DEM generation, the baseline should be less than critical baseline[30].

The phase difference corresponding to same pixel point in two SAR images or interferometric phase ($\Delta\phi$) is proportional to the propagation path difference between the two acquisitions.

$$\Delta\phi = \phi_2 - \phi_1 = \frac{4\pi}{\lambda}(\Delta R) \qquad (2)$$

λ is the wavelength of the transmitted signal. In repeat pass interferometry, the interferometric phase is a summation of various components as given by the following equation :

$$\Delta\phi_{total} = \Delta\phi_{flat} + \Delta\phi_{topo} + \Delta\phi_{dis} + \Delta\phi_{atm} \qquad (3)$$

where, $\Delta\phi_{flat}$ and $\Delta\phi_{topo}$ are the phase differences due to changes in satellite-target distance for flat-earth and topography. $\Delta\phi_{flat}$ can be computed accurately from the precise orbital information and to get the value of $\Delta\phi_{topo}$, an auxiliary DEM is needed where topographic phase can be extracted from the elevation. $\Delta\phi_{atm}$ is the phase difference due to changes in atmospheric conditions in between two passes. $\Delta\phi_{dis}$ the phase difference due to displacement of earth surface in LOS direction. Hence, to get the phase due to deformation $\Delta\phi_{dis}$, all the three components in the right side of eqn 3 need to be subtracted from $\Delta\phi_{total}$.

III. ITG-TOOL & ITS Processing Stages

Interferometric Tool for Ground observation (ITG-tool), a GUI based DInSAR processing software has been developed by Indian Institute of Technology, Kharagpur along with Space Applications Center (SAC), ISRO, Ahmedabad during the tenure of a purely R&D project sponsored by ISRO. A screen shot of the main window of ITG-tool is shown in Fig. 3. This software has been designed in such a way that remote sensing users with a preliminary knowledge of InSAR processing, can process interferometric mode SAR data using step by step processing to generate a Differential DEM (DDEM) or a deformation map of a particular area of

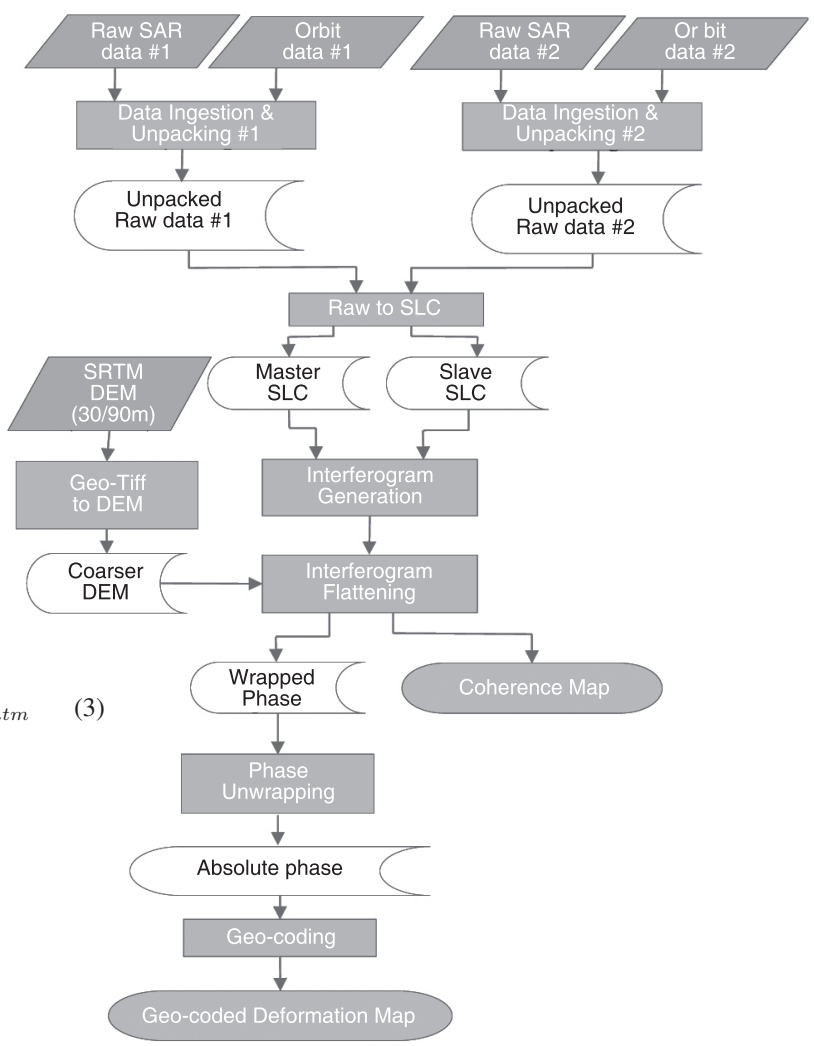

Fig. 4 : Flow diagram of InSAR processing steps using ITG tool.

interest during a finite time interval. This tool is able to process starting from raw SAR data with viewing facility of each intermediate result at the end of every processing step. Output results at each step can be taken and analyzed to understand and interpret the final findings. ITG-tool has been designed and developed for both the expert user and the novice in the InSAR processing field. Two modes of processing facilities are available in this software. The first one is 'piece-wise processing' for advanced users who knows all the sub-processing stages related to InSAR processing. In this flow, there are options to halt and see the intermediate results for understanding and analyzing the most recent outputs files or images) generated in between the processing stages. The other processing method is 'two steps processing' where only two steps are there where the first step is 'data unpacking' and the second step starts from unpacked data to the generation of the end result i.e. geo-coded deformation map[34],[35]. All the important steps associated with the ITG tool-based DInSAR processing for 'piece-wise processing' mode have been shown in Fig. 4 using a flow diagram containing all the sub-processing steps with its inputs and outputs. In the flow chart red, blue, white and green colored boxes indicate input data, different sub-process steps, intermediate results and the end results. DInSAR processing through ITG-tool is done in two-pass method, i.e. using two SAR data & an external DEM of the same area. The standard resolution of some of well-known DEM missions vary from 90m to 10m or even finer. The only requirement is that the input DEM needs to be converted to a 2-byte signed integer binary file where the coordinates are either in EQA or UTM projection so that the DEM can be read by the software. So, the inputs of the ITG-tool are : two SAR CEOS format raw data, orbit data (PRC type or ODR type) containing the satellite orbit information at the instant of imaging the corresponding scene and one external DEM (SRTM DEM in TIFF format). From these inputs, ITG-tool can generate deformation map as the end product.

So, in the present version, the software has the capacity of processing SAR data of all three different frequency bands L-band (ALOS PALSAR), C-band (ERS-1&2, EnviSat) and X-band (CSK) with strip map mode data acquisition. It has the ability to process both raw and SLC data sets. The processing facility associated with recent SAR sensor data like, TSX & Sentinel-1 and other acquisition mode (e.g. Spotlight, Scan SAR and TOPS) might be added in future. In this context, the authors will appreciate any indigenous development of such modules from the users and other research groups.

A. A brief summary of each sub-processing steps of ITG-tool

Differential SAR Interferometry (DInSAR) is an advanced interferometric technique with which any topographic surface change or displacement can be measured with high accuracy. In ITG-tool, first we need two SAR images are taken over the same area with some temporal gap. Using these two SAR images and one external DEM of the same area, interferogram can be generated to distinguish the height difference occurred during the period between two image acquisitions. In next sections, a brief summary of each sub-processing steps associated with ITG-Tool has been described.

1) ***Data Ingestion & Unpacking :*** SAR data usually comes in several formats; some of them are Committee for Earth Observation Satellites (CEOS), Sky Telemetry Format (STF) and Alaska Satellite Facility (ASF) etc. In each of this format, mainly two different processing level data are available which are either in RAW data (*.raw) or in SLC data (*.slc) of different air-borne or space-borne satellites. Generally RAW data are termed as level-0 and SLC data as level-1. Sometimes this level naming convention can be slightly different for some of space agencies[30],[36]. The data encoding techniques for different satellites are different, for this reason data from each mission should be decoded differently in the onboard pre-processing stages. ITG-tool is capable of processing from the very beginning i.e. level-0 or RAW data. For this subprocessing stage, two SAR raw data and their corresponding orbit information are required. As the satellite sensor is revolving around the earth on its specific orbital path at a very high speed (7 km/sec approx.) [14], and the earth itself is also rotating on its own axis, Doppler computation is an important step to focus the raw data to form an image. At the end of this step, we will get two unpacked raw data with their corresponding Doppler information file.

2) ***Raw to SLC :*** The basic idea of SAR processing is to have a 2-D complex image from 3-D projection of the earth. In this step, raw data are focused to generate a complex image through some of the complicated techniques. In 'ITGtool' SAR processing is done using range-doppler algorithm (RDA). In RDA, when a coded pulse is transmitted from the antenna, the replica of the same pulse

is stored at the receiver and when returned signal received at the receiving end, it needs to be compared with the stored replica to cancel out the noise added during the travel time. This technique is called Matched Filtering[37]. The received response from any point target on earth spreads out both across the track (range direction) and along the track (azimuth direction). So, to get back the focused point target image, first the matched filter operation is done on range responses on frequency domain as range compression[15],[16]. As the spacecraft moves along its track, the same point in a footprint are illuminated from different places at varying angles generates an arc-shaped response for different range to target distances. Range cell migration (RCM) is another important technique to get a straightened image response[38]. Finally, the same matched filter is applied in azimuth frequency domain, called azimuth compression and then we get a focused single look complex (SLC) image[29].

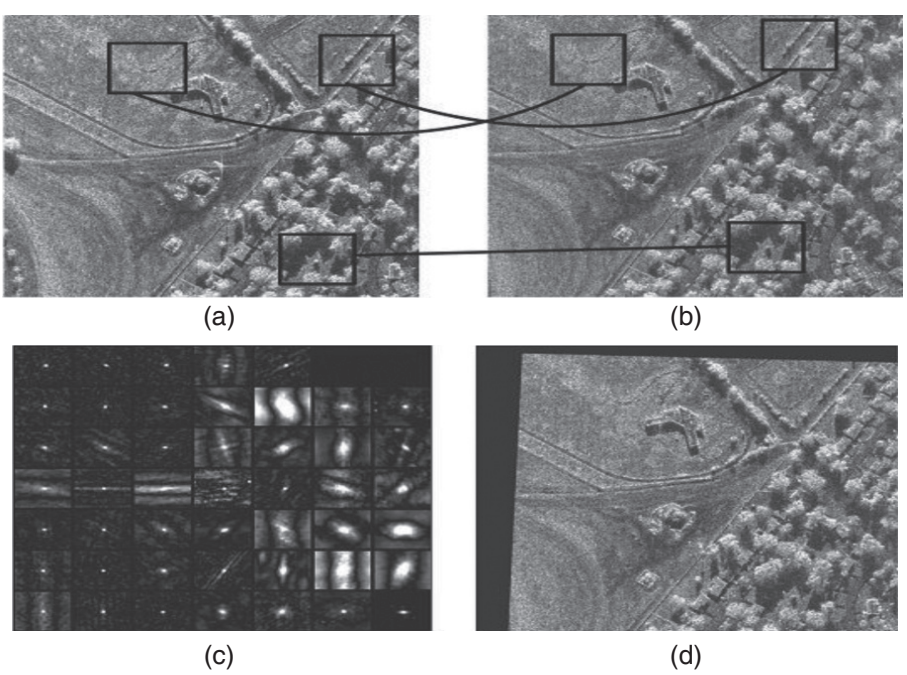

Fig. 5 : Representation of image co-registration via tie point mapping. (a) Three chosen sub-regions of master image for co-registration. (b) A visible shift in the same three common regions in slave image.
(c) Illustration of magnitudes of 7x7 array of sub-image cross-correlation function.
(d) Slave image after the alignment to register with master image[39]

3) ***Image Co-registration :*** The height estimation of any area depends on the phase difference of the echo pulses from each pixel at the two receivers at the same time (one-pass) or during two different satellite pass (repeat-pass) over the same area. So, it is necessary to ensure that the amplitude and phase of same ground pixels in master and slave are compared for interferometry[40]. The difference between the image co-ordinates of the same point in master and slave is called offset. SAR image co-registration is used to warp slave image to align well with the master with the help some rotation and translation techniques[41]. If the offsets are more, then it's difficult to co-register two images. The co-registration associated with InSAR processing is done twice. At first coarse co-registration where pixel by pixel are compared and then fine co-registration where up to (1/10)th pixel accuracy is maintained[42]. Then the amplitude and phase of each pixel in slave image has been recalculated by interpolation using bilinear or cubic convolution function. The co-registration in InSAR uses a series of cross-correlations between small subimages which are common in both master and slave image, to develop a warping function. This concept, called control point mapping or tie point mapping [43],[44] which is depicted in Fig. 5. The two SLC images f (l,m) and g (l,m) are shown in sub-fig. (a) and (b) of the Fig. 5, as master and slave images respectively. By examining the boxed sub-regions carefully, it is clear that one image is a bit shifted with respect to the other. By considering f(l,m) as the master image, so that slave image g(l,m) will be warped to align with the master image f(l,m). The procedure begins by subdividing both images into small sub-images; in this example, a 7x7 subdivision of the images is shown in Fig. 5(c). Similarity index between the like pixels in master and slave image is well approximated by cross correlation function. The two-dimensional (range & azimuth) correlation co-efficient is given by :

$$s^n_{fg}(l,m) = \frac{E\left[f(l,m)g^*(l,m)\right]}{\sqrt{E\left[|f(l,m)|^2\right]E\left[|g(l,m)|^2\right]}} \qquad (4)$$

The 2-D cross-correlation $s^n_{fg}(l,m)$ is calculated for each of the corresponding pairs of sub-images; the superscript n indicates the n^{th} sub-image. The magnitudes of the 49 cross-correlation functions are shown in Fig. 5(c). If a well-defined cross-correlation peak occurs at lag (0,0); it suggests that

no shift or offset is there or two sub-images are well aligned in both range and azimuth direction. If the cross-correlation peak occurs at some non-zero lag (kl, km), it indicates that the area of the slave image is offset from the corresponding region of the master image by kl pixels in range and km pixels in azimuth. If a sub-region has low reflectivity due to shadow or a relatively featureless terrain such as a water body, the correlation peak will diffuse and this may be a poor indicator of the required warping. Such sub-images can be detected by measuring the peak-to-rms ratio of the sub-image correlation.[39]

$$\xi = \frac{max\left\{s_{fg}^2(l,m)\right\}}{\sqrt{\frac{1}{LM}\sum_l \sum_m s_{fg}^2(l,m)}} \qquad (5)$$

ξ will have the higher values for sharp correlation peaks than for diffuse peaks. A threshold value of ξ can be fixed to eliminate unreliable sub-image correlations.

4) ***Interferogram generation :*** Once two images are coregistered, the phase of each pixel of slave image is subtracted from corresponding pixels of the master image. This complex operation is done by multiplication between the master image and complex conjugate of slave image[45]. The generated phase contained image from this step is called interferogram. The wrapped phase of the interferogram is calculated by[21] :

$$\phi_{fg}[l,m] = arg\left\{\sum_{n=1}^{N} f[l,m]g^*[l,m]\right\} \qquad (6)$$

Where, N is interferogram samples.

The interferogram phase is computed for each target P in the (azimuth, slant range) plane. The difference in the sensor target path distance for the two satellites is given by[30] :

$$\phi(P) = \frac{4\pi}{\lambda}[r_M(P) - r_S(P)] \qquad (7)$$

Where, $r_M(P)$ and $r_S(P)$ are the slant range distance for common pixels of master and slave image respectively.

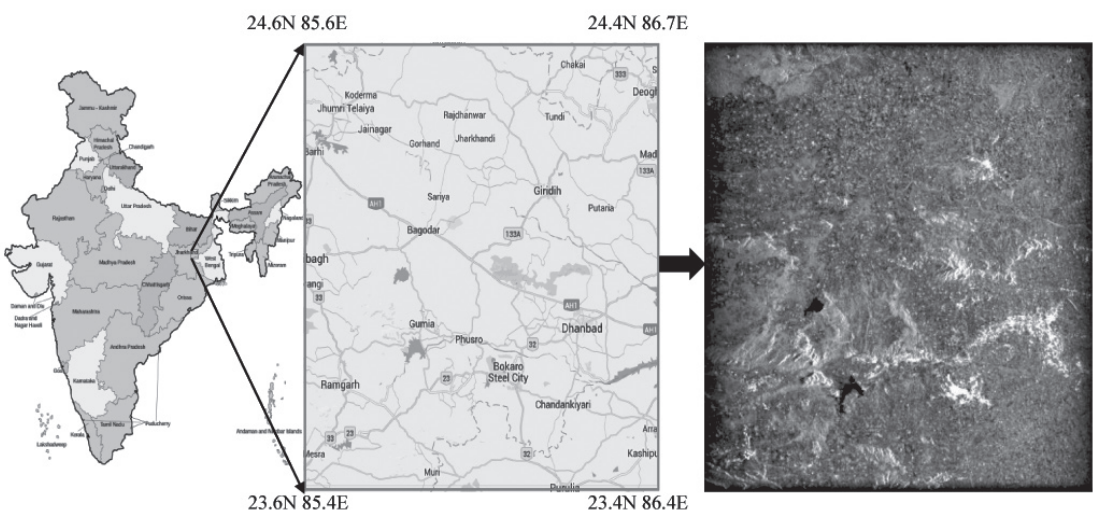

Fig. 6 : The study area and its SLC image.

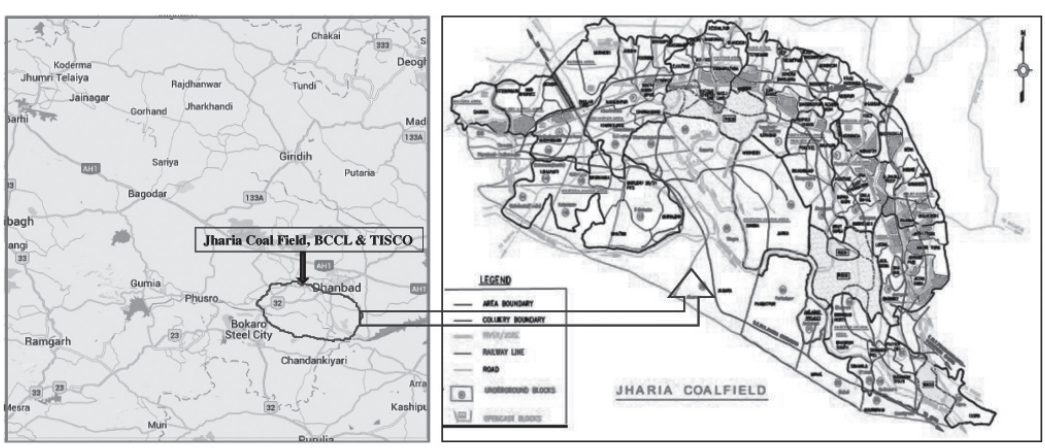

Fig. 7 : Detailed mining map of Jharia Coal Field.

5) **Interferogram Flattening** : In the generated interferogram, two unintended factors, i.e. orbital fringes and topographic contents are available. To get the ground deformation, these two factors are to be removed. For these purpose an external DEM (SRTM-90m has been used for this study) is required. The coarser external DEM helps in two ways in In-SAR processing. With the help of precise orbital information, firstly, it estimates and removes the topography in the final interferogram[30],[45]. Finally, this generates a 'differential interferogram' (DInSAR) suitable for monitoring and detecting the surface changes. Secondly, the external DEM is used to provide an optimal removal of 'baseline de-correlation'[30]. SRTM DEM generally comes in image format (as geo-tiff file) and to incorporate this in ITG-tool, a format conversion step is needed namely, Geo-tiff to DEM. In this step, basically the image file is converted to binary file. From the coarser DEM, a synthetic interferogram is generated by just applying 'height to phase' formula[36]. The phase of the synthetic interferogram can be subtracted from the interferogram to remove the known topography, hence providing a differential interferogram, for monitoring the deformation occurred in between the two image acquisitions. After the interferogram flattening, the numbers of fringes are reduced. At the end of this step, coherence map is generated to observe the similarity and change took place during the acquisition interval on a scale ranging from 0 to 1.

6) ***Phase Unwrapping :*** The flattened interferogram provides an ambiguous interpretation of the relative terrain altitude as the interferometric phase is wrapped in a modulo 2π nature, which makes it necessary to unwrap the phase to derive topographic information. The phase variation between two points in the flattened interferogram gives a measurement of the actual altitude variation, only after adding the appropriate number of altitudes of ambiguity (equivalent to an integer number of 2π phase cycles). The process of adding the correct integer multiple of 2π to the interferometric fringes is called phase unwrapping[19],[22],[46]. In ITG-tool, phase unwrapping technique is done using the very popular branchcut method described in[46]. Once the interferometric phases are unwrapped, an elevation map is obtained but in image coordinate. This is the first step towards getting a Digital Elevation Model (DEM)[25].

7) Geo-coding : In all the above steps mentioned earlier, all the operations were carried out in radar co-ordinate, i.e. range and azimuth. The final unwrapped phase contained image needs to be converted from radar co-ordinate to geographic co-ordinate[47],[48]. The deformation map should then be referred to a conventional ellipsoid (e.g. WGS84) and resampled on a different grid (e.g. UTM). Geo-coded products are usually a subset of the external DEM area, but has the same grid spacing and shifted by an integer number of DEM pixels. In the geocoded deformation map, every 2π radian fringe difference is meant to be half of the wave length path difference. Here the deformation is along the slant range direction[12],[29]. This is the final result of generated from ITG-Tool.

IV. STUDY AREA & DATA USED

The study site has been chosen for DInSAR study based on the fact that the area should have some history of surface change phenomenon due to anthropogenic activities[23],[33]. Deformation monitoring over mining area using various geodetic techniques has been carried out successfully by previous researchers[8]–[11],[33],[49].

For the present study, a coal mining site located at Dhanbad and its vicinity (in eastern part of India) which covers 100*100 Km^2 is selected. It is located between 23.4°–24.6°N and 85.4°–86.7°E as shown in Fig. 6. The area is mostly flat but a large number of coal mines are there in and around the area of Asansol-Dhnabad region. A small part of this area on which our detailed study is based upon, is Jharia Coal Field (JCF) area where three mining companies are there, they are : Bharat Coking Coal Limited (BCCL), Tata Iron & Steel Company (TISCO) & Indian Iron & Steel Company (IISCO)[49]. These three mining companies have more than hundred mines (both underground & open cast) in this area as shown in detailed map of JCF area in Fig. 7. In this map, the green color indicates the open cast mines and pink dots represent underground mines. So, it is observed that open cast mines are located in the farthest periphery of the map and the rest of the area is covered by underground mines.

Three pairs of CEOS format ERS raw data have been used to see the deformation due to mining activities as described in

TABLE I : Detailed specifications of used data sets

Sensor Name	Date of acquisition	Orbit	Track	Frame	Scene Center	Pass	Polarization	Perperndicular baseline (m)
ERS-1	19930224	8423	262	3122	23.54N 85.93E	Descending	VV	203
	19930331	8924	262	3122	23.54N 85.93E	Descending	VV	
Tandem ERS	19960517	25300	262	3122	23.54N 85.93E	Descending	VV	120
	19960518	5627	262	3122	23.54N 85.93E	Descending	VV	
ERS-2	19960413	5126	262	3122	23.54N 85.93E	Descending	VV	161
	19960518	5627	262	3122	23.54N 85.93E	Descending	VV	

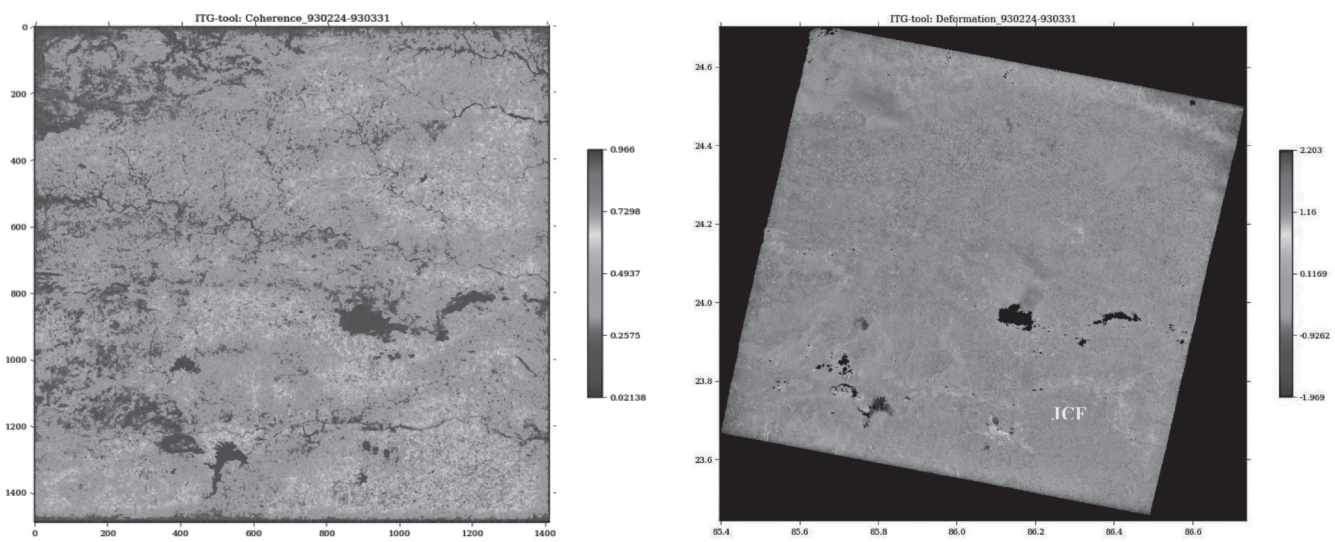

(a) (b)

Fig. 8 : (a) Coherence map (b) Geo-coded deformation map along slant range direction for ERS-1 data pair.

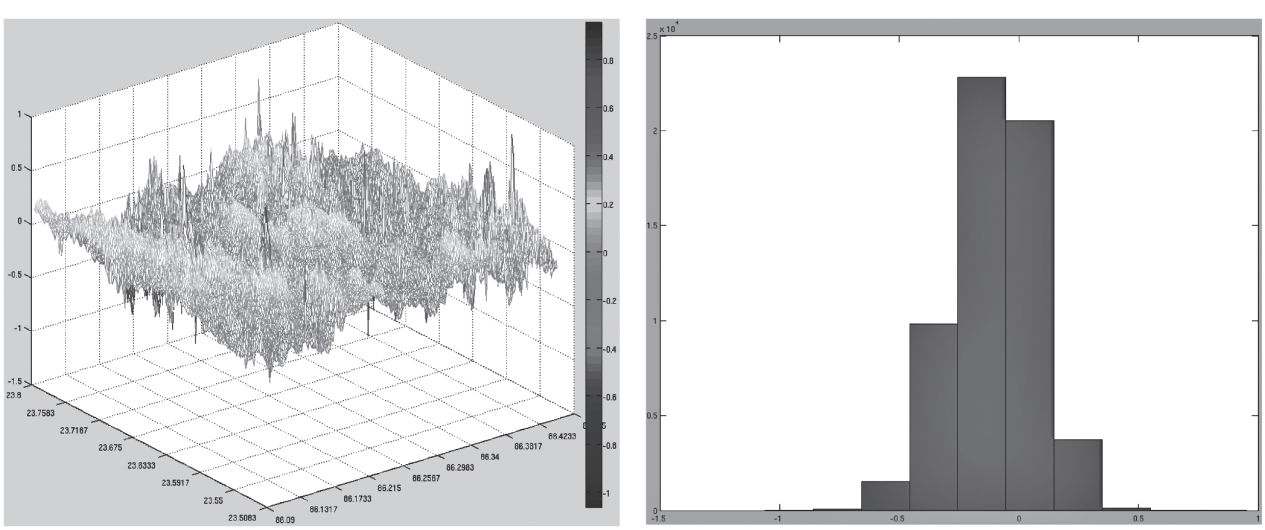

(a) (b)

Fig. 9 : (a) 3-D Mesh plot of deformation of JCF area; (b) Histogram of 3-D mesh plot for ERS-1 data pair.

Table 1. First pair is of ERS-1 dated on 24th February 1993 and 31st March 1993 i.e. with 35 days interval. Second pair is Tandem-ERS i.e. ERS-1 dated on 17th May 1996 and ERS-2 on 18th May 1996 with 24 hours interval between ERS-1 & ERS-2 satellite pass. The third pair is ERS-2 dated on 13th April 1996 and 18th May 1996. All the data are in descending mode and VV polarization.

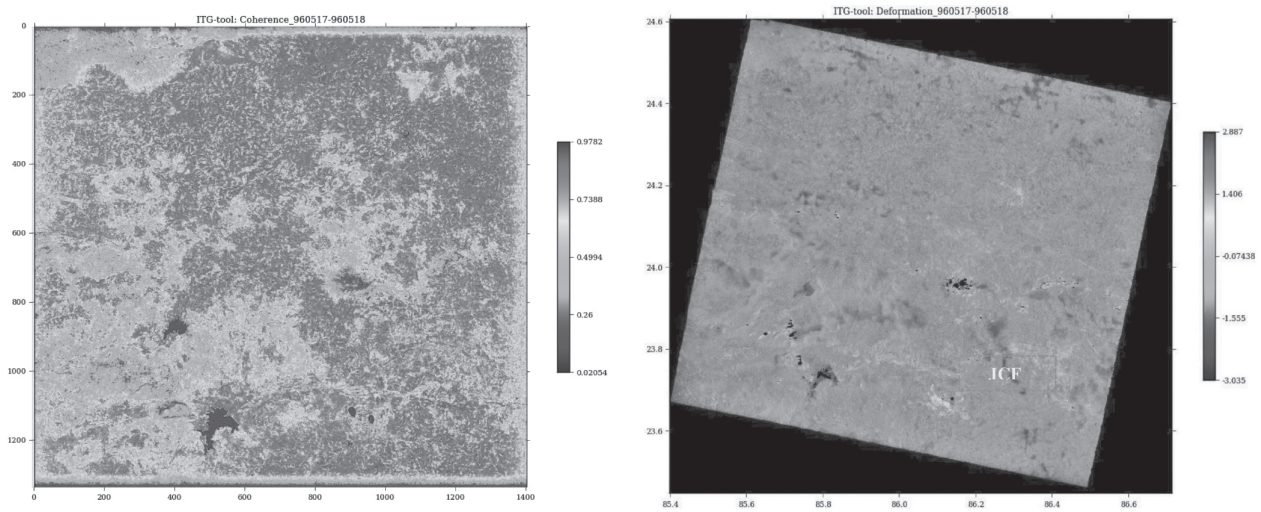

(a) (b)

Fig. 10 : (a) Coherence map (b) Geo-coded deformation map along slant range direction for Tandem-ERS data pair.

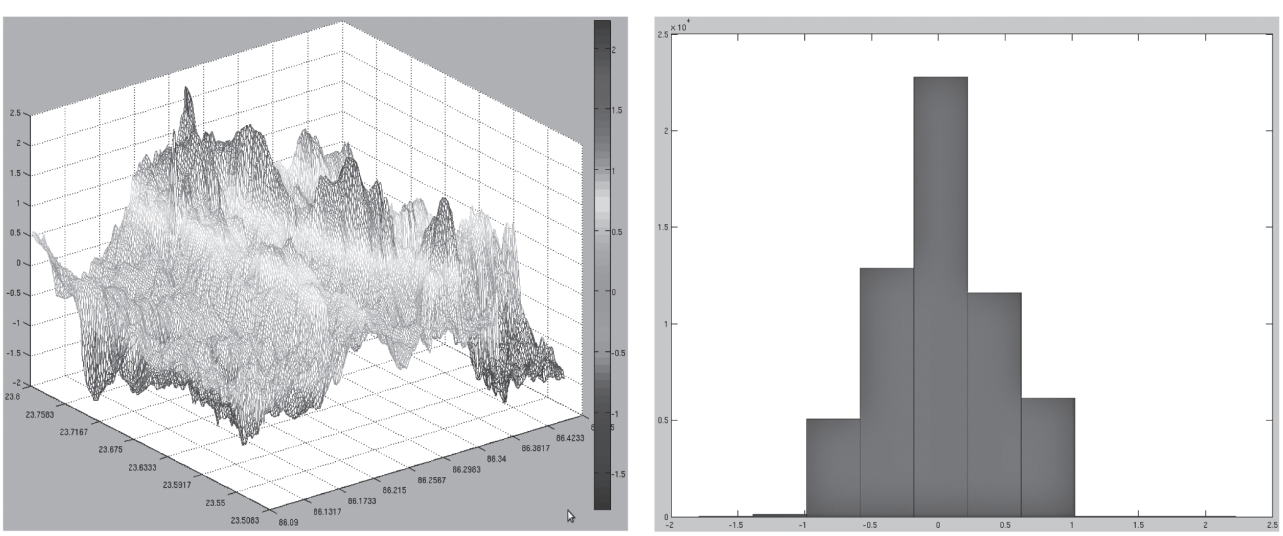

(a) (b)

Fig. 11 : (a) 3-D Mesh plot of deformation of JCF area; (b) Histogram of 3-D mesh plot for Tandem-ERS data pair.

V. RESULTS & DISCUSSION

A. Case-I : ERS-1

For viewing of results generated from 'ITG-tool', a python based viewer has been developed. However, for further analysis of the software generated results, such as : 3-D displacement mapping, deformation histogram plot, etc., a licensed MATLAB can be used. The ERS-1 data pair (930224-930331) has been processed and coherence maps & deformation maps are viewed in python viewer. The other two results, i.e., 3-D mesh plot and histogram of the deformation map are shown using our own written MATLAB code.

The coherence map generated from the above mentioned data pair is shown in Fig. 8(a). A color bar is showing the range between 0-1. Where 0 or blue color represents the least coherence and 1 or red color represents the highest coherence. The final geo-coded deformation map is shown in Fig. 8(b) and it is tilted towards right side due to satellite's right look and

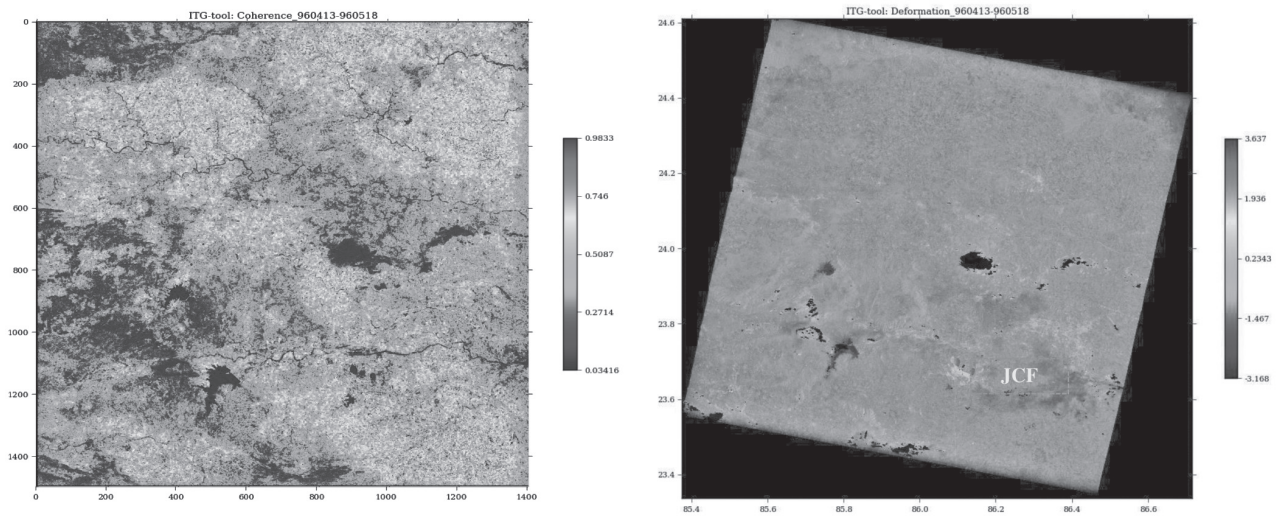

(a) (b)

Fig. 12 : (a) Coherence map (b) Geo-coded deformation map along slant range direction for ERS-2 data pair.

descending (i.e. from South Pole to North Pole) motion. The color value of each pixel represents the change in sensor to target or LOS distance. As the master and slave images are considered to be the former and latter acquisitions respectively and we are subtracting phase of slave from the phase of master image. So, positive pixel value indicates decrease of phase in slave compared to master or decrease in the LOS distance and vice versa[50]. Hence, any positive value denotes an emergence or upliftment and negative value signifies the subsidence. From the whole study area, one small portion which is Jharia Coal Field (JCF) region as shown in red dotted line in Fig. 8(b), has been taken for further analysis. JCF area is located at 23.64° – 23.80°N and 86.09° – 86.46°E.

The 3-D mesh plot of JCF area is shown in Fig. 9(a) where, X-axis, Y-axis and Z-axis are longitude, latitude and deformation in cm respectively. A histogram plot is drawn from the 3-D plot as shown in Fig. 9(b) where X-axis is the deformation in cm and Y-axis is number of pixels lying in a specific deformation interval. It is clearly shown that most of the area is facing slight subsidence in the range of 0 to -0.5 cm, while some of the distinct portions appear to be uplifted as indicated in red color in Fig. 9(a). This might be due to increase in the height of over-burden dumps near the opencast mines that may have taken place during the 35 days acquisition interval.

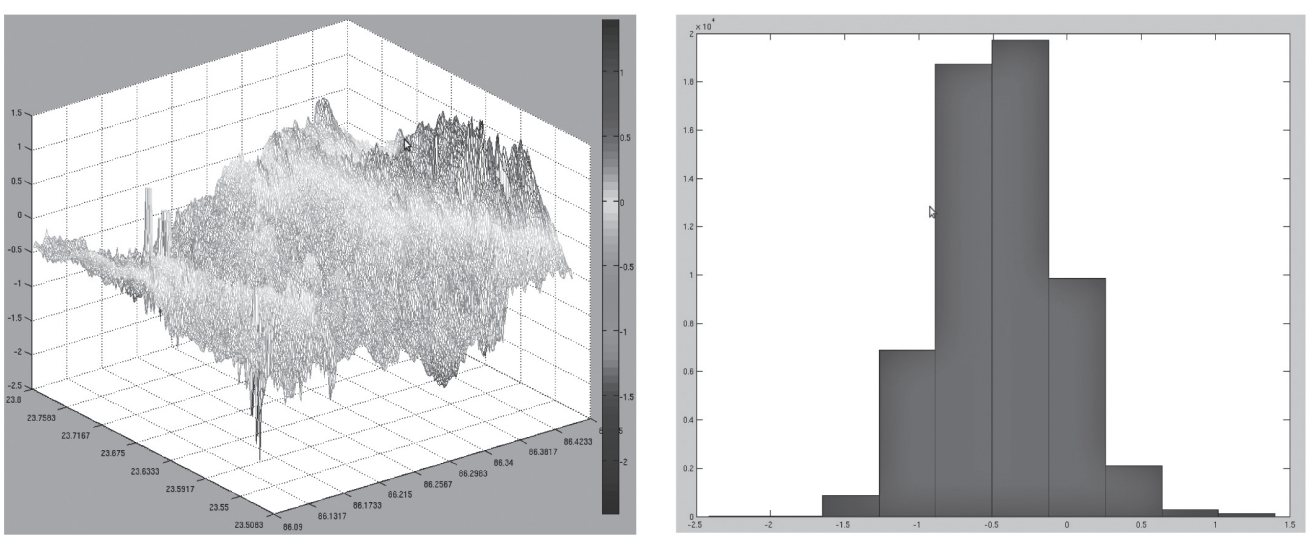

(a) (b)

Fig. 13 : (a) : 3-D Mesh plot of deformation of JCF area; (b) Histogram of 3-D mesh plot for ERS-2 data pair.

B. Case II : Tandem-ERS

The Tandem-ERS mission gave some advantages and benefits for both research and applications by flying two identical sets of instruments (ERS-1 and ERS-2) in the same orbital configuration, for a unique SAR data set could be collected in interferometric applications[51]. The temporal baseline between the tandem pass happens to be 24-hours interval[30]. A pair of Tandem-ERS data (960517-960518) has been processed through ITG-Tool. The coherence is expected to be much better due to only 24-hours time gap between two acquisitions. Most of the points are lying near to 1 (i.e. high coherence), apart from some vegetation and water reservoir area as blue patches shown in Fig. 10(a). From the geo-coded deformation map shown in Fig. 10(b), the same JCF area is taken for generating the 3-D mesh plot to see the deformation due to anthropogenic activities. From the Fig. 11(a), it is seen that pixels are ranging from -1.5 to +2.5 cm with an undulating nature. Those can be due to orbital affects for the two different satellites. There are some positive peaks which may be due to the same overburden dumps caused due to open cast mining activities during the interval between tandem pass. The histogram of the 3-D plot depicted in Fig. 11(b) indicates that most of the pixels are lying at 0 cm and its neighborhoods.

C. Case III : ERS-2

Lastly, a pair of ERS-2 data sets over the same mining area has been processed. The coherence map and geo-coded deformation map is shown in Fig. 12(a) and Fig. 12(b) respectively. The 3-D plot of the JCF area has been presented in Figure 13(a). From the histogram plot as indicated in Figure 13(b), it can be demonstrated that most of pixels are lying below 0 cm value. So, apart from some small regions most of the JCF area is experiencing subsidence up to -1.5 cm for the duration of 35 days acquisition interval. From a closer view of this 3-D plot, the farthest periphery is experiencing some upliftment as most of the open cast mines are located on that particular area. Whereas, rest of the area is experiencing subsidence due to underground mining activities which is fully supporting the detailed area map of JCF as shown in Fig. 7. The upliftment observed is due to increase in the height of overburden dumps lying beside the open cast mines.

Numerous researchers had conducted similar kind of studies which showed that DInSAR can detect mining induced deformation upto sub-centimeter accuracy[4],[7],[52],[53]. The present study was specifically carried out to exhibit the efficacy of the developed software tool to measure ground deformation as a result of underground mining operations. However, validation of DInSAR based results with ground truth data will be taken up as a future scope for the betterment of this developed tool.

VI. CONCLUSION

The study area is facing problems with subsidence due to the century old history of underground mining from the coal blocks stored beneath the surface. To quantify and analyze the mining subsidence, DInSAR can be a very effective tool from the perspective of sub-centimeter level of accuracy and its ability to remotely monitor a large area in a regular interval. So, the developed ITG-Tool can be very useful for DInSAR processing and analysis for monitoring the surface deformation over a large area with reasonable accuracy level.

ACKNOWLEDGMENT

The authors would like to thank Indian Space Research Organisation for funding this research study, European Space Agency for providing the required data, and National Aeronautics and Space Administration for some technical assistance. They would also like to thank Dr. Ran Novitsky Nof (Berkeley Seismological Laboratory) for his valuable suggestions during the development of the image viewer. They acknowledge the anonymous reviewer for his/her reviewing remarks and suggestions.

REFERENCES

[1] C. R. Dunrud, “Coal mine subsidence western united states,” Reviews in Engineering Geology, vol. 6, pp. 151–194, 1984.

[2] L. Ge, H.-C. Chang, C. Rizos, M. Omura et al., “Mine subsidence monitoring: a comparison among envisat, ers, and jers-1,” in 2004 ENVISAT Symposium, 2004, pp. 4–9.

[3] H.-C. Chang, L. Ge, and C. Rizos, “Dinsar for mine subsidence monitoring using multi-source satellite sar images,” in Geoscience and Remote Sensing Symposium, 2005. IGARSS’05. Proceedings. 2005 IEEE International, vol. 3. IEEE, 2005, pp. 1742–1745.

[4] S. Dong, H. Yin, S. Yao, and F. Zhang, “Detecting surface subsidence in coal mining area based on

dinsar technique," Journal of Earth Science, vol. 24, no. 3, pp. 449–456, 2013.

[5] C. Casta˜neda, F. Guti´errez, M. Manunta, and J.P. Galve, "Dinsar measurements of ground deformation by sinkholes, mining subsidence, and landslides, ebro river, spain," Earth Surface Processes and Landforms, vol. 34, no. 11, pp. 1562–1574, 2009.

[6] L. Ge, H.-C. Chang, and C. Rizos, "Mine subsidence monitoring using multi-source satellite sar images," Photogrammetric Engineering & Remote Sensing, vol. 73, no. 3, pp. 259–266, 2007.

[7] G. Herrera, M. A´. Ferna´ndez, R. Toma´s, C. Gonza´lez-Nicieza, J. M. Lo´pez-Sa´nchez, and A. A´. Vigil, "Forensic analysis of buildings affected by mining subsidence based on differential interferometry (part iii)," Engineering Failure Analysis, vol. 24, pp. 67–76, 2012.

[8] A. H.-M. Ng, L. Ge, K. Zhang, H.-C. Chang, X. Li, C. Rizos, and M. Omura, "Deformation mapping in three dimensions for underground mining using InSAR - Southern highland coalfield in New South Wales, Australia," International Journal of Remote Sensing, vol. 32, no. 22, pp. 7227–7256, 2011.

[9] J. Engelbrecht, "Parameters Affecting Interferometric Coherence and Implications for Long-term Operational Monitoring of Mining-induced Surface Deformation," Ph.D. dissertation, University of Cape Town, 2013.

[10] M. Ji, X. Li, S. Wu, Y. Gao, and L. Ge, "Use of SAR interferometry for monitoring illegal mining activities : A case study at Xishimen Iron Ore Mine," Mining Science and Technology (China), vol. 21, no. 6, pp. 781–786, Nov. 2011.

[11] L. Ge, C. Rizos, S. Han, and H. Zebker, "Mining Subsidence Monitoring using the Combined InSAR and GPS Approach Mining," in The 10th FIG International Symposium on Deformation Measurements, 2001, pp. 1–10.

[12] D. Massonet and K.L. Feigl, "Radar interferometry and its application to changes in the earth's surface," Review of Geophysics, vol. 36, no. 4, pp. 441–500, 1998.

[13] Y.K. Chan and V.C. Koo, "An Introduction to Synthetic Aperture Radar (SAR) Y.K. Chan and V.C. Koo," Progress in Electro magnetics Research B, vol. 2, pp. 27–60, 2008.

[14] R.F. Hanssen, Radar Interferometry : Data Interpretation and Error Analysis, M.S. Meer, Freek van der, Michael Abrams, Paul Curran, Arnold Dekker, Steven de Jong, Ed. Kluwer Academic Publishers, 2002.

[15] A. Hein, Processing of SAR Data : Fundamentals, Signal Processing, Interferometry. Springer, 2004.

[16] J.C. Curlander and R.N. McDonough, Synthetic Aperture Radar Systems and Signal Processing, J. A. Kong, Ed. John Wiley & Sons, Inc., 1991.

[17] H. Balzter, "Forest mapping and monitoring with interferometric synthetic aperture radar (InSAR)," Progress in Physical Geography, vol. 25, no. 2, pp. 159–177, 2001.

[18] N. Madsen, H.A. Zebker, and J. Martin, "Topographic Mapping Using Radar Interferometry : Processing Techniques," IEEE Transactions on Geoscience and Remote Sensing, vol. 31, no. 1, pp. 246–256, 1993.

[19] P. A. Rosen, S. Hensley, I. R. Joughin, F. K. Li, S. R.N. Madsen, E. Rodr´ıguez, and R. M. Goldstein, "Synthetic Aperture Radar Interferometry," Processdings of the IEEE, vol. 88, no. 3, pp. 333–382, 2000.

[20] S. Barbot, Y. Hamiel, and Y. Fialko, "Space geodetic investigation of the coseismic and postseismic deformation due to the 2003 Mw7.2 Altai earthquake : Implications for the local lithospheric rheology," Journal of Geophysical Research : Solid Earth, vol. 113, no. 3, pp. 1–15, 2008.

[21] R. Bamler and P. Hartl, "Synthetic aperture radar interferometry," Inverse Problems, vol. 14, pp. 1–54, 1998.

[22] M. Simons and P.A. Rosen, "Interferometric Synthetic Aperture Radar Geodesy," Treatise on Geophysics, vol. 3, pp. 391–446, 2007.

[23] P. Milillo, B. Riel, B. Minchew, S.-H. Yun, M. Simons, and p. Lundgren, "On the synergistic use of sar constellations' data exploitation for earth science and natural hazard response," Selected Topics in Applied Earth Observations and Remote Sensing, IEEE Journal of, vol. PP, no. 99, pp. 1–6, 2015.

[24] J. Catalao, G. Nico, P. Lollino, V. Conde, G. Lorusso, and C. Silva, "Integration of insar analysis and numerical modeling for the assessment of ground subsidence in the city of lisbon, portugal,"

Selected Topics in Applied Earth Observations and Remote Sensing, IEEE Journal of, vol. PP, no. 99, pp. 1–11, 2015.

[25] H.a. Zebker, S. Hensley, P. Shanker, and C. Wortham, "Geodetically accurate InSAR data processor," IEEE Transactions on Geoscience and Remote Sensing, vol. 48, no. 12, pp. 4309–4321, 2010.

[26] N.B.D. Bechor and H.a. Zebker, "Measuring two-dimensional movements using a single InSAR pair," Geophysical Research Letters, vol. 33, no. 16, pp. 1–5, 2006.

[27] N. Bechor, "Extending Interferometric Synthetic Aperture Radar Measurement from One to Two Dimensions," Ph.D. dissertation, Stanford University, 2006.

[28] I.H. Woodhouse, "intro2radar : A Visual Introduction to Radar Remote Sensing," 2013.

[29] G. Franceschetti and R. Lanari, Synthetic Aperture Radar Processing. CRC Press, 1999.

[30] A. Ferretti, A. Monti-guarnieri, C. Prati, F. Rocca, and D. Massonet, InSAR Principles : Guidelines for SAR Interferometry Processing and Interpretation, Karen Flethcher, Ed. Noordwijk, Netherlands : ESA Publications, ESTEC, 2007, no. TM-19.

[31] H. Zebker and K. Chen, "Accurate Estimation of Correlation in InSAR Observations," IEEE Geoscience and Remote Sensing Letters, vol. 2, no. 2, pp. 124–127, 2005.

[32] L.C. Graham, "Synthetic Interferometeric Radar for Topographic Mapping," Proceedings of the IEEE, vol. 62, no. 6, pp. 763–768, 1974.

[33] C. Carnec and C. Delacourt, "Three years of mining subsidence monitored by SAR interferometry, near Gardanne, France," Journal of Applied Geophysics, vol. 43, no. 1, pp. 43–54, Jan. 2000.

[34] T.K. Dey, B. Manna, D. Chakravarty, B. Samanta, and A.R. Misra, "ITG-tool : An InSAR processing software for measuring surface change using DInSAR technique," in International Expert Meet on Microwave Remote Sensing. IEEE GRSS Gujarat Chapter, 2013, pp. 33–35.

[35] B. Manna, T.K. Dey, D. Chakravarty, A.R. Misra, and B. Samanta, ""ITG-Tool": A GUI Based Software for Interferometric SAR Processing for Monitoring Surface Deformation," in NISAR Science Workshop, SAC Ahmedabad, India, 2014, pp. 1–6.

[36] R. Burgmann, P.A. Rosen, and E.J. Fielding, "Synthetic Aperture Radar Interferometry to Measure Earth's Surface Topography and it's Deformation," Annual Review of Earth and Planetary Sciences, vol. 28, pp. 169–209, 2000.

[37] S. Haykin, Communication Systems, 4th ed. Wiley India (P.) Ltd., 2009.

[38] I.G. Cumming and F.H. Wong, Digital Processing of Synthetic Aperture Radar Data. Artech House Inc., 2005.

[39] M.A. Richards, "A Beginner's Guide to Interferometric SAR Concepts and Signal Processing," IEEE A&E Systems Magazine, vol. 22, no. 9, pp. 5–29, 2007.

[40] R. Scheiber and A. Moreira, "Coregistration of interferometric sar images using spectral diversity," Geoscience and Remote Sensing, IEEE Transactions on, vol. 38, no. 5, pp. 2179–2191, Sep 2000.

[41] W. Zou, Y. Li, Z. Li, and X. Ding, "Improvement of the accuracy of InSAR image co-registration based on tie points - A review," Sensors, vol. 9, no. 2, pp. 1259–1281, 2009.

[42] U.G. Sefercik and I. Dana, "Crucial Points of Interferometric Processing for Dem Generation Using High Resolution Sar Data," ISPRS - International Archives of the Photogrammetry, Remote Sensing and Spatial Information Sciences, vol. XXXVIII-4/, no. June, pp. 289–296, 2012.

[43] T. Wang, S. Jonsson, and R. Hanssen, "Coregistration between sar image subsets using pointwise targets," in Proceedings of 'Fringe 2011 Workshop', vol. ESA SP-697, no. January 2012, 2012, pp. 1–6.

[44] B. Zitov´a and J. Flusser, "Image registration methods : A survey," Image and Vision Computing, vol. 21, no. 11, pp. 977–1000, 2003.

[45] S.H. Yun, H. Zebker, P. Segall, A. Hooper, and M. Poland, "Interferogram formation in the presence of complex and large deformation," Geophysical Research Letters, vol. 34, no. 12, pp. 1–6, 2007.

[46] H.A.Z. Richard M. Goldstein and C.L. Warner, “Satellite Radar Interferometry : Two-dimensional Phase Unwrapping,” Radio Science, vol. 23, no. 4, pp. 713–720, 1988.

[47] O. Mora, R. Lanari, J. Mallorqui, P. Berardino, and E. Sansosti, “A new algorithm for monitoring localized deformation phenomena based on small baseline differential SAR interferograms,” IEEE International Geoscience and Remote Sensing Symposium, vol. 2, no. 11, pp. 2375–2383, 2002.

[48] F.I. Okeke, “InSAR Operational and Processing Steps for DEM Generation InSAR Operational and Processing Steps for DEM Generation,” pp. 1–13, 2006.

[49] R.S. Chatterjee, R.C. Lakhera, and V.K. Dadhwal, “Insar coherence and phase information for mapping environmental indicators of opencast coal mining: a case study in jharia coalfield, jharkhand, india,” Canadian Journal of Remote Sensing, vol. 36, no. 4, pp. 361–373, 2010.

[50] D. Ghosh and D. Chakravarty, “Integration of DInSAR Technique and Conventional Methods through GIS for Verification of Quantified Surface Changes,” Journal of the Indian Society of Remote Sensing, vol. 40, no. 2, pp. 179–190, 2012.

[51] J. Slacikova and M. Potuckova, “Evaluation of Interpolation Methods in InSAR DEM Derivation from ERS Tandem Data,” in 31st EARSeL Symposium, L. Halounova, Ed., 2011, pp. 544–551.

[52] M. Przyłucka, G. Herrera, M. Graniczny, D. Colombo, and M. B´ejar- Pizarro, “Combination of conventional and advanced dinsar to monitor very fast mining subsidence with terrasar-x data : Bytom city (poland),” Remote Sensing, vol. 7, no. 5, pp. 5300–5328, 2015.

[53] V. Spreckels, U. Wegm¨uller, T. Strozzi, J. Musiedlak, and H.-C. Wichlacz, “Detection and observation of underground coal mining-induced surface deformation with differential sar interferometry,” in ISPRS Workshop” High Resolution Mapping from Space, 2001, pp. 227–234.

COMPARISON OF EFFICIENCY OF USE OF POLYURETHANE COATING OF HYDROTRANSPORT PIPELINES AND STEEL PIPELINES ON THE BASIS OF PARAMETERS OF ABRASIVE WEAR

Prof Victor Alexandrov*, Prof Maria Vasilyeva**, Prof Olga Kochergina***

ABSTRACT

The paper presents analytical calculations of specific pressure loss in hydraulic transport of the Kachkanarsky GOK iron ore processing tailing slurry. The calculations are based on the results of the experimental studies on specific pressure loss dependence upon hydraulic roughness of pipelines internal surface, lined with polyurethane coating. The experiments proved that hydraulic roughness of polyurethane coating is by the factor of four smaller, than that of steel pipelines, resulting in decrease of hydraulic resistance coefficients entered into calculating formula of specific pressure loss - the Darcy-Weisbach formula. Relative and equivalent roughness coefficients are calculated for pipelines with polyurethane coating and without it. Comparative calculations show that hydrotransport pipelines polyurethane coating application is conductive to specific energy consumption decrease in hydraulic transport of the Kachkanarsky GOK iron ore processing tailings slurry by the factor of 1.5.

Keywords : roughness, hydraulic resistance coefficient, equivalent roughness, slurry, specific pressure loss.

1. INTRODUCTION

Pressure loss is one of the main parameters of hydraulic transport raw minerals processing, as actually determined operational energy costs in the hydraulic transport system. Modern trends in productivity growth as a result of the mining enterprise engaging in the processing of large volumes of all ores are responsible for increasing the load on the hydraulic transport system and tail slurries - on the tailings storage, respectively. The operational system of hydrotransport efficiency can be estimated at the cost of a particular energy transportation process [Aleksandrov V. I. et al, 2015, 2012]

It is known that the main energy losses arise when the liquid flow rubs against the inner surface of the pipeline. They depend on the value of the coefficient of hydraulic resistance included in the formula for Darcy-Weisbach [Darcy H., 1857].

Hydraulic drag coefficient is a function of the relative pipe wall roughness and Reynolds numbers [Heywood N. et al, 1978, 2003] and determines the fluid flow regime, i.e.

$$\lambda = f(\varepsilon, \mathrm{Re}), \qquad (1)$$

At the Kachkanar GOK, industrial testing of high density polyethylene pipelines was carried out. The tests did not show a significant increase in the service life of the slurry pipeline. The outlet pipeline was made of polyethylene pipes installed on the pipeline of the distribution slurry during the working week, when the through hole is worn by solid particles.

At the same factory angular rotations of technical fluids were used, lined with internal walls of polyurethane coating. Operation with a polyurethane coating turns shows that in this case, the service life of more than 10 times longer than the angular rotations of steel without a polyurethane coating.

2. HYDRAULIC DRAG COEFFICIENT AND THE FLOW REGIME

From hydraulics know that the coefficient of hydraulic resistance does not depend on the roughness of the inner surface of the pipeline and in laminar regime ($\mathrm{Re} \leq 2300$) is a function only of the Reynolds number by the Stokes formula or by the Blasius formula for hydraulically smooth pipes. Such regimes are possible with hydraulic transport of highly concentrated fine-dispersed mixtures, when rheological properties appear in the flow of pulp.

In practice all hydrotransport pipelines operating mode in the transition to turbulent and turbulent regimes, determining when the magnitude value of the hydraulic resistance value has a pipe wall roughness [Kumar U. et al, 2015; Schmitt D. J., 2004].

* *Head of Department Mining Transport Machines, Saint-Petersburg Mining University, 199106, Saint Petersburg, 21 Linia 2, RUSSIA, victalex@mail.ru*

** *Associate Professor of the Department of Mining Transport Machines, Saint-Petersburg Mining University, 199106, Saint Petersburg, 21 Linia 2, RUSSIA, saturn.sun@mail.ru*

*** *Associate Professor, PhD, Department of Foreign Languages, Saint-Petersburg Mining University*

Let's calculate the value of the Reynolds number for the conditions of Kachkanar GOK by formula :

$$\mathrm{Re} = \frac{vD\rho_h}{\mu}, \qquad (2)$$

Let us assume for the calculation of the following values of the basic parameters: D = 1000 mm; v=4,8 m/s; ρ_h=C_v(ρ_h-1)+1=0.033(3.3-1)+1=1092 kg/m^3; μ = 1.017.10^{-3} 3 Pa·s.

In the calculation it is assumed that the mass concentration is equal to the tailings slurry CP = 10%, which corresponds to $c_v \cong 3\%$ by the formula :

$$c_v = c_p \frac{\rho_h}{\rho_s} = 0.1\frac{1092}{3300} = 0.033 .$$

For pipe 1000 mm, the Reynolds number :

$$\mathrm{Re} = \frac{4.8 \cdot 1.0 \cdot 1092}{1.017 \cdot 10^{-3}} = 5.154 \cdot 10^6.$$

For pipeline 900 mm and average velocity of pulp v = 4.0 m/s and similar parameters, the Reynolds number is equal to :

$$\mathrm{Re} = \frac{4.0 \cdot 0.9 \cdot 1092}{1.017 \cdot 10^{-3}} = 3.865 \cdot 10^6.$$

In fact, we find that the pulp flow regime in pipes is developed turbulent.

When developed turbulent regime the hydraulic drag coefficient is independent of the Reynolds number, as determined by the relative roughness coefficient in accordance with the formula Shifrison

$$\lambda = 0{,}11\varepsilon^{0.25} . \qquad (3)$$

2.1 Physical roughness of the inner surface of pipes

Experimental investigations of surface roughness of pipelines with polyurethane coating were carried out in the hydraulic laboratory of the St. Petersburg Mining University. The coating material is polyurethane having a hardness Shore surface - 83A, 85A and 90A . Experienced coated pipe samples are shown in Fig. 1.

Surface roughness of the coating is measured using a special device, SJ-210. Contact profilometer (surface roughness meter) is an inductive sensor (detector in the form of a probe) with a diamond needle and based on the measured area. The needle (probe) moves perpendicular to the inspected surface. The sensor generates pulses that pass through an electronic amplifier. Emerging with mechanical oscillation probe converted into a digital signal. Statistical analysis of several of these signals allows us to calculate the average value of the parameter - quantitative characteristic plot irregularities based on a certain length.

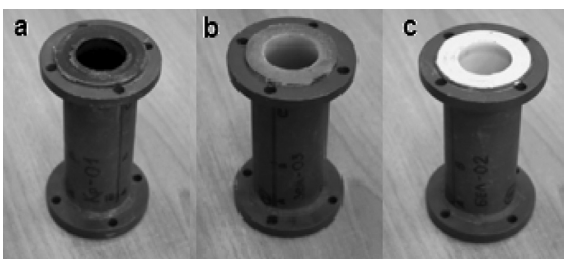

Fig. 1 General view of the prototypes pipes with polyurethane coating: a - hardness Shore 83A; b - hardness of 85A; c- hardness 90A

The test installation was assembled to carry out the measurements, the general form of which is shown in Fig. 2.

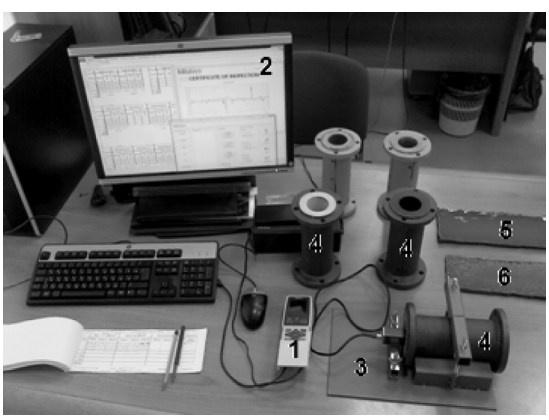

Fig. 2 General view of the measurement setup: 1 - profilometer, 2 – PC, 3 - lodgment, 4 - prototypes with a polyurethane coating, 5 - element of the steel pipe (new pipe), 6 - element of a steel pipe with a run-roughness (trumpet, the former in operation)

Measurements of the surface roughness of prototype tubes made according to the three coating forming on the inner length of 120 mm, a next bend in the samples 120° and three line samples on steel pipes. The total number of measurements at each measurement sample was equal to 27. The measured values were averaged. The arithmetic mean value is taken as the absolute surface roughness . The results of each measurement to be displayed on the computer screen in the form of a spectrogram and characteristic table values.

The absolute roughness prototypes pipelines are given in Table. 1, where Ra means arithmetic average.

Table 1 : Surface roughness prototypes pipes coated with polyurethane

The measuring point	hardness 83A			hardness 85A			hardness 90A		
	Line I	Line II	Line III	Line I	Line II	Line III	Line I	Line II	Line III
	The measured values of roughness (Ra), μm								
A	1.343	0.379	0.54	1.266	0.642	0.564	0.780	0.798	0.636
B	0.73	0.996	0.696	1.389	1.248	0.877	0.799	0.730	0.726
C	0.893	0.57	0.457	0.876	1.039	1.135	0.91	0.554	0.412
R_a	0.988	0.648	0.564	1.177	0.976	0.859	0.830	0.694	0.591
$R_a = \Delta$	**0.734**			**1.004**			**0.705**		

Similar measurements were performed for roughness elements wall steel pipe - new and used, see Table. 2.

Table 2 : Measured values of the inner surface of steel pipe roughness

The measuring point	New pipe			Pipe with a run-roughness (used pipe)		
	Line I	Line II	Line III	Line I	Line II	Line III
	The measured values of roughness (Ra) , μm					
A	2.749	2.809	2.821	5.147	4.199	3.883
B	4.742	4.883	4.913	4.2	3.964	4.088
C	4.903	4.358	4.306	4.618	5.199	5.199
R_a	4.131	4.016	4.306	4.618	4.454	4.39
$R_a = \Delta$	**4.053**			**4.499**		

For assess the nature and intensity changes with a polyurethane coating roughness prototypes pipes experiments on an operating time of roughness were performed on a laboratory hydraulic installation.

In linear part of the pipeline installed three prototypes of pipes with a polyurethane coating. In supply tank of installation capacity of 100 liters poured slurry tailings Kachkanarsky GOK with a weight solids content of 10%. The slurry was pumped through a pipeline with an internal diameter of 50 mm with using the centrifugal pump CP30/18. Pump flow was controlled by a frequency converter. Pump capacity is at maximum motor speed was 45 m3/h. From the pipeline slurry gets into the measuring tank, which is used to determine the flow rate, and then poured into the supply tank.

The practice of hydrotransport shows that the steady value of the surface roughness of steel pipe occurs approximately after one month of continuous operation of the pipeline, which corresponds to 720 hours. The average flow rate in the current pipeline (1000 mm) from the pumping station No. 1 of Kachkanarsky GOK (according to the company) is 4.8 m/s. These data were used to determine the total flow time of the slurry tailings through line pipes and prototypes until a steady operating time the inner surface roughness. Estimated time was 484 hours. To determine the nature and dynamics of the roughness of polyurethane coatings prototypes pipes total run time of the pump unit was divided into several time intervals: 4, 24, 24, 96, 96, 240 (hours). The pump was turned off after each time interval experienced pipe dismantled and measured the accumulated roughness. Values accumulated roughness of experienced pipe samples are shown in Table. 3.

Table 3 : Values accumulated roughness of experienced pipe samples

Sample pipe with a Shore hardness	The average surface roughness (Ra x 10^3 μm) for the operating time, h						
	0	4	28	52	148	242	484
83A	0,734	0,815	0,908	0,876	0,764	0,95	0,828
85A	1,004	1,031	0,975	1,063	0,782	0,788	0,822
90A	0,705	0,783	0,872	0,962	0,983	0,854	0,935
The average value	0,814	0,815	0,918	0,967	0,843	0,864	0,862

From the data of Table. 3 it follows that the roughness after 484 hours working time for all samples experienced pipeline varies slightly. The roughness values are in the range from 0.814 to 0.862 μm. As a result of experimental data processing methods of mathematical statistics was obtained empirical formula for calculating the roughness, depending on the time of operation of the pipeline

$$Ra = 0.814 + 9.92 \cdot 10^{-5} T_{op} . \qquad (4)$$

where Ra - the average roughness of the pipe wall, μm; T_{op}- working time of the pipeline, h.

By equation (4), the value of the accumulated roughness can be calculated as a function of the pipeline working time. For example, at time T_{op} = 2000h (3 months) of continuous operation of hydrotransport system, the average roughness of the inner surface is equal to Ra = 1.012 μm; for T_{op} = 4000 h (5 months) $\rightarrow$ Ra = 1.211 μm; T_{op} = 8000 h (approximately 1 year) $\rightarrow$ Ra = 1.608 μm.

3. Definition of roughness, coefficients hydraulic resistance and the losses of pressure

Adopted in hydraulics method of determining the roughness it takes into account that the natural (geometric $R_a = \Delta$) always heterogeneous - peaks and troughs have different shapes, sizes and location. Surface microrelief internal pipe wall depends on many factors including the material, method of manufacturing pipes and physicochemical properties of the fluid and lifetime. Since the natural roughness has multiple irregular shape (Fig.4a), set by any geometrically methods the averaged value of the height of hillocks, determining the effect of roughness on the pressure loss, it is impossible to. Therefore, the parameter of roughness is considered as a conditional value determined by a special scale of artificial homogeneous roughness (Fig. 4b).

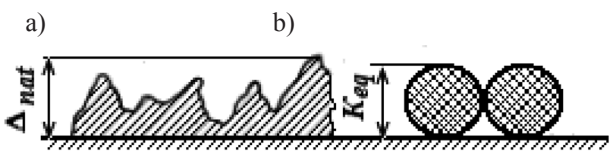

Fig.4 Natural (a) and equivalent roughness (b)

Scale of roughness is constructed with the help of calibrated grains of sand, glued to the smooth surface of the pipe. A set of such pipes with different grain diameters gives a number of values of relative roughness, in the function of which values are obtained (I. Nikuradze's formula) [Nikuradse J., 1932, 1933; Yagi T et al, 1972]

$$\lambda = \frac{1}{\left(2\lg\frac{\Delta}{D} + 1{,}14\right)^2} . \qquad (5)$$

By means of such a scale, the absolute roughness is taken to be its equivalent value, that is, the size of the grains of artificial roughness sand, which in the quadratic region of friction with respect to the hydraulic resistance is equivalent to this inhomogeneous surface.

The results of studies [13] of the relationship between the coefficient of equivalent and natural roughness on 13 samples of low-pressure and high-pressure polyethylene pipes with diameters from 25 to 400 mm, as well as the results of studies carried out by G.A. Trukhin (two reinforced concrete collectors with diameters of 1.6 and 1.94 m) VNII VODGEO (eight water pipes from various materials with diameters from 0.7 to 1.2 m) made it possible to establish a mathematical dependence for determining this connection:

$$K_{eq} = 2 \cdot \Delta^{1{,}33} , \qquad (6)$$

where $\Delta = R_a$ - the natural roughness, μm.

Based on these assumptions, we calculate the value of the equivalent roughness coefficient by the formula (10), given by the operating time of the hydrotransport pipeline T_{op} = 1000 hours. We'll have

$$K_э = 2 \cdot \left(0{,}814 + 9{,}92 \cdot 10^{-5} \cdot 1000\right)^{1{,}33} = 1{,}772 \text{ μm}.$$

Thus, the expected value of the equivalent roughness for a pipeline with a polyurethane coating on the inner surface of the pipe with hardness in the range 83A-95A, after the operating T_{op} = 1000 hours, when pumping the slurry of the Kachkanarsky GOK processing tailings with a mass concentration of solid about 10%, is equal to K_{eq} = 1,772 μm.

We assume the obtained value of the equivalent roughness to calculate the coefficient of hydraulic resistance λ and the specific head loss I .

We determine the coefficient of equivalent roughness for a steel pipe that was in operation. In accordance with GOST 8.586 1-2005 (ISO 5167-2003), the equivalent roughness for steel pipelines is calculated by the formula

$$K_{eq} = \mu R_a \qquad (7)$$

For calculation K_{eq}, we use the value of the natural roughness of the hydrotransport pipeline element (R_a - 4, 49 μm), Table 2.

$$K_{eq} = \pi \cdot 4{,}49 = 14{,}1 \text{ μm}.$$

It can be seen that the equivalent roughness values for a steel pipeline are significantly higher than the values for a coated pipeline (almost eight times). Accordingly, the coefficients of hydraulic resistance and the specific head loss will be significantly different.

The coefficient of hydraulic resistance, which is a function of the relative roughness in the quadratic area of friction (resistance), for a pipe of 1000 mm with an inner polyurethane coating (λ_{coat}), according to Shifison's formula, will be equal to:

$$\lambda_{coat} = 0{,}11 \cdot \varepsilon^{0{,}25} = 0{,}11\left(\frac{K_{eq}}{D}\right)^{0.25} = 0{,}11 \cdot \left(\frac{1.772 \cdot 10^{-3}}{1000}\right)^{0.25} = 0{,}004 .$$

The coefficient of hydraulic resistance for a steel spent pipeline (λ_{st}), will be equal to

$$\lambda_{st} = 0{,}11\left(\frac{14{,}1 \cdot 10^{-3}}{1000}\right)^{0{,}25} = 0{,}007 .$$

Specific head losses are calculated for the conditions of the Kachkanarsky GOK, taking into account the new values of the coefficients of hydraulic resistance λ_{coat} and λ_{st}. We will have for head losses in the pipeline lined with a layer of polyurethane with a hardness of Shore from 83A to 90A:

$$I = I_в + \Delta I_в = \lambda_{фут} \frac{v^2}{2gD} + k_ρ \delta \sqrt[4]{j} \cdot \sqrt[3]{c_{об}^2} ;$$

$$I = 0{,}004 \frac{4{,}8^2}{2 \cdot 9.81 \cdot 1{,}0} + 3.3 \cdot 0{,}056 \cdot \sqrt[4]{0{,}2} \cdot \sqrt[3]{0{,}04^2} = 0{,}0155 .$$

In the steel pipeline (without coating) :

$$I = I_0 + \Delta I_0 = \lambda_{st} \frac{v^2}{2gD} + \Delta I_0 ;$$

$$I = 0{,}007 \frac{4{,}8^2}{2 \cdot 9.81 \cdot 1{,}0} + 3.3 \cdot 0{,}056 \cdot \sqrt[4]{0{,}2} \cdot \sqrt[3]{0{,}04^2} = 0{,}0232 .$$

The results of calculations of the roughness coefficients, hydraulic resistances and specific head losses are given in Table. 4. The results of calculations of the roughness coefficients, hydraulic resistances and specific head losses are given in Table. 4.

Table 4 : Calculated values of coefficients of roughness, hydraulic resistances and specific head losses (pipeline *D* = 1000 MM mm)

Pipeline	Parameters			
	Natural roughness (Δ), μm	Equivalent roughness (K_{eq}), μm	Coefficient of hydraulic resistance (λ)	Specific head loss (*I*), m w.c./m
Polyurethane coating	0,913	1,772	0,004	0,0155
Steel	4,49	14,1	0,007	0,0232

4. CONCLUSION

1. Established values of the surface roughness of polyurethane coatings, the values of the relative roughness coefficients and the calculated values of specific head losses confirm the efficiency of using pipelines with a polyurethane coating of the pipeline inner surface in hydrotransport system of tail pulp.
2. Hardness of the surface of polyurethane coatings in the Shore scale from 83A to 90A (experimental coatings) does not have a practical effect on the intensity of the change in the roughness of the coating surface.
3. Hydraulic drag coefficient in pipeline during the transportation of tail pulp with a mass concentration of solid phase c_p = 10% is proportional to the ratio of equivalent roughness (K_{eq}) to the diameter of the pipeline by the formula $\lambda = 0.11\left(\frac{K_{eq}}{D}\right)^{0.25}$. For the working diameter of the pipeline *D* = 1000 mm, when working in the zone of quadratic friction

(developed turbulent flow regime of the slurry), the hydraulic resistance coefficient on average for 1000 hours of continuous operation will not exceed $\lambda = 0.004$.

4. Calculated values of the specific head losses in the pipeline with polyurethane coating for hydraulic transport of the slurry of the concentration tailings with a solid concentration of 10% is $I_{Coat} = 15.5$ m w.c./km, which is almost 1.5 times less than in the uncoated steel pipeline ($I = 23.2$ m w.c./km).

ACKNOWLEDGMENTS

Reported study was funded by the Kachkanarsky Ore Mining and Processing Enterprise (EVRAZ KGOK), according to the research project No. 160038y/356 From May 26, 2016.

REFERENCES

1. Aleksandrov V.I., Vasylieva M. A. 2015. The rheological properties of high concentration slurry at pipeline transportation on example of copper-nickel ore tailings. Reports of the XXIII Int. Sci. Symp. «Miner's week — 2015», 452–460.
2. Aleksandrov V.I., Gorelkin I. M. 2012. Energy inputs minimization in slurry hydraulic transportation. Mineral Processing, 3, 39–42.
3. Darcy H. Recherches expérimentales relatives au mouvement de l'eau dans les tuyaux. 1857. Paris, Malet-Bachelier.
4. Heywood, N. Richardson J., 1978. Head loss reduction by gas injection for highly shear-thinning suspensions in horizontal pipe flow. Proc. Hydrotransport 5, BHRA Fluid Engineering, C1, 146–152.
5. Heywood N., Alderman J., 2003. Developments in slurry pipeline technologies. Chem. Eng. Prog., 4, 100–107.
6. Kumar U., Singh S.N., Seshadri V., 2015. Bi-modal slurry pressure drop characteristics at high concentration in straight horizontal pipes. Int. J. of Engineering and Technical Research (IJETR), 3(4), 394–397.
7. Schmitt D.J., 2004. Experimental investigation of surface roughness microstructures and their effects on pressure drop characteristics in rectangular minichannels. M. S. thesis. Rochester Institute of Technology.
8. ISO 868—85. Plastics and ebonite. Determination of indentation hardness by means of a duromater (Shore hardness). Moscow, Committee for Standardization and Metrology of the USSR.
9. Portable Surface Roughness Tester SURFTEST SJ-210 Series. Mitutoyo America Corporation. URL: http://www.mitutoyo.com/Images/003/316/2140_SJ-210.pdf, date of the application: 1.12.2016.
10. Nikuradse J. 1932. Gesetzmässigkeiten der turbulenten Strömung in glatten Rohren. Ver. Deut. Ing. Forschungsheft, 356.
11. Nikuradse J. 1933. Stromungsgesetze in rauhen Rohren. *Ver. Deut. Ing. Forschungsheft*, 361.
12. Yagi T., Okude T., Miyazaki S., Koreishi A. 1972. An analysis of the hydraulic transport of solids in horizontal pipes. Report of the Port & Harbour Research Institute (Japan), 11(3).
13. Dobromyslov A. I. 2004. Tables for the hydraulic calculation of pipelines made of polymer materials. Moscow, VNIIVP, 209 pp.

LIST OF MGMI SPECIAL PUBLICATIONS

Name of Publication	Year	US$	Rs
Progress of the Mineral Industry* (Golden Jubilee Vol 1906-1956)	1956	12	60
Dr DN Wadia Commemorative Volume*	1965	15	100
Small Scale Mining in India and abroad*	1991	45	450
New Finds of Coal In India–Resource potential and Mining Possibilities	1993	30	300
Computer Applications in Mineral Industry	1993	40	400
Indian Mining Directory (4th Edition)*	1993	40	400
Asian Mining 1993	1993	85	850
Mine Productivity & Technology	1994	75	500
Maintenance Management for Mining Machinery*	1995	60	600
High Production Technology for underground Mines*	1996	50	500
Mineral Industry Development in India–Issues, Perspective & Policy	1996	20	200
Disaster Prevention Management for Coal Mines, Vol I	1996	50	500
Disaster Prevention Management for Coal Mines, Vol II	1996	50	500
Business and Investment opportunities in Mining Industries (BIMI '96)*	1996	40	400
Indian Mining Directory (5th Edition)	1996	50	500
Information Technology in Mineral Industry (MGMIT'97)*	1997	50	500
Technological Advances in Opencast Mining (Opencast '98)*	1998	80	800
Management of Mining Machinery (MMM 1999)	1999	80	800
Mining & Marketing of Minerals (MMM 2000)	2000	80	800
Mechanisation and Automation in Mineral Industry (MAMI 2001)	2001	80	800
Mineral Industry: Issues on Economics, Environment and Technology (MEET 2002)	2002	80	800
Development of Indian Mineral Industry Looking Ahead (DIMI 2003)	2003	20	200
Emerging Challenges in Mining Industry (ECMI 2003)	2003	50	500
Future of Indian Mineral Industry (FIMI 2004)	2004	80	800
Bridging the Demand Supply Gap in Indian Coal Industry*	2005	30	300
Asian Mining Towards A New Resurgence (Vol I & II)	2006	175	2400
Indian Mining Directory (6th Edition)	2006	60	600
Turnaround Stories of Coal Companies and Future Strategies	2006	20	200
Reprints of Holland Memorial Lecture	2006	40	400
Glimpses from Transactions	2006	30	300
Coal Beneficiation & Development of Coal Derivatives*	2007	40	400
2nd Asian Mining Congress* (Vol I & II)	2008	200	2000
Glimpses of Hundred years of MGMI of India (1906–2006)	2008	50	500
3rd Asian Mining Congress (Vol I & II)	2010	160	2000
4th Asian Mining Congress	2012	100	1000
5th Asian Mining Congress 2014 (CD available)	2014	100	1000
6th Asian Mining Congress 2016 (Pen Drive available)	2016	100	1000
7th Asian Mining Congress 2017 (Pen Drive available)	2017	100	1000

*out of stock

MGMI TRANSIT HOUSE

The Mining, Geological and Metallurgical Institute of India

GN-38/4, Sector V, Salt Lake, Kolkata 700 091
Phones : +91 33 4000 5168, +91 33 2357 3482/3987, Telefax : +91 33 2357 3482
E-mail : secretary@mgmiindia.in, office@mgmiindia.in, Web : www.mgmiindia.in

Rules & Regulations

1. Room Rent is as follows :

Accommodation	AC	Accommodation	AC
Single Occupancy	Rs. 1,500/-	Triple Occupancy	Rs. 2,500/-
Double Occupancy	Rs. 2,000/-	Extra Bed	Rs. 600/-

2. 50% discount will be offered to MGMI member for self occupancy only.
3. Full tariff will be applicable for the nominee of MGMI member.
4. Full tariff for the employees of the Corporate Member or Patron Member.
5. 100% advance has to be deposited for confirmation of block booking (three or more rooms for two or more days).
6. Caution money @Rs. 500/- per day, per room has to be deposited along with room rent in advance. This will be refunded in full or part thereof depending on the damage caused by the Guests.
7. Cancellation of confirmed booking Period Prior to date of Occupancy Cancellation fee to be deducted from advance

   a. Cancellation before Seven days 5%
   b. Cancellation before Three days 10%
   c. Cancellation before One day 25%

8. Check-in time 12.00 noon
9. Check-out time 11.00 a.m.
10. GST : Less than Rs. 1,000/- No GST
    Rs. 1,001/- to 7,500/- 12% (6% + 6% GST)
    Above Rs. 7,501/- 18% (9% + 9% GST)

LIFT Facility Available

For Booking Please Contact MGMI Office
Mobile : 88840 00362, E-mail : secretary@mgmiindia.in, office@mgmiindia.in, Web : www.mgmiindia.in

Published by : Honorary Secretary, **The Mining, Geological and Metallurgical Institute of India**
GN-38/4, Sector V, Salt Lake, Kolkata 700 091
Phones : +91 33 4000 5168, +91 33 2357 3482 / 3987, Telefax : +91 33 2357 3482
E-mail : secretary@mgmiindia.in, office@mgmiindia.in, Web : www.mgmiindia.in
Printed at : Graphique International, Kolkata - 700 015, Phone : (033) 2251 1407